Sharp bend flow

Comparison of Delft3D-FLOW with LES and measurements for sharp bends

Graduation committee:

Prof. dr. ir. H.J. de Vriend (Deltares/TU Delft, Hydraulic Engineering section)

Dr. ir. E. Mosselman (Deltares/TU Delft, Hydraulic Engineering section)

Ir. W. Ottevanger (TU Delft, Hydraulic Engineering section)

Dr. ir. C.J. Sloff (Deltares/TU Delft, Hydraulic Engineering section)

Prof. dr. ir. W.S.J. Uijttewaal (TU Delft, Enviromental Fluid Mechanics section)

Deltares
Enabling Delta Life

TU Delft

MSc thesis

Arco van Sabben

Faculty of Geosciences and Civil Engineering

Delft University of Technology

June 2010

The figure at the cover is a sharp bend in the river Mosel at Trittenheim, Germany (postcard)

Preface

This report contains the findings of a study on the applicability of Delft3D-FLOW in sharp open-channel bends. This research was performed as a Master thesis for the Hydraulic Engineering section at the Delft University of Technology (Delft, the Netherlands). This research was conducted at Deltares and was focused on the applicability of Delft3D-FLOW in sharp open-channel bends and to find aspects in this engineering tool that possibly needs to be improved such that it may be used in sharply curved open channel bends. Use is made of results of previous research. Manifold use is made of the results of the Large Eddy Simulations performed at the Delft University of Technology and the experimental results of the experiments performed at the Ecole Polytechnique Fédérale Lausanne (EPFL, Lausanne, Switzerland). Both researches used in this thesis are part of a joint research program focused on implementation of improvements obtained by this research in engineering modelling tools. This study tries to contribute to the development of good engineering tools.

In the first part of this thesis the used models are described. The second part contains a comparison of the results. This thesis provides insight in the shortcomings of the different models and contains suggestions to improve Delft3D-FLOW in the area of sharp bend flows.

Arco van Sabben

Delft, June 2010

Summary

For a proper management of rivers and river bends in particular, it is important to have good models to predict the flows through bends. It is important that those developed models are well validated with measurements to demonstrate the usefulness of the models. At the Ecole Polytechnique Fédérale Lausanne (EPFL, Lausanne, Switzerland) detailed measurements of a flume with a sharp bend (as a rule of thumb is taken the radius over the width should be smaller than two or three, see the figure) were conducted. These measurements are suitable for comparison with the results of numerical models. At the TU Delft, these measurements were compared with a Large Eddy Simulation (LES) model. Another widely used model in engineering practice is Delft3D-FLOW. The main question of this research is aimed at the applicability of Delft3D-FLOW in sharp bends:

- To what extent is Delft3D-FLOW able to predict the hydrodynamic processes in sharp open channel bends?

To find an answer to this question, we used the measurements conducted at the EPFL and the LES's conducted at the TU Delft.

The two sub-questions which are addressed are:

- What are the differences between the LES and Delft3D-FLOW and how can these differences be explained?

- What is the effect of changes in the turbulent viscosity on the flow?

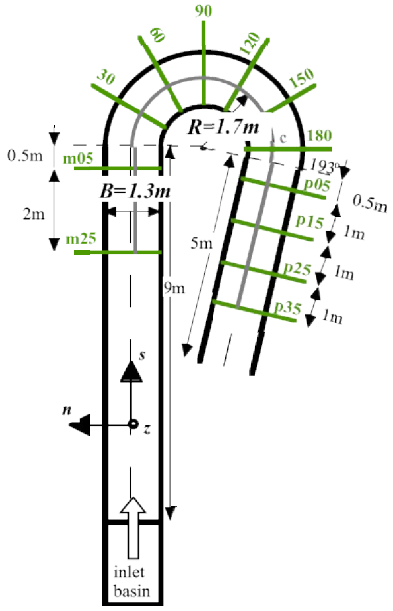

Plan view of the flume used at the EPFL (Blanckaert, 2002)

The results of the measurements and the LES's were compared with simulations of Delft3D-FLOW. Two cases were compared: a flat-bed (Q89) and an equilibrium-bed (M89) case. The measurements were compared with the Delft3D-FLOW simulation to find out to what extent Delft3D-FLOW is able to predict the flow. The results of the simulations were compared with the results of the LES too. The M89-case was compared to show the applicability of Delft3D-FLOW in the engineering practice because in general the bottom is not flat in practice. Based on the comparison of the Delf3D-FLOW results with the measurements and the LES, the causes of possible shortcomings in the prediction of the flow are sought. These comparisons were conducted for both the flat-bed and the equilibrium-bed case.

To answer the last question about the turbulent viscosity, two Delft3D-FLOW simulations of the flat-bed case, were compared. For one of these simulations the horizontal turbulent viscosity is enlarged to $\nu_{hor} = 10^{-2}$ m^2/s, which is an order of magnitude larger than what was chosen in the other simulation).

From the comparison of the measurements with the Deflt3D-FLOW simulation, it turned out that especially the transverse velocities (secondary flow) were not predicted correctly by Delft3D-FLOW. Several phenomena did not appear in the simulations. One of them is the '*outer-bank cell*' which is a cell at the outer bank of the flume that rotates opposite to the primary secondary cell. Another important one was the internal shear layer at the inner bend. From the comparison of the LES and the measurements it turned out that the LES is able to predict these phenomena better. This is especially caused by the way the turbulent stresses were predicted. This is also visible in the turbulent shear stresses. These were predicted better by the LES in the flat-bed case. Delft3D-FLOW underestimated the turbulent shear stresses and the patterns in the cross-section often did not compare. The turbulent kinetic energy is concentrated along the borders of the flume and the outer-bank cell and along the internal shear layer. These are the regions where the turbulent kinetic energy is generated.

In the equilibrium-bed case (M89), the comparison between the results of Delft3D-FLOW and the measurements decreases. The transverse velocities are underestimated even more. The same holds for the results of the LES although the comparison between LES and measurements is better than the comparison between Delft3D-FLOW and the measurements. When taking a look at the shear stresses, it turns out that these were underestimated for both the LES and the Delft3D-FLOW simulation. The distribution of the calculated turbulent shear stresses diverges from what was measured.

The comparison of the two Delft3D-FLOW simulations with different turbulent viscosity, gives insight in the effect of the turbulent viscosity on the flow. It appears that an increase of the turbulent viscosity increases the exchange of momentum. This is clearly visible in the distribution of the velocity over the width of the flume. Peaks are smoothed out and the velocities (both the downstream and the transverse velocities) are more even distributed over the flow. The turbulent shear stresses are larger than in the simulation with the low turbulent viscosity. This can be explained partly because of the relation (by the Boussinesq hypothesis) between the turbulent viscosity and the turbulent shear stresses. In the Boussineq hypothesis are the shear stresses proportional to the turbulent viscosity. Besides that, the shear stresses are coupled to the gradients of the velocities. In its turn, the velocities depend on the turbulent stresses via the momentum balance.

As was mentioned, the prediction of the flow by the LES is better than the prediction by Delft3D-FLOW, generally spoken. This is due to the way the turbulent shear stresses are predicted by the LES, which causes that the LES is able to predict phenomena like the outer-bank cell. The LES gives in the flat-bed case a better prediction of the turbulent shear stresses than Delft3D-FLOW. The change of the turbulent viscosity, and in that way turbulent shear stresses, influences the distribution of the velocities. Therefore it can be stated that it is important for a good prediction of flows and details of the flow, to have a good prediction of the turbulent stresses.

Samenvatting

Voor een goed beheer van rivieren en met name rivier bochten, is het van belang om goede modellen te hebben om voorspellingen te kunnen doen van de stroming door bochten. Het is van belang dat de ontwikkelde modellen goed gevalideerd zijn met praktijk metingen om de bruikbaarheid van het model aan te tonen. Bij de Ecole Polytechnique Fédérale Lausanne (EPFL, Lausanne, Zwitserland) zijn gedetailleerde metingen verricht aan een goot (zie de figuur) met een scherpe bocht (als een vuistregel wordt wel aangehouden dat een bocht scherp is wanneer de straal gedeeld door de breedte van de stroom kleiner is dan 2 of 3). Deze metingen zijn geschikt om numerieke modellen mee te vergelijken. Op de TU Delft zijn deze metingen vergeleken met Large Eddy Simulaties. Een ander veel gebruikt model in de ingenieurs praktijk is Delft3D-FLOW. De hoofdvraag van dit onderzoek is gericht op de toepasbaarheid van Delft3D-FLOW in scherpe bochten en luidt dan ook:

- In hoeverre is Delft3D-FLOW in staat om stroming door scherpe bochten te voorspellen?

Om een antwoord te vinden op deze vraag is er gebruik gemaakt van de metingen die uitgevoerd zijn aan de EPFL en de LES's die uitgevoerd zijn aan de TU Delft.

De twee subvragen die daarbij geprobeerd zijn te beantwoorden zijn:

- Wat zijn de verschillen tussen de LES en Delft3D-FLOW en hoe kunnen deze verschillen worden verklaard?

- Wat is het effect van veranderingen van de turbulente viscositeit op de stroming?

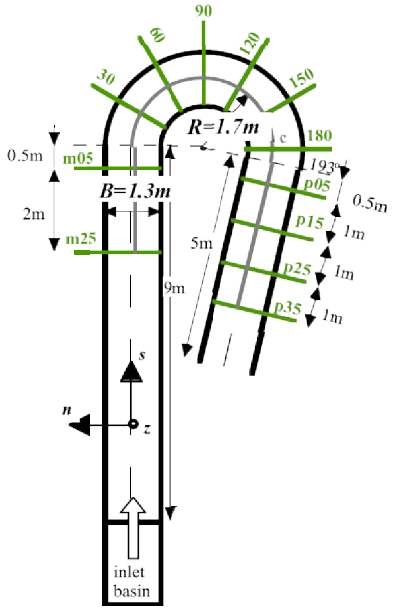

Bovenaanzicht van de goot, gebruikt bij de EPFL metingen (Blanckaert, 2002)

Om een antwoord te vinden op deze vragen zijn de resultaten van de metingen en de LES's vergeleken met simulaties van Delft3D-FLOW. Twee situaties zijn vergeleken: een vlakke bodem (Q89) en een evenwichtsbodem (M89). De metingen zijn vergeleken met de Delft3D-FLOW simulaties om te onderzoeken in hoeverre Delft3D-FLOW in staat is de stroming te voorspellen. Het geval met de evenwichtsbodem is vergeleken uit het oogpunt van toepasbaarheid van Delft3D-FLOW in de ingenieurs praktijk. Daarnaast zijn de metingen ook vergeleken met de LES's. Aan de hand van deze twee vergelijkingen is gekeken waar mogelijke oorzaken liggen van betere of slechtere voorspellingen van de stroming. Deze

vergelijkingen zijn gedaan voor zowel de vlakke bodem situatie als de evenwichtsbodem situatie.

Om de laatste onderzoeksvraag over het effect van de turbulente viscositeit te beantwoorden zijn er twee simulaties van Delft3D-FLOW (vlakke bodem) met elkaar vergeleken. Hierbij is bij een van de twee simulaties de horizontale turbulente viscositeit vergroot (een orde groter dan in de andere simulatie, naar $\nu_{hor} = 10^{-2}$ m^2/s).

Bij de vergelijking van de metingen met de Delft3D-FLOW simulatie bleek dat met name de dwars snelheden (secundaire stromingen) niet goed worden voorspeld door Delft3D-FLOW. Een aantal verschijnselen komen niet terug in de simulatie. Dit zijn onder andere de 'outer-bank cell' en het ontstaan van de interne schuif laag. De 'outer-bank cell' is een circulatie in de buitenbocht die in tegengestelde richting draait als de primaire secundaire circulatie. Uit de vergelijking van de LES met de metingen blijkt dat de LES beter in staat is om deze verschijnselen te voorspellen. Dit heeft met name te maken met de manier waarop de turbulente spanningen zijn gemodelleerd. Dit is ook terug te zien in de turbulente schuifspanningen. Deze worden in het Q89 geval beter gesimuleerd door de LES. Delft3D-FLOW onderschat de turbulente schuifspanningen en de verdeling over de doorsnede komt ook vaak niet overeen. De turbulente kinetische energie is met name geconcentreerd langs de randen van de goot en de outer-bank cell en langs de interne schuiflaag. Dit zijn de plaatsen waar de urbulente kinetische energie wordt gegenereerd.

In het geval van de evenwichtsbodem (M89) is de overeenkomst tussen Delft3D-FLOW en de metingen minder goed. De dwars snelheden worden nog meer. Dit geldt tevens voor de resultaten van de LES alhoewel de overeenkomst tussen LES en meting nog steeds beter is dan de overeenkomst tussen Delft3D-FLOW en de metingen. Als we kijken naar de turbulente schuifspanningen dan blijkt dat deze voor zowel de LES als de Delft3D-FLOW simulatie sterk onderschat worden. Ook de verdeling van de turbulente schuifspannignen wijkt sterk af van wat gemeten is.

De vergelijking van de twee simulaties van Delft3D-FLOW voor het Q89 geval waarbij de turbulente viscositeit is gewijzigd, geven inzicht in het effect van de turbulente viscositeit op het stromingsbeeld. Het blijkt dat een toename van de turbulente viscositeit zorgt voor meer uitwisseling van impuls. Dit is goed zichtbaar in de verdelingen van de snelheid over de stroming. Pieken zijn afgevlakt en de snelheden (zowel de stroom afwaarts gerichte als de dwarssnelheden) zijn meer egaal verdeeld over de stroming. De turbulente schuifspanningen zijn groter dan in de simulatie met de lage viscositeit. Dit is deels te verklaren doordat de schuifspanningen zijn bepaald met behulp van de Boussinesq hypothese. Hierin zijn de turbulente schuispanningen evenredig met de viscositeit. Verder zijn de turbulente schuifspanningen, in de Boussinesq hypothese, gekoppeld aan de verdeling van de snelheidscomponenten (de gradiënten). De verdeling van de snelheid is op zijn beurt weer gekoppeld aan de turbulente spanningen, via de impulsbalans.

Er kan worden geconcludeerd dat de voorspelling van de stroming door de LES, over het algemeen beter is dan de voorspelling door Delft3D-FLOW. Dit heeft onder andere te maken met een andere wijze van berekenen van de turbulente schuifspanningen bij de LES waardoor hier fenomenen als de outer-bank cell wel worden berekend. De verandering van de turbulente viscositeit, en indirekt dus ook de turbulente schuifspanning, heeft invloed op de verdeling van de snelheden. Daarom kan er gesteld worden dat het goed voorspellen van de turbulente spanningen van belang is voor het goed voorspellen van stromingen en details van stromingen. De LES doet dat in het geval van een horizontale bodem beter dan Delft3D-FLOW.

Table of contents

1 Introduction

1.1 Motivation

Many river training works have been performed in the past, nowadays more attention is paid to a more natural development of rivers. A way to realize the natural development of streams is to let them (re-)meander. For a good management of the rivers, and especially the river bends, good models, software tools and a good understanding of the behaviour of the river is needed. The recent flooding problems (in June, 2010) in middle Europe also show the necessity of a good prediction of the water level along the river. As is known (Blanckaert, 2002), the water level is influenced by bends. The spreading of transported matter is also strongly influenced by bends because of the mixing capacity of the secondary flow in bends. This leads also to the question what happens with morphologic phenomena along bends. How does the morphological phenomena influence the conveyance capacity and of the rivers and streams? Until recently not much research was done on flows through sharp open-channel bends. The curvature of a bend is sometimes denoted by the radius to width ratio (R/B). There are other ways to define the sharpness of a bend but in this report we will call a bend sharp when R/B < 2 or 3 (Blanckaert, 2002). At present most analytical and numerical models are based on mild curvature assumptions (high R/B). The focus of experimental research to be used for model validation is also mostly on mild curvature bends. As a result, most numerical models have not been validated for sharp curvature bends. An exception to this is the research done by Van Balen (2010) who validated a Reynolds Average Navier-Stokes (RANS) model and a Large Eddy Simulation (LES) model with the help of experimental results obtained by Blanckaert (2002). Blanckaert conducted several detailed measurements in a flume with a sharp open channel bend (Blanckaert, 2002). The data from these experiments are well suited to validate the numerical models. One of the numerical modelling systems that often is used to calculate flows through channels and rivers is Delft3D-FLOW. It is a model, based on the Reynolds equations where the turbulent stresses are modelled with a closure model.

This study tries to contribute to this field of research. It will focus on a Delft3D-FLOW model and its applicability to sharp open channel bends. The results of this study should contribute to a better understanding of the shortcomings of the Delft3D-FLOW model and tries to suggest possible improvements of the model. Finally it should lead to a proper tool for the engineering practice in real life problems. Therefore the (improved) model should be validated with measurements in existing sharp river bends. Especially in rivers it is of importance that morphological phenomena are properly simulated but therefore it is firstly needed that the hydrodynamic aspects are properly represented. This study will therefore focus on the hydrodynamic aspects of sharp open-channel bends in Delft3D-FLOW.

1.2 Objectives

As was described in section 1.1 it is interesting to know to what extent the numerical models used to simulate flows through sharp open channel bends are applicable. In this research a numerical model based on the Delft3D-FLOW code is chosen to be validated extensively. The main question to be answered is:

To what extent is Delft3D-FLOW able to predict the hydrodynamic processes in sharp open channel bends?

By answering this question, particular attention is paid to secondary circulation and wall shear stresses.

Van Balen compared LES and RANS-simulation with results of the measurements performed by Blanckaert (van Balen, 2010). An interesting second objective arises: what are the differences between LES and Delft3D-FLOW simulations and how can these differences be explained?

Once this is clear it is possible to conclude which model gives better results.

An important difference between LES and Delft3D-FLOW is the way the turbulence is modelled (Delft3D-FLOW manual, 2008 and Uijttewaal, 2008). Because the turbulence in Delf3D-FLOW is strongly related to the eddy viscosity, which is an input parameter in Delft3D-FLOW, the effects of the eddy viscosity on the flow are investigated, to identify the effects of changes in this viscosity.

1.3 Outline of the report

The set up of this report is as follows:

Chapter 1 contains the introduction and the motivation for this research. The objectives of this research are described in chapter 1 as well. In chapter 2 some theoretical information is summarized. The models and measurements used are described and the method to compare the different data sets is written down. Chapter 3 is dedicated to the flat-bed case. It consists of an analysis of the measurements followed by a comparison of the Delft3D-FLOW results with the measurements and the LES. In the last part of chapter 3 the effects of an increase of the viscosity are analyzed. Chapter 4 contains the comparison of the equilibrium-bed case. Here too, the results of the measurements are analyzed and compared with the results of a Delft3D-FLOW simulation. The last two chapters contain the discussion and the conclusions.

2 Methodology

In the first part of this chapter some theoretical background information is given. After that, the experiments and models used are described and in the last part of the chapter the methodology is described.

2.1 Physical modelling

2.1.1 Navier-Stokes equations

Flows can mathematically be described by the Navier-Stokes equation, considering the conservation of momentum and mass. By adopting the cylindrical coordinate axes as shown in Figure 2-1 with rθ the downstream coordinate, r the transverse and z the vertical direction with u, v, w the corresponding velocities, we can write the Navier-Stokes equations as (assuming incompressible flow, see van Balen, 2010):

$$\rho\left(\frac{\partial u}{\partial t}+v\frac{\partial u}{\partial r}+\frac{u}{r}\frac{\partial u}{\partial \theta}+\frac{uv}{r}+w\frac{\partial u}{\partial z}\right)= -\frac{1}{r}\frac{\partial p}{\partial \theta}+\eta\left[\frac{1}{r}\frac{\partial}{\partial r}\left(r\frac{\partial u}{\partial r}\right)-\frac{u}{r^2}+\frac{1}{r^2}\frac{\partial^2 u}{\partial \theta^2}+\frac{2}{r^2}\frac{\partial v}{\partial \theta}+\frac{\partial^2 u}{\partial z^2}\right] \quad (2.1)$$

$$\rho\left(\frac{\partial v}{\partial t}+v\frac{\partial v}{\partial r}+\frac{u}{r}\frac{\partial v}{\partial \theta}-\frac{u^2}{r}+w\frac{\partial v}{\partial z}\right)= -\frac{\partial p}{\partial r}+\eta\left[\frac{1}{r}\frac{\partial}{\partial r}\left(r\frac{\partial v}{\partial r}\right)-\frac{v}{r^2}+\frac{1}{r^2}\frac{\partial^2 v}{\partial \theta^2}-\frac{2}{r^2}\frac{\partial u}{\partial \theta}+\frac{\partial^2 v}{\partial z^2}\right] \quad (2.2)$$

$$\rho\left(\frac{\partial w}{\partial t}+v\frac{\partial w}{\partial r}+\frac{u}{r}\frac{\partial w}{\partial \theta}+w\frac{\partial w}{\partial z}\right)= -\frac{\partial p}{\partial z}+\rho g+\eta\left[\frac{1}{r}\frac{\partial}{\partial r}\left(r\frac{\partial w}{\partial r}\right)+\frac{1}{r^2}\frac{\partial^2 w}{\partial \theta^2}+\frac{\partial^2 w}{\partial z^2}\right] \quad (2.3)$$

$$\frac{1}{r}\frac{\partial (rv)}{\partial r}+\frac{1}{r}\frac{\partial u}{\partial \theta}+\frac{\partial w}{\partial z}=0 \quad (2.4)$$

with

u,v,w = velocities in θ, r and z direction [m/s]

ρ = fluid density [kg/m^3]

p = pressure [N/m^2]

η = molecular diffusion coefficient [kg/m/s]

Equation (2.1) to equation (2.3) describe the conservation of momentum and equation (2.4) describes the conservation of mass.

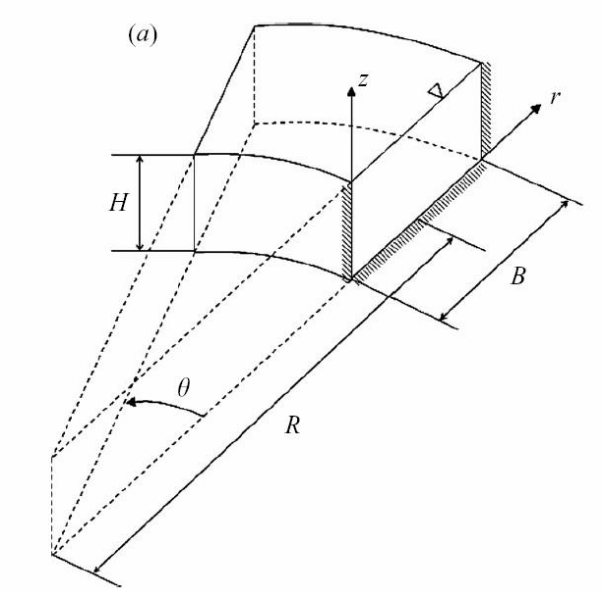

Figure 2-1 Definition sketch (van Balen, 2009a)

There are no analytical solutions for these equations for flows with relatively high Reynolds numbers (Re>1000, Uijttewaal, 2008) because of instabilities and other non-linear phenomena of the solutions. One way to solve them is by brute computational power but this is very time consuming and for engineering purposes not attractive and maybe even infeasible. The number of grid points needed to solve the problem properly is proportional to $Re^{9/4}$ (Pope, 2000, pag. 347). If we take into account the time scale to be solved, the number of floating-point operations required to perform a simulation is proportional to the product of the number of modes and the number of steps. Pope (2000, pag. 347) explained that the number of floating-point operations is proportional to Re^3. This shows the very steep rise with the Reynolds number. The simulation of a practically relevant flow with a Re of about 10^5 will therefore not yet be possible to simulate in the next decades (Uijttewaal, 2008). An other way to solve flows with a high Reynolds number, is to simplify the Navier-Stokes equations by decomposing the velocities and pressure in an ensemble averaged part and a fluctuating part ($v_i = \overline{v}_i + v_i'$ and $p = \overline{p} + p'$) and averaging the resulting equations. By doing this we arrive at the Reynolds equations which resemble the Navier-Stokes equations:

$$\rho\left(\frac{\partial\overline{u}}{\partial t}+\overline{v}\frac{\partial\overline{u}}{\partial r}+\frac{\overline{u}}{r}\frac{\partial\overline{u}}{\partial\theta}+\frac{\overline{uv}}{r}+\overline{w}\frac{\partial\overline{u}}{\partial z}\right)+\rho\left(\frac{\partial(\overline{v'u'})}{\partial r}+\frac{1}{r}\frac{\partial(u'u')}{\partial\theta}+\frac{\overline{u'v'}}{r}+\frac{\partial(\overline{w'u'})}{\partial z}\right)= -\frac{1}{r}\frac{\partial\overline{p}}{\partial\theta}+\eta\left[\frac{1}{r}\frac{\partial}{\partial r}\left(r\frac{\partial\overline{u}}{\partial r}\right)-\frac{\overline{u}}{r^2}+\frac{1}{r^2}\frac{\partial^2\overline{u}}{\partial\theta^2}+\frac{2}{r^2}\frac{\partial\overline{v}}{\partial\theta}+\frac{\partial^2\overline{u}}{\partial z^2}\right] \quad (2.5)$$

$$\rho\left(\frac{\partial\overline{v}}{\partial t}+\overline{v}\frac{\partial\overline{v}}{\partial r}+\frac{\overline{u}}{r}\frac{\partial\overline{v}}{\partial\theta}-\frac{u^2}{r}+\overline{w}\frac{\partial\overline{v}}{\partial z}\right)+\rho\left(\frac{\partial(\overline{v'v'})}{\partial r}+\frac{1}{r}\frac{\partial(\overline{u'v'})}{\partial\theta}-\frac{(\overline{u'u'})}{r}+\frac{\partial(\overline{w'v'})}{\partial z}\right)= -\frac{\partial\overline{p}}{\partial r}+\eta\left[\frac{1}{r}\frac{\partial}{\partial r}\left(r\frac{\partial\overline{v}}{\partial r}\right)-\frac{\overline{v}}{r^2}+\frac{1}{r^2}\frac{\partial^2\overline{v}}{\partial\theta^2}-\frac{2}{r^2}\frac{\partial\overline{u}}{\partial\theta}+\frac{\partial^2\overline{v}}{\partial z^2}\right] \quad (2.6)$$

$$\rho\left(\frac{\partial\overline{w}}{\partial t}+\overline{v}\frac{\partial\overline{w}}{\partial r}+\frac{\overline{u}}{r}\frac{\partial\overline{w}}{\partial\theta}+\overline{w}\frac{\partial\overline{w}}{\partial z}\right)+\rho\left(\frac{\partial(\overline{v'w'})}{\partial r}+\frac{1}{r}\frac{\partial(\overline{u'w'})}{\partial\theta}+\frac{\partial(\overline{w'w'})}{\partial z}\right)=$$
$$-\frac{\partial\overline{p}}{\partial z}+\rho g+\eta\left[\frac{1}{r}\frac{\partial}{\partial r}\left(r\frac{\partial\overline{w}}{\partial r}\right)+\frac{1}{r^2}\frac{\partial^2\overline{w}}{\partial\theta^2}+\frac{\partial^2\overline{w}}{\partial z^2}\right] \quad (2.7)$$

The extra term in the equations (2.5) to (2.7) represents the fluctuating part of the velocities and the covariances of these fluctuating velocities can be interpreted as a stress-tensor:

$$\tau_{ij}=\rho\overline{v_i'v_j'} \quad (2.8)$$

with i and j representing the orthogonal directions r, θ and z.

These stresses are called Reynolds stresses. When i = j, the stresses are called normal stresses, otherwise they can be denoted as shear stresses. The normal Reynolds stresses can be neglected for cases with a high Reynolds number (Uijttewaal, 2008).

To solve the Reynolds equations, we need extra relations for the Reynolds stresses, based on ensemble averaged quantities. This is called the closure problem.

The Boussinesq hypothesis states that the turbulent Reynolds stresses are a function of the mean velocity gradients. This is mathematically written as:

$$-\overline{v_i'v_j'}=\nu_t\left(\frac{\partial\overline{v}_i}{\partial x_j}+\frac{\partial\overline{v}_j}{\partial x_i}\right)-\frac{2}{3}k\delta_{ij} \quad (2.9)$$

Where ν_t is the turbulent viscosity or eddy viscosity, k is the turbulent kinetic energy defined as $\sum_{i=1,2,3}\overline{v_i'v_i'}/2$, δ is the Kronecker delta and u the velocity component. The prime means the turbulent fluctuation of the velocity (Pope, 2000, pag. 93 and Wu, 2007).

The problem is now shifted to determining the turbulent viscosity. For determining the turbulent viscosity, the eddy viscosity can be seen as the product of a velocity and a length scale. In this view, several models are developed to determine that specific velocity scale and length scale. These models are often called the turbulence closure models.

The mixing-length hypothesis

One of the first developed models is the Prandtl mixing-length hypothesis. The Prandtl mixing-length hypothesis says that the velocity scale is proportional to the velocity difference (of the mean flow) over a distance l_m over which the momentum transport takes place. The length scale is taken equal to l_m. This results in the following relation:

$$\tau_{ij}=\rho\overline{v_i'v_j'}=-\rho\underbrace{l_m^2\left|\frac{\partial v_i}{\partial x_j}\right|}_{\nu_t}\frac{\partial v_i}{\partial x_j} \quad (2.10)$$

For flows near a wall the length scale l_m is take proportional to the distance from the wall: $l_m = \kappa z$, in which κ is the Von Karman constant (about 0.4) and z is the distance to the wall. This results in a logarithmic velocity profile.

The disadvantages of the mixing-length hypothesis are:

- No turbulent transport can take place at places where the velocity gradient is zero

- Mixing-length models do not account for advective and diffusive transport processes

- In some cases (e.g. in recirculating flows) the relation between the shear stress and the velocity gradient is more complex.

The k-ε model

The k-ε model determines the length scale by means of a transport equation of the energy dissipation (ε) which is related to the length scale. The velocity scale is related to the turbulent kinetic energy whereas the idea is that the velocity scale should stand for the fluctuating velocity of the large eddies. The turbulent kinetic energy is determined by a transport equation.

The k-ε model is one of the more advanced models but the resulting eddy viscosity is isotropic which is often not the case in reality. Recent progress is made with a non-linear k-ε model which is able to predict anisotropic turbulence (c.f. Kimura *et al.*, 2008).

Reynolds stress modelling

Another way to resolve the closure problem is by determining the Reynolds stresses by a transport equation. In the transport equation of the Reynolds stresses some terms appear which also need a closure (terms like production, dissipation, pressure rate of strain tensor and diffusion). These terms are closed with other approximations and constants. It is quite an expensive way of modelling and it is not clear if this way of solving the closure problem is advantageous.

Large eddy simulations

With large eddy simulation only the large scale turbulent structures are solved. The small scale structures are often more isotropic and are filtered out of the equations by filtering them over the volume of one or several grid cells. The resulting equations apply only to the mean flow and the large scale turbulent structures. The small scale turbulence structures are resolved by a closure model. The use of a mixing length model is now better justified. Several closure models are developed for the small scale structures containing most of the turbulent kinetic energy and being anisotropic. These models are also called 'sub-grid models'. It turns out that some of these models transfer energy from the small scales to the large scale structures which is in contradiction with the concept of the energy cascade. The idea of the energy cascade is that energy is transferred from the larger scale to the smaller scale structures where the energy is dissipated. This is one of the reasons to develop dynamic sub-grid models which do not show the transfer of energy from small scale to large scale structures (Uijttewaal, 2008).

2.1.2 Secondary flow

By looking at the flow through a bend we can make some simplifications to gain more insight in the behaviour of bend flows. We can write equation (2.2) for the transverse momentum equation as (assuming ρ as a constant):

$$\frac{\partial v}{\partial t}+\frac{1}{r}\frac{\partial rvv}{\partial r}+\frac{1}{r}\frac{\partial uv}{\partial \theta}+\frac{\partial wv}{\partial z}-\frac{u^2}{r}=-\frac{1}{\rho}\frac{\partial p}{\partial r}+visc.diff. \qquad (2.11)$$

Assuming stationary, uniform flow (time derivative and advection can be neglected), neglecting the resistance (diffusion term) because of the relatively short distance in transverse direction, the only two terms remaining form the transverse momentum balance are the centrifugal force and the pressure gradient in transverse direction.

$$\frac{u^2}{r}=\frac{1}{\rho}\frac{\partial p}{\partial r} \qquad (2.12)$$

These two forces result in a local imbalance. Because of this local imbalance of the hydrostatic pressure and the centrifugal force in a river bend, a secondary circulation flow occurs. These two forces are the driving mechanism of the secondary circulation. The left hand side of equation (2.12) represents the centrifugal force per unit of mass and is given as:

$$a_n = \frac{u^2}{r} \qquad (2.13)$$

The gradient of the hydrostatic pressure per unit of mass is given as:

$$\frac{\partial p}{\partial r} = \rho g \frac{\partial h}{\partial r} \qquad (2.14)$$

with:

a_n = centrifugal force per unit of mass (acceleration) in transverse direction [N/kg or m/s^2]

u_s = downstream velocity [m/s]

r = radius [m]

ρ = density [kg/m^3]

g = gravitational constant [m/s^2]

$\frac{\partial h}{\partial r}$ = water level gradient in transverse direction [-]

A graphic representation of the velocity profile due to the centrifugal force (1), the gradient of the hydrostatic pressure (2) (which is a constant force over the depth) and the resulting transverse velocity profile (3) is shown in Figure 2-2.

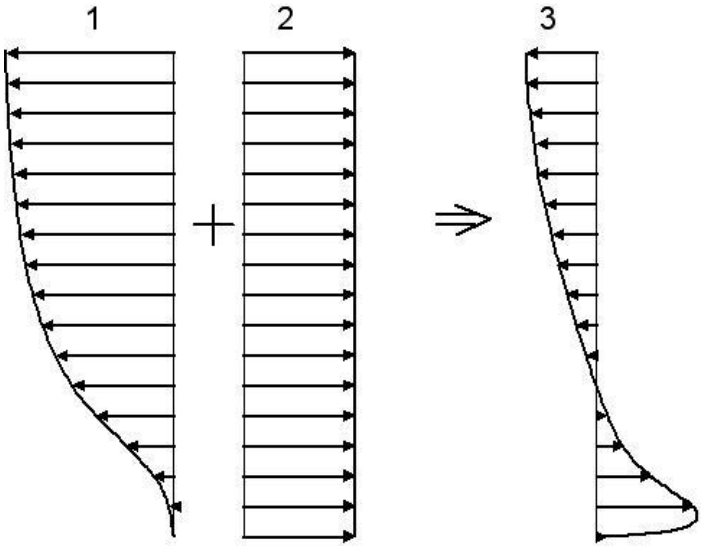

Figure 2-2 Secondary flow in a bend, 1 is the centrifugal acceleration, 2 is the hydrostatic pressure gradient and 3 is the resulting velocity profile due to the combination of both forces

This secondary flow influences the spreading of momentum and suspended matter over the width. Several models have been developed in the past to simulate the secondary flow in a less time consuming way (de Vriend, 1977, Rosovskii, 1957). These models are derived for mild curvatures (large R/B) and therefore neglect the feedback mechanism between streamwise and transverse flow. This feedback mechanism causes a flattening of the streamwise velocity profiles and this in turn leads to a reduction of the strength of secondary

flow for sharp bends (R/B< 2 or 3,m c.f. Blanckaert and de Vriend, 2003) who developed a model including this feedback mechanism). Mild curvature models therefore over predict the momentum redistribution due to secondary flows.

2.2 Experimental setups

This research will mainly concentrate on the possibility of Delft3D-FLOW to predict the flow through sharp open channel bends. The results of the Delft3D-FLOW simulation are compared with measurements and results of LES. Use is made of the measurements conducted by Blanckaert at EPFL (École Polytechnique Fédérale de Lausanne, Lausanne, Switzerland). Figure 2-2 shows a plan view and a cross-section of the flume he used for the experiments. A detailed description of the experiment can be found in Appendix A.1 and A.2

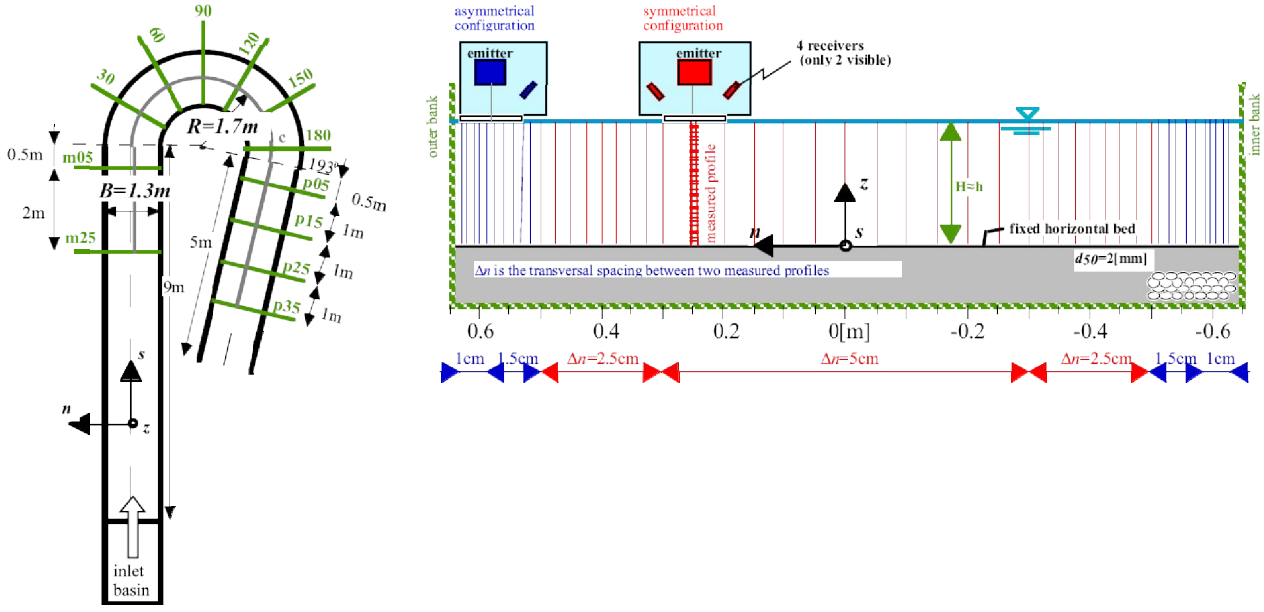

Figure 2-3 Flume used for the experiments conducted at EPFL, with measured cross-sections and profiles (source: Blanckaert, 2002)

In Table 2-1 some quantities of four of the conducted experiments are represented. The experiments denoted with a '*Q*' are experiments with a flat-bed. The experiment denoted with an '*M*' is an experiment where the flow is fed with sediment. This feeding of the flow with sediment resulted in an equilibrium-bed profile. When the equilibrium-bed was reached, the bed was fixed by spraying paint on it. Afterward the hydrodynamic quantities were measured.

Label	Q [l/s]	q_s [kg/s/m]	H [m]	U [m/s]	u* [m/s]	C [$m^{1/2}/s^{-1}$]	Re [10^3]	Fr [-]	R/B [-]	R/H [-]
Q56	56	0	0.108	0.40	0.039	32	43	0.39	1.31	15.6
Q89	89	0	0.159	0.43	0.040	34	69	0.35	1.31	10.6
Q104	104	0	0.212	0.38	0.033	35	81	0.26	1.31	8.0
M89	89	0.023	0.141	0.49	0.049	31.3	68	0.41	1.31	12.1

Table 2-1 Four of the experiments conducted at the EPFL (Blanckaert, 2009), Q denotes the discharge, q_s denotes the sediment discharge, H is the flume average water depth, U denotes the flume averaged velocity, u_* the flume averaged shear velocity (based on H and the average streamwise water surface slope), $C= g^{1/2}(U/u_*)$ the Chezy friction coefficient, $Re = UH/\nu$ the Reynolds number, $Fr = U/(gH)^{1/2}$ the Froude number, R the radius of the centre line of the bend and B the width of the flume.

The results of two of the experiments from Table 2-1 are used during this research, the flat-bed experiment Q89 as a reference case and the equilibrium-bed experiment M89 as a relatively good reflection of flows and streams in practical problems.

2.3 Computational models

2.3.1 Delft3D-FLOW

This section is a short summary of the most important principles of Delft3D-FLOW which are of importance for the simulations performed. The information is adopted from the Delft3D manual.

Delft3D-FLOW is capable to calculate the motion of water in 2D (depth averaged) and 3D domains. In both situations the non-linear shallow water equations are solved. In the vertical direction it is possible to choose between a σ-layer grid or a Z-layer grid in Delft3D-FLOW. A σ-layer grid means that a grid layer covers a certain percentage of the water depth and with a Z-grid the layer thickness represents an absolute thickness (see Figure 2-4). At present it is not possible to perform non-hydrostatic simulations with Delft3D-FLOW when using a σ-layer grid. This means that vertical accelerations are not accounted for. When vertical accelerations become important it is possible to account for the vertical accelerations in Delft3D-FLOW but it is needed to change to a Z-grid in that case. The Delft3D-FLOW simulations in this research are performed all with a σ-grid which has as a consequence that all simulations are hydrostatic simulations.

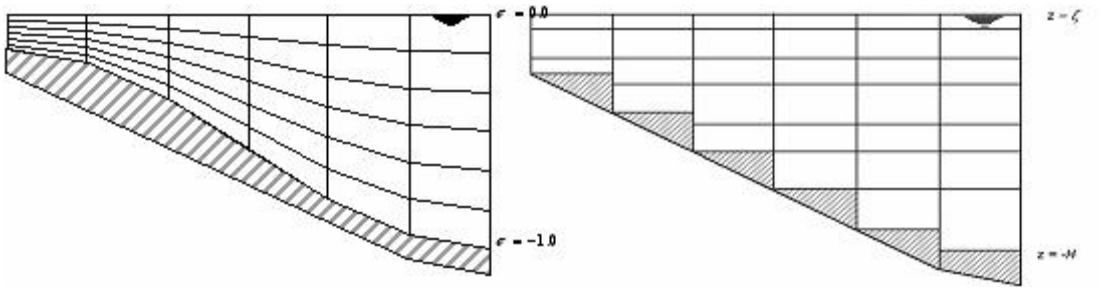

Figure 2-4 Example of σ-grid, left and Z-grid, right [source: DELFT3D-FLOW manual]

The following assumptions and approximations are made in Delft3D-FLOW:

For the spatial discretization of the horizontal advection terms, three options are available, *WAQUA*-, *Cyclic*- and the *Flooding*-scheme. The first and second option use higher-order dissipative approximations of the advection terms. The time integration is based on the Alternating Direction Implicit (ADI) method. The ADI-method splits one time step into two stages. Each stage consists of half a time step. In both stages, all the terms of the model equations are solved in a consistent way with at least second order accuracy in space. Because of that, the *WAQUA* and *Cyclic* method does not impose a time step restriction for the horizontal advection. For the *Flooding* scheme, the integration of the advection term is explicit and the time step is restricted by the Courant number for advection (Delft3D-manual, 2008, p.293). For staircase shaped boundaries, the ADI method (used in the *Cyclic*- and *WAQUA*-schemes) is inaccurate for Courant numbers larger than $4\sqrt{2}$ (Delft3D-manual, 2008, p.295). This is irrelevant during this research because all boundaries are smooth. The *Flooding*-scheme can be applied for problems that include rapidly varying flows, which is probably the case at the point bar of the equilibrium bottom.

To solve the (simplified) Navier-Stokes equations, a closure model for the turbulent stresses is needed. The reason for this is that the turbulent stresses are represented as time and space averaged quantities in the (simplified) Navier-Stokes equations. They are generated in sub-

grid scale processes and therefore they are not taken into account in the advection equations. In Delft3D-FLOW there are four different closure models for the turbulent stresses:

- Constant coefficient
- Algebraic Eddy viscosity closure Model (AEM)
- k-L turbulence closure model
- k-ε turbulence closure model

The closure models determine the vertical eddy viscosity. The horizontal eddy viscosity coefficients are normally much larger than the vertical ones because the horizontal length scales of the flow are larger than the depth. In Delft3D-FLOW are the horizontal eddy viscosity coefficients assumed to be a superposition of a 2D-turbulence part, a 3D-turbulence part (determined by the closure model) and the molecular viscosity. According to the manual the 2D-turbulent part of the horizontal coefficient is approximately an order of magnitude larger than the vertical coefficients determined by the turbulence closure model. The 2D-turbulent part of the horizontal coefficient is not directly calculated by Delft3D-FLOW when using one of the closure models mentioned above and therefore it must be included in the horizontal background viscosity.

Delft3D-Flow has additionally a sub-grid scale model to determine the horizontal eddy viscosity, HLES called. This Horizontal Large Eddy Simulation is a formulation of the horizontal component of the sub-grid eddy viscosity making use of a high-pass filter. It is possible to choose the relaxation time in such a way (less than zero) that the high-pass filter is cancelled which reduces the computational time but it still gives an estimation of the horizontal eddy viscosity.

Something has to be said about the roughness. The input of the roughness can be done in different parameters, depending on the model you choose. For 3D calculations the following models are available:

- Manning (n in $s/m^{1/3}$)
- Chezy (C in $m^{1/2}/s$)
- White-Colebrook (k_s in m)
- Z0 (z_0 in m)

All these parameters are converted to the Chezy coefficient which is used in the bed boundary condition to calculate the bed shear stress τ_b (Delft3D-manual, 2008)

2.3.2 Delft3D-FLOW set up Q89 simulation

To simulate the Q89 experiment, several simulations were done to calibrate the model. The settings of these simulations can be found in Appendix B. The final settings of the simulation that is used to compare with the measurements and the LES data are described in this section. This simulation is referred to as '*simulation Q89_1_D3D*'. A second simulation of Delft3D-FLOW is to see what the effect of the viscosity is on the flow. This simulation is referred to as '*simulation Q89_2_D3D*'.

For simulation Q89_1_D3D a grid is used of 0.05 m by 0.05 m. The complete flume is modelled. The vertical water column is divided in 20 layers with an equidistant distribution. The σ-grid is used. The complete flume is simulated to be sure that possible disturbances from the upper boundary do not influence the flow results in the bend.

For the simulations two boundary conditions are needed. The first boundary is at the upstream end of the flow and represents the inflow. The discharge at the inflow is set at 0.089 m^3/s and is distributed over the width according to the following relation:

$$q_i = \frac{B_i h_i^{1.5} C_i}{\sum_{j=1}^{N} B_j h_j^{1.5} C_j} Q \qquad (2.15)$$

where B_i, h_i and C_i are the width, water depth and Chezy roughness of grid cell *i* respectively, N is the number of boundary points and Q is the total discharge imposed (Delft3D-manual, 2008).

The second boundary is at the downstream end of the grid and represents the water level. This water level is linearly extrapolated from the measured water levels at the centre line. The downstream boundary is set at a water depth of 0.149 m above reference level.

The initial water level is set at 0.15 m above reference level.

The roughness of the bottom is determined during the calibration of the model. It seemed that the resistance was to high when taking into account the sand grain size that was used (d_{50} of about 2 mm, according to van Rijn (1984) this results in a k_s of 6 mm). For the Q89 experiment, the roughness is set at k_s = 3 mm. A possible explanation for the reduction of the roughness can be found in the way the sand was fixed. This was done by spraying paint on the sand which possibly reduces the roughness. For the wall roughness, the option '*Partial Slip*' is chosen to bring into account some effects of the walls. The roughness length is set at $5*10^{-6}$ m. This is quite small because the walls are made of Plexiglas.

As turbulence model is the k-ε model used which is the most advanced model available in Delft3D-FLOW at the moment. The background viscosity is varied. In simulation Q89_1_D3D a background viscosity of $\nu_{hor;back} = 1*10^{-6}$ m^2/s is chosen, which is equal to the molecular viscosity. In simulation Q89_2_D3D the horizontal background viscosity is set at $\nu_{hor;back} = 1*10^{-2}$ m^2/s, which is an order of magnitude larger than the vertical viscosity calculated by the k-ε model. The horizontal background viscosity is given this value because of strong fluctuations that aroused in the simulation of the M89-experiment at the inflow boundary. To smooth these fluctuations out, the viscosity was increased in the simulation of the M89-experiment. To see what the effect is of the increased viscosity on the flow, the Q89_1_D3D and Q89_2_D3D simulations are compared.

Most of these settings are obtained from the measurements performed by Blanckaert (2002 and 2009) and by means of several parameter variations (see Appendix B).

2.3.3 Delft3D-FLOW set up M89 simulation

To simulate the M89 experiment with the fixed equilibrium bottom, the same grid is used as for the simulation of the Q89 experiment. The flat-bed is replaced by the equilibrium-bed topography. The bottom topography is only measured from 3.5 m upstream the bend entrance to 3.2 m downstream the bend exit. Therefore the simulated area is reduced to a part of the flume, starting 6.5 m upstream of the bend entrance and ending 3.5 m downstream the bend exit. The bottom topography is extrapolated in the regions where no measurements were available.

At the upstream boundary the discharge is set at a constant value of 89 l/s. The downstream boundary condition is a water level and is taken from the measurements. In the inner bend the water level is set at 0.1198 m above reference and the outer bend is set at 0.1192 m above reference level.

The initial water level is set at 0.15 m above reference level.

The roughness of the bottom is determined from the results of the measurements (Blanckaert, 2009). The k_s is 6.4 $*10^{-3}$ m and z_0 is about 0.002 m (see Appendix B.5). For the wall roughness, the option '*Partial Slip*' is chosen to bring into account some effect of the walls. The roughness length for the walls is set at $5*10^{-6}$ m.

The turbulence model that is used, is the k-epsilon model. The horizontal background eddy viscosity is set at $1*10^{-2}$ m^2/s and the vertical background eddy viscosity is set at 10^{-6} m^2/s. The horizontal background viscosity is given this relatively high value to damp some large fluctuations that aroused at the inflow boundary. The simulation, used for the analysis of Delft3D-FLOW, is referred to as '*simulation M89_1_D3D*'.

Label	**Case**	**Grid size [m*m]**	**Nr of vertical layers**	**Downstream boundary [m] above reference**	**ν_{hor} [m^2/s]**
Q89_1_D3D	Q89	0.05*0.05	20 (equidistant)	0.149	10^{-6}
Q89_2_D3D	Q89	0.05*0.05	20 (equidistant)	0.149	10^{-2}
M89_1_D3D	M89	0.05*0.05	20 (equidistant)	≈0.119	10^{-2}

Table 2-2 Delft3D-FLOW simulations performed

2.3.4 Large Eddy Simulation and RANS simulation

At the TU Delft several simulations of the flume described in section 2.2 were performed by van Balen (2010). Van Balen performed a Reynolds averaged Navier-Stokes (RANS) simulation as well as a Large Eddy Simulation (LES) of the experiments in the flume that was used by Blanckaert. The focus of his study was on the mechanisms of the secondary flow. He investigated the turbulence and the influence of the depth on the secondary flow. Besides that he made a comparison of the RANS simulation and the LES. Three LES's were performed with different depths and a flat-bed; a shallow, a medium and a deep one (see Table 2-3). The medium simulation was set up to simulate the Q89 experiment conducted at EPFL. The results of this simulation will be compared with the results of a Delft3D-FLOW simulation. Some results of the RANS simulation will be used to compare to what extent the Delft3D-FLOW simulation deviates from a non-hydrostatic RANS simulation. The equilibrium-bed experiment was also simulated with the LES by van Balen. The results of this simulation will be used to compare with the results of the belonging

Label	**Case**	**Description**
Q56_LES	Q56	LES, flat-bed case, rigid lid, H = 0.108 m, Q = 60 ls^{-1}
Q89_LES	Q89	LES, flat-bed case, rigid lid, H = 0.159 m, Q = 89 ls^{-1}
Q104_LES	Q104	LES, flat-bed case, rigid lid, H = 0.206 m, Q = 115 ls^{-1}
M89_LES	M89	LES, equilibrium-bed case, rigid lid, H = 0.141 m, Q = 89 ls^{-1}
Q89_RANS	Q89	RANS, flat-bed case, rigid lid, H = 0.159 m

Table 2-3 Some of the simulations performed by van Balen (van Balen, 2010)

For the LES's, the full three dimensional Navier-Stokes equations are solved to model the flow. The equations are solved on a staggered grid. The grid size in the Q89_LES is 0.68 cm * 0.68 cm * 0.68 cm. For the spatial discretization, the midpoint rule is used and for the time integration the explicit, second order Adams-Bashford scheme is used. To model the sub grid-

scale stresses, the standard Smagorinsky model is used with a model constant of 0.1, reduced near solid walls with a standard Van Driest damping function (van Balen *et al*., 2009b).

The free surface is treated as a horizontal rigid lid with free-slip condition which is set at 0.159 m above the bottom in the case of the simulation of the Q89 experiment. The walls are modelled with the help of the standard law-of-the-wall (van Balen *et al*., 2008).

The LES set up for the simulation of the M89 experiment is nearly the same as for the Q89 simulation. There are two major differences. The first is the bottom topography. The bottom topography is adapted for the equilibrium-bed. The other difference is the water depth. The water level is changed to 0.429 m above the lowest point of the bottom level. Due to this change, the grid in the vertical changes as well, now more cells are needed to cover the whole flume. The size of the grid cells change a little too. The grid size becomes about 0.68 cm * 0.107 cm * 0.6 cm. The bend is modelled from 3.8 m upstream of the bend to 3.8 m downstream the bend in both the Q89_LES and M89_LES cases.

The RANS model uses the Reynolds averaged Navier-Stokes equations, which means that we need a turbulence model to solve the equations. The simulation that provides the data that are used in this research uses the standard k-ε model. This model is unable to predict an anisotropic eddy viscosity (van Balen *et al*., 2008, Demuren and Rodi, 1984).

The free surface and the walls are modelled in the same way as was done for the LES. The free surface is modelled as a rigid lid with free-slip condition and the walls are modelled as smooth walls with the help of a two-layer model (van Balen *et al*., 2008).

2.4 Methodology

The capability of Delft3D-FLOW to simulate the flow through sharp bends is analyzed by comparing the results of the Q89 and M89 experiments with the results of the Delft3D-FLOW simulations Q89_1_D3D and M89_1_D3D.

To find an answer to the question about the differences between LES and Delft3D-FLOW simulations and how these differences can be explained (the second objective, see section 1.2), use is made of the results of the LES conducted at TUDelft by van Balen (van Balen, 2010). He simulated the experiments described in section 2.2 with a LES. The flat-bed cases were also simulated by Van Balen with a RANS simulation. The LESs will be compared with the results of the Delft3D-FLOW simulations for both the flat-bed and equilibrium-bed case. The RANS simulation is only used in one specific case, namely to compare the transverse velocities in the flat-bed case. This is to check how the assumptions made in Delft3D-FLOW will result in differences in the flow.

With the Q89 results of the measurements, the Delft3D-FLOW model is calibrated as well as possible. The results of the calibrated model are compared with the results of the Q89 experiment and the Q89_LES. Simulation Q89_2_D3D is done to see the effect of a change in the viscosity. For that case, the same settings are used as in the Q89_1_D3D simulation but now the viscosity is increased. Simulation M89_1_D3D is done to simulate the M89 experiment. The results of this simulation are also compared with the results of the M89 experiment and the LES M89. In Table 2-4 the simulations are shown which are used in the comparison.

Label	Case	Type of simulation	Bed	Surface	Eddy viscosity
Q89_LES	Q89	LES	Flat-bed	Rigid lid, 0.159 m above reference level	-
M89_LES	M89	LES	Equilibrium-bed	Rigid lid, 0.141 m above reference level	-
Q89_RANS	Q89	RANS	Flat-bed	Rigid lid, 0.159 m above reference level	-
Q89_1_D3D	Q89	Delft3D-FLOW	Flat-bed	Free surface	$\nu_{hor} = 10^{-6}$ m^2/s
Q89_2_D3D	Q89	Delft3D-FLOW	Flat-bed	Free surface	$\nu_{hor} = 10^{-2}$ m^2/s
M89_1_D3D	M89	Delft3D-FLOW	Equilibrium-bed	Free surface	$\nu_{hor} = 10^{-2}$ m^2/s

Table 2-4 Overview simulations used during this research

The quantities and phenomena which are compared are:

- The water levels and water level gradients
- Downstream and transverse velocities
- The downstream vorticity (ω_s) and the downstream vorticity balance (only for the Q89 case)
- The turbulent stresses
- The turbulent kinetic energy (only for the Q89 case)

To find answers to the objectives, use is made of the comparisons as described above.

3 Results of the flat-bed case

In this chapter the results of the experiment and simulations of the Q89 case are shown and compared. The set up that is used for the Delft3D-FLOW simulation is described in section 2.3.2. The sections gives the comparison of simulation Q89_1_D3D with the results of the LES and the M89 experiment. Section 3.1 contains the comparison of the water level, in section 3.2 is the downstream velocity compared, in section 3.3 the transverse velocity. Section 3.4 contains the comparison of the most important terms of the downstream vorticity balance. Section 3.5 contains the comparison of the turbulent velocities. In section 3.6 the turbulent kinetic energy is analyzed. In section 3.7 simulation Q89_2_D3D is compared with simulation Q89_1_D3D to see what the effect is of an increase of the viscosity. The last section is a short summary of the conclusions.

3.1 Water level

In this section, the results of the Q89 simulation are compared with the results of the experiment. The water level will be described and the reason for possible differences will be investigated.

The flow through the flume is a gravity driven flow. Therefore firstly we will take a look at the water elevation and the water level gradient. The LES-simulation is done with a stress-free rigid lid to represent the free surface of the flow. The use of such a rigid lid is justified as long as the gradients of the water surface are small enough (van Balen *et al.*, 2009). The pressures calculated during the LES simulation are transformed to water levels according to the following relations (van Balen *et al.*, 2009b):

$$\frac{\partial h}{\partial r} = \frac{1}{\rho g}\left(\frac{\partial p}{\partial r}\right)_s \quad \text{and} \quad \frac{\partial h}{\partial r} = \frac{1}{\rho g}\left(\frac{\partial p}{\partial \theta}\right)_s \qquad (3.1)$$

With H = 0.159 m as averaged water level, this results in Figure 3-2.

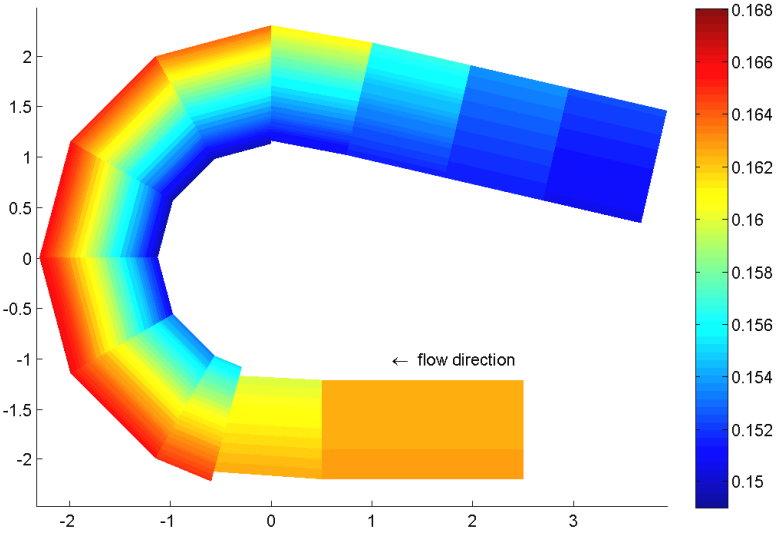

Figure 3-1 Water level according to measurements

Figure 3-1 gives the measured water level for the Q89 experiment. In the bend the transverse tilting of the water level is visible (see also Figure 3-6). This transverse water level gradient exists to counteract the centrifugal force due to the downstream velocity. These two forces show a local imbalance over the depth. Because of this imbalance a secondary circulation occurs in river bends.

When comparing Figure 3-2 with Figure 3-1, the LES gives somewhat (about 2 mm) higher values than the measurements, especially in the upstream straight reach and the outer part of the first half of the bend.

Figure 3-3 gives the water depth according to simulation Q89_1_D3D. Figure 3-4 gives the difference between the LES and simulation Q89_1_D3D. The maximum difference is 3.5 mm (LES gives higher values) which is about 2 % of the average water depth. Towards the exit of the flume, the water depth given by simulation Q89_1_D3D has lower values (about 2 mm). The reason for this can be a wrongly imposed downstream boundary. The boundary is derived from the measurements. Because the grid of simulation Q89_1_D3D extends beyond the measured grid, the downstream boundary is linearly extrapolated which could have introduced an error in the downstream boundary of simulation Q89_1_D3D and therefore also in the water level gradient. In a narrow strip along the inner bend (which becomes wider towards the exit of the bend) the difference between the LES and simulation Q89_1_D3D increases.

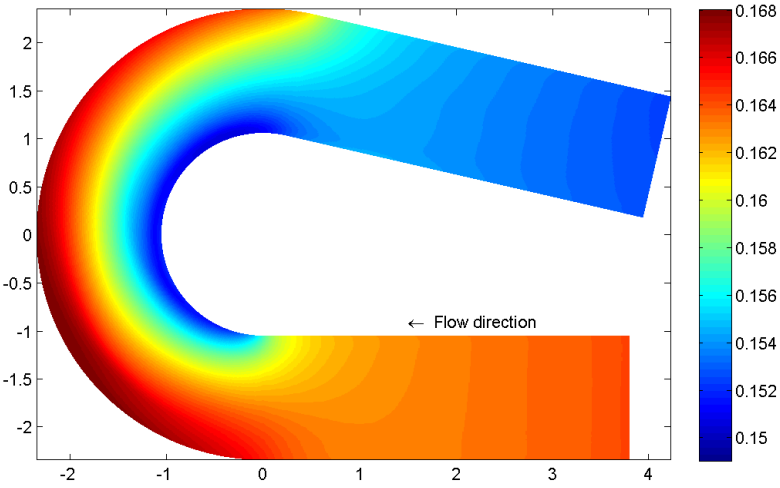

Figure 3-2 Water level according to LES-simulation

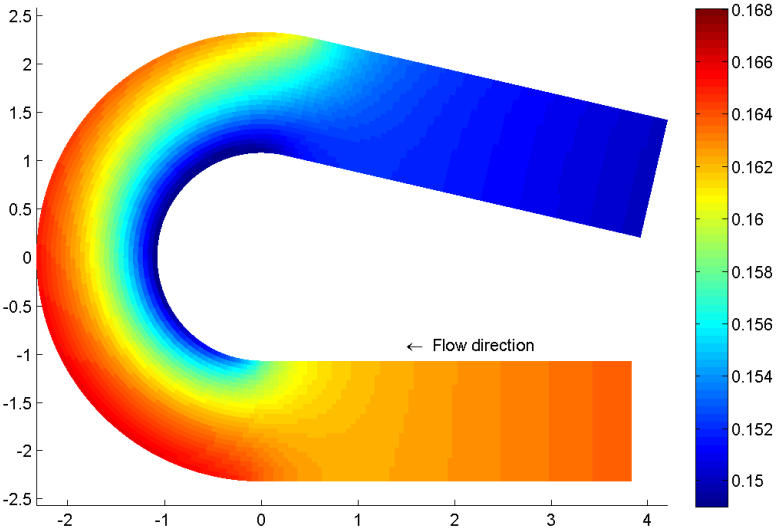

Figure 3-3 Water level according to Delft3D-FLOW simulation Q89_1_D3D

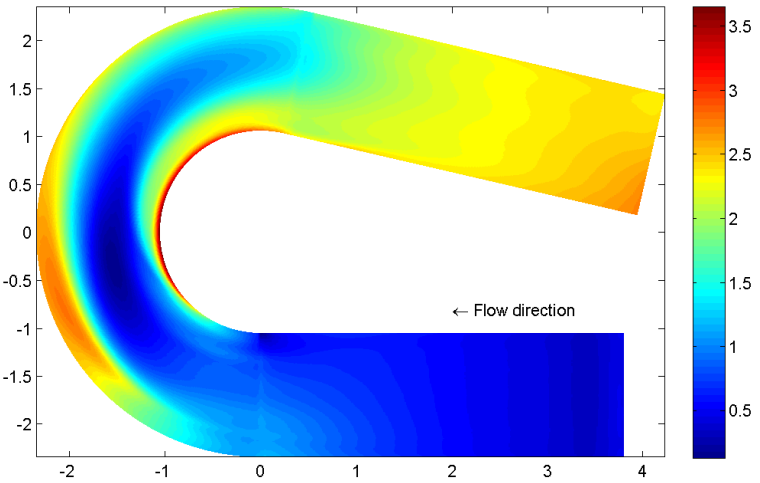

Figure 3-4 Difference in water level between LES and DELFT3D simulation Q89_1_D3D (in mm)

Figure 3-5 shows the water level along the *centre* line for simulation Q89_1_D3D, the LES and the measurements. When comparing these results it can be concluded that the downstream gradient of the water level along the bend is better predicted by the LES data than by simulation Q89_1_D3D. Simulation Q89_1_D3D predicts a to steep gradient over the entire bend. At the start of the bend the gradient decreases strongly, which is also visible from the LES (it is also visible in the measurements but there it is less clear).

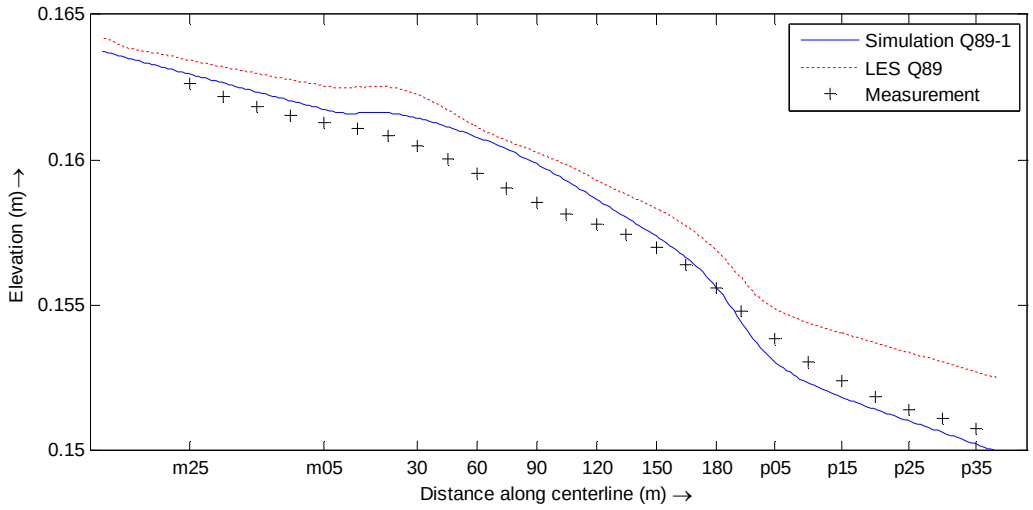

Figure 3-5 Water level along centreline of the flume

Where the LES data shows an increase of the gradient to a constant value around 15° in the bend, the water level gradient predicted by simulation Q89_1_D3D reaches a constant value around the 120 cross-section. In the upstream straight reach, both the LES and simulation Q89_1_D3D predict a too gentle water level gradient according to the measurements. In the downstream straight reach, the gradients of the LES and simulation Q89_1_D3D nearly equal the measured water level gradient.

The increase of the water level gradient throughout the bend is caused by the extra resistance in the bend. Several processes contribute to the extra resistance in the bend. Firstly, there is an additional transversal bottom shear stress component (τ_n) due to the secondary circulation. Secondly, due to the advective momentum transport by the secondary circulation, the downstream velocity profile is flatter with respect to the velocity profile in the straight uniform flow. Because the shear stress is determined by the near-bed velocity gradients, this

will cause an increase of the bottom shear stress (τ_b) for the same depth averaged velocity (Blanckaert, 2002 pag. IV.6).

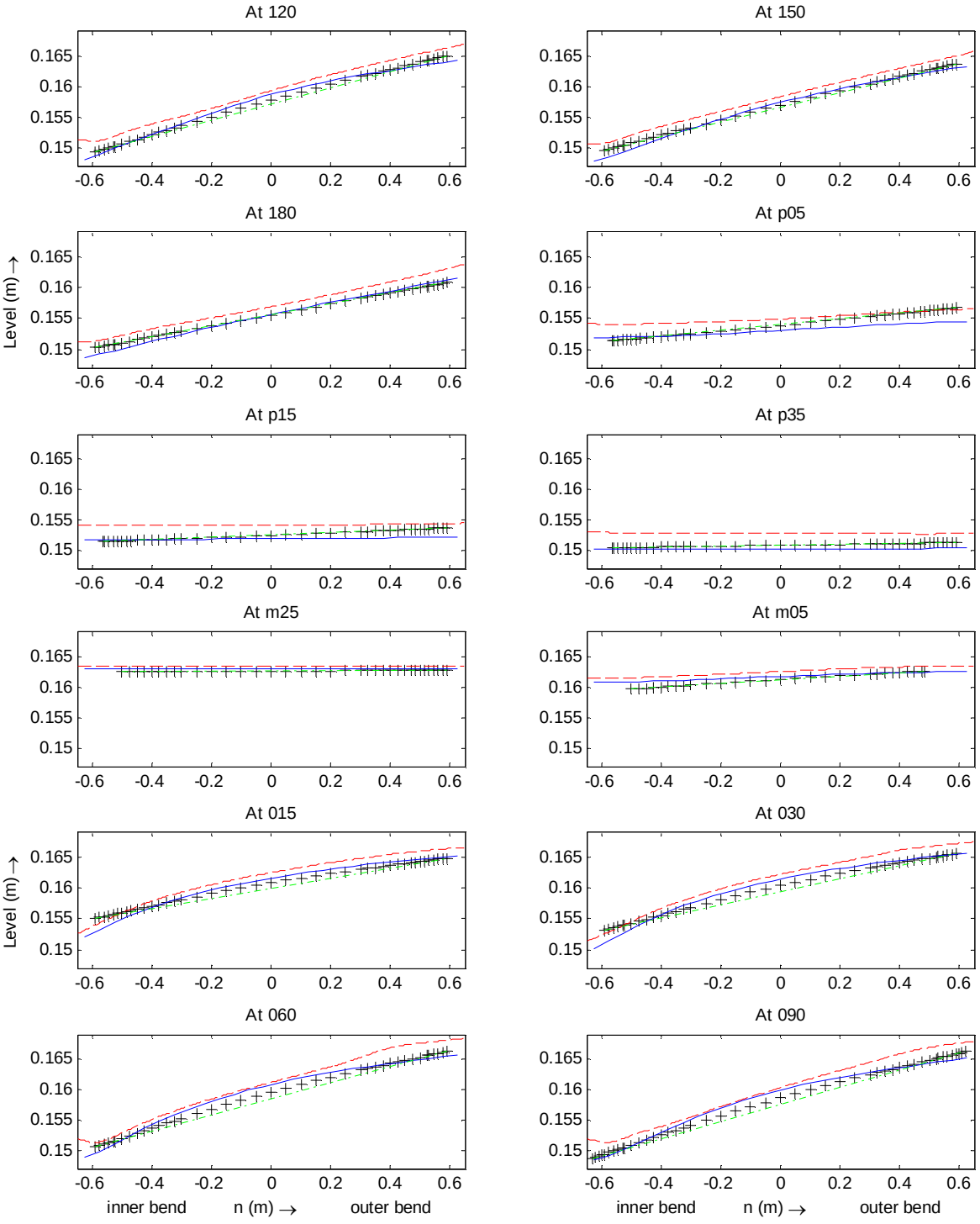

Figure 3-6 Transverse water levels at different cross-sections [legend same as in Figure 3-5: red -- = LES; black + = measurement; blue-=DELFT3D-FLOW simulation; green-. = straight line]

Figure 3-6 shows the transverse water levels at several cross-sections. These are consistent with each other besides some small differences. From Figure 3-6 it is also visible that the LES gives a somewhat higher water level than was measured which already was concluded in the first part of this section.

In the inner bend from the 060 to 150 cross-sections, a rise of the water level is visible for the LES results. This rise of the water level is absent for the simulation Q89_1_D3D and the measurements. The reason for this water level rise is unclear.

An other remarkable phenomena is that all data show a kind of hump in the centre of the flow during the bend (compare the green -.line, which is a straight line between the first and last measured water level point, with the other data lines). This hump is best visible for the 060 to 120 cross-sections. The hump is about twice as big for the simulations (LES and simulation Q89_1_D3D) than for the measured data. This hump causes a decrease of the transverse water level gradient along the outer bend of the flume and an increase along the inner bend of the flume. Especially for simulation Q89_1_D3D. This can (partly) be a reason for the under prediction of the transverse velocity.

3.2 Downstream velocity

In this section the downstream velocities of the different data sets will be compared with each other.

First we will take a look at the depth averaged downstream velocities. Figure 3-7 shows the measured depth averaged velocity U and Figure 3-8 shows the depth averaged velocity U predicted by the LES. Because the LES is computed with a rigid lid, which means that the calculations were done with an equal grid height, the height of the grid cells is scaled with H/h_{LES} to give the velocities of the LES a more equal weight compared to the measurements. With H the flow depth of the LES (0.159 m) and h_{LES} the local water depth according to the pressures at the surface of the flow, predicted by the LES.

In both figures are visible:

a.) Fluctuations of the velocity over the width in the upstream straight reach (four peaks are visible). These fluctuations are caused by secondary cells. The secondary cells have a width of approximately the water depth. They grow there because of anisotropic turbulence near the walls of the flume (c.f. Nezu and Nakagawa, 1993 and Blanckaert, 2002, part II, pp. 32). The downstream velocity peaks exist at the points where the secondary cells bring water with high downstream momentum down to the bottom and increase the downstream velocity at the bottom which results finally in an increase of the depth averaged downstream velocity of the water column at that point.

b.) The second remarkable thing is the outward shift of the core of the downstream velocity in the bend. Besides that, the maximum of the downstream velocity in the core decreases and the width of the core increases towards the end of the bend. This shift and widening of the core of the downstream velocity are caused by the exchange of momentum due to the secondary flow (see also: Blanckaert, 2002, part II, pp. 30). Several other phenomena arise along the inner bend of the flume which has to do with this outward shift of the core. A sharp edge is visible between water with a high depth averaged downstream velocity and water with a lower depth averaged downstream velocity. This boundary indicates the place where an internal shear layer exists (van Balen, 2010) due to the outward transport of momentum. More towards the inner wall a narrow strip with a high value of depth averaged downstream velocities is visible. This strip is not clearly visible in the measured data, there are only some very small fluctuations.

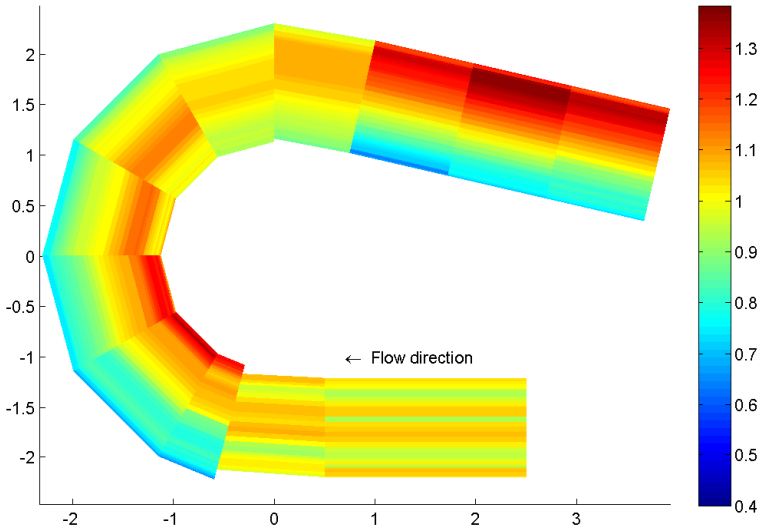

Figure 3-7 Depth averaged downstream velocity according to measurements, normalized by U_{bulk} = 0.43 m/s

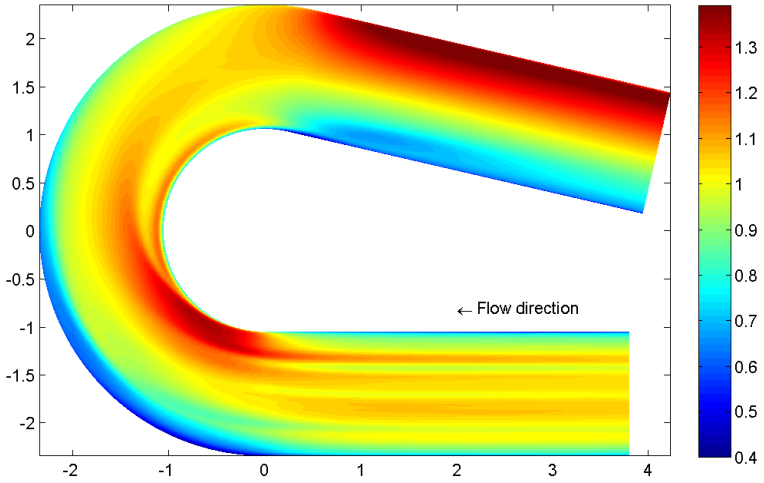

Figure 3-8 Depth averaged downstream velocity according to LES, normalized by U_{bulk} = 0.43 m/s and scaled by H/h_{LES}

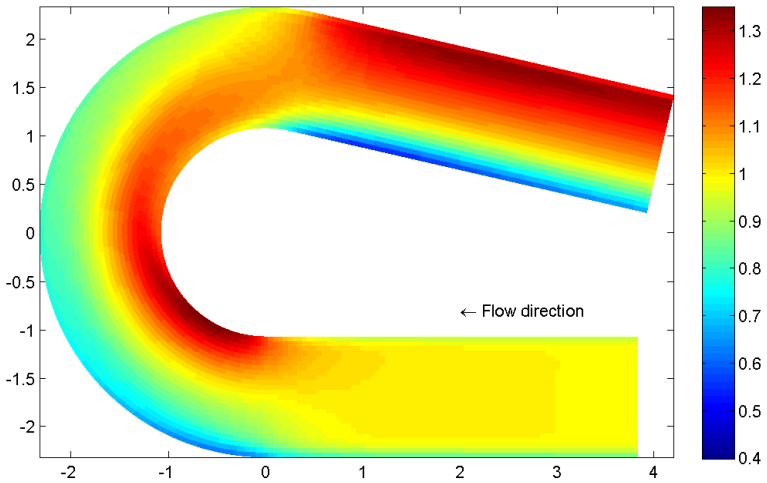

Figure 3-9 Depth averaged downstream velocity according to simulation Q89_1_D3D, normalized by U_{bulk} = 0.43 m/s

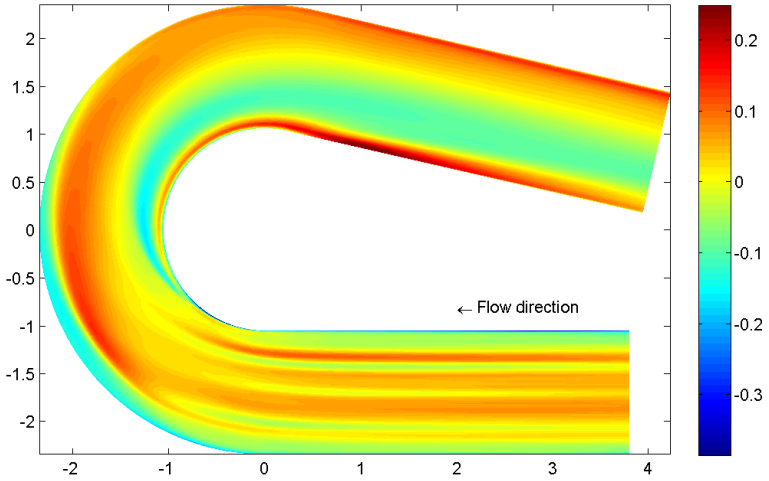

Figure 3-10 Difference in depth averaged downstream velocity between LES (scaled by H/h_{LES}) and simulation Q89_1_D3D, normalized by U_{bulk}

c.) Another thing that can be mentioned is the clear separation of downstream velocities with a large and with a low magnitude in the straight outflow. Along the outer wall the depth averaged downstream velocity has higher values than along the inner wall. This distribution extends along the whole straight outflow. A reason why the distribution of the depth averaged downstream velocity does not really change along the straight outflow, is the decrease of the secondary flow that caused the mixing of momentum in the bend.

d.) A layer with low downstream momentum along the outer bend of the flume which disappears towards the end of the bend. This strip is strongly related to the existence of the outer-bank cell. A clear relation is not yet known but it can be imagined that the water in the outer-bank cell is strongly affected by the presence of the wall and the downstream momentum exchange with the core of the flow is poor.

It can be said that the LES gives a good prediction of the depth averaged downstream velocity. This result is used to compare with the results of simulation Q89_1_D3D.

Figure 3-9 shows the depth averaged downstream velocity, predicted by simulation Q89_1_D3D. Figure 3-10 shows the difference between the LES and simulation Q89_1_D3D. From these two figures some important differences are made clear.

a.) The secondary cells in the straight inflow are not modelled by simulation Q89_1_D3D. This is because of the shortcomings of the k-ε model and presumably the course grid (0.05 cm width, the secondary cells have a width of about 0.10 cm). The linear k-ε model is unable to predict anisotropic turbulence which is the cause of the secondary cells in the straight inflow (Zeng *et al.*, 2008 and Demuren and Rodi, 1984).

b.) The core of the flow with the highest depth averaged downstream velocity, does not shift to the outer bend during the flow through the bend. It stays at the inner bend until the end of the bend where it shifts over a short distance towards the outer bank. All phenomena causing and caused by the shift of this core (such as the existence of the internal shear layer) are absent along the inner bend.

c.) The poor mixing in the straight outflow is also visible in the results of simulation Q89_1_D3D. However, the LES gives higher respectively lower values at the outer respectively inner bank while simulation Q89_1_D3D gives a wider distribution of the core of depth averaged downstream velocity.

d.) Simulation Q89_1_D3D gives in the outer bend a wider strip of low valued depth averaged downstream velocities compared to the LES but the magnitude of the velocities in this low valued strip are somewhat higher than was predicted by the LES. A reason for the wider strip can be the absence of the shift for simulation Q89_1_D3D. A reason for the high values can be sought in both the absence of the shift of the core and the outer-bank cell.

When comparing the values of the depth averaged downstream velocity (see also Figure 3-10) it can be seen that in the outer part of the core of the flow the LES gives about 10% higher values than simulation Q89_1_D3D. In the inner bend and the inner wall around the outflow, simulation Q89_1_D3D gives 10% higher values. This has all to do with the shift of the core which is absent in simulation Q89_1_D3D. The difference between LES and simulation Q89_1_D3D along the outer bend of the flume can be caused by the outer-bank cell.

Now taking a look at the downstream velocity profiles over the depth, some remarks can be made. The profiles for all measured cross-sections can be found in Appendix C.1. Generally spoken, the profiles of the LES fit somewhat better than the ones of simulation Q89_1_D3D, especially in the second half of the bend. In the second half of the bend, the upper part of the inner bend shows a clear reduction of the downstream velocity (see Figure 3-11). This reduction shifts towards the centre when the flow moves on through the bend. This reduction can be associated with the flow separation at the inner bend and the corresponding outward shift of the core of the downstream flow. In the centre region after the bend, in the straight outflow, there is still some reduction visible in the LES data while this reduction is nearly absent in simulation Q89_1_D3D and the measurements (see Figure 3-12). In the first part of the outer bend, both the LES and the measurements show a reduction of the downstream velocity in the upper part of the flow. This reduction of the downstream velocity initiates the outer-bank cell (van Balen *et al.*, 2008). Simulation Q89_1_D3D does not show this reduction of the downstream velocity nor the outer-bank cell.

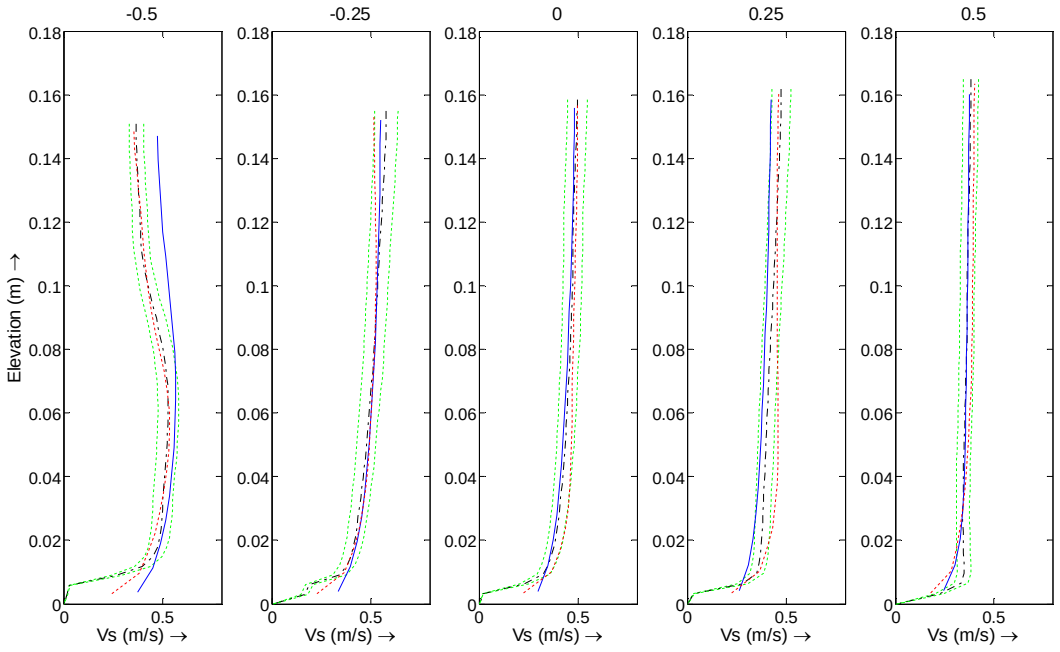

Figure 3-11 Downstream velocity profiles over the depth at 90 [black -. = measurement; red := LES; blue -- = simulation Q89_1_D3D; green := 10% margin of measurements]

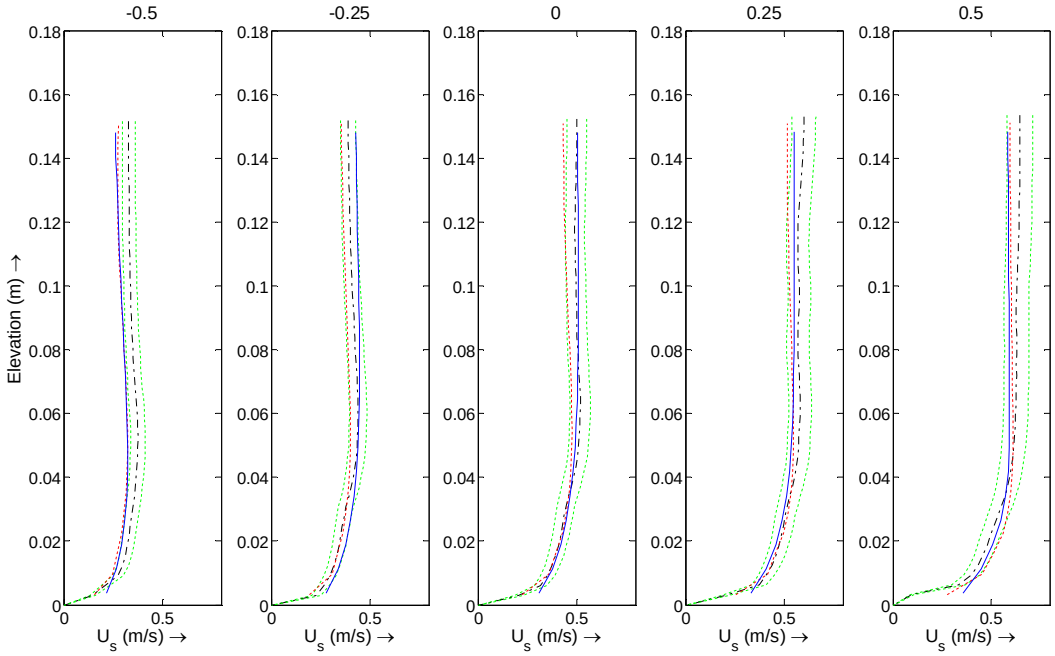

Figure 3-12 Downstream velocity profiles over the depth at p15 [black -. = measurement; red := LES; blue -= simulation Q89_1_D3D; green := 10% margin of measurements]

3.3 Transverse velocity

In this section the transverse velocities of the different data sets will be compared.

The depth averaged transverse velocities are presented with the help of a pseudo-stream function ψ which is a measure for the strength of the secondary circulation. ψ is based on continuity in a cross-section and defined as (van Balen *et al.*, 2009b):

$$\psi = \frac{1}{2}(\psi_r + \psi_z) \qquad (3.2)$$

$$\psi_r = -\int_{z_b}^{z} v^* r dz \qquad (3.3)$$

$$\psi_z = \int_{-B/2}^{r} w dr + A \qquad (3.4)$$

Whereas v^* represents the circulatory part of the transverse velocity obtained by subtracting the depth-averaged part V from the total transverse velocity v. w is the vertical velocity component, and R is radius of curvature of the bend, n is the coordinate of the associated velocity in the transverse direction with respect to the centre line. A is an integration constant, it is chosen such that the cross-sectional-averaged values of ψ_r and ψ_z are equal. For the LES the water depth is taken equal to the overall mean flow depth because of the rigid lid approximation and dz is calculated by dividing this depth by the number of grid points in the vertical. The pseudo-stream function is normalized by multiplying ψ by 100/(UH).

Looking at Figure 3-13, the pseudo stream function ψ for the experiment is shown. In the inflow there is some circulation caused by the secondary cells. While entering the bend, the secondary flow increases strongly and reaches a maximum around the 090 cross-section.

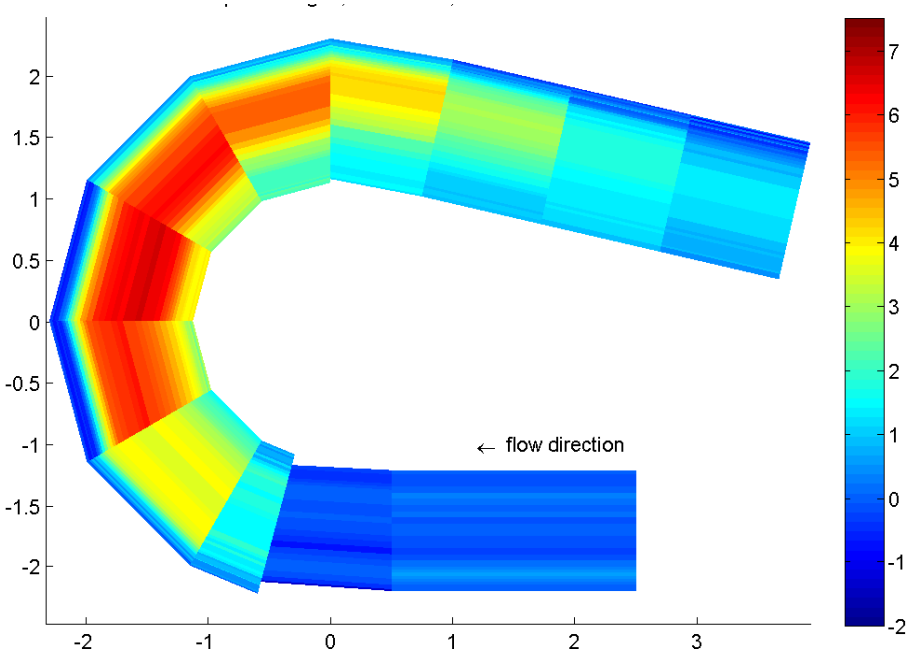

Figure 3-13 Distribution of the depth averaged cross-stream circulation strength, according to the measurements, ψ is normalized by: 100/(U_{bulk}*H)

Around the exit of the bend, the secondary flow decreases. In the outer bend a narrow strip with negative values for ψ is visible. This shows the existence of the outer-bank cell. In the upper half at the outer bank of the bend, often a so called 'outer-bank cell' exists. This cell rotates in the direction opposite to the secondary flow. The outer-bank cell is caused by turbulence anisotropy (van Balen, 2010). The outer-bank cell rotates in the opposite direction as the centre region cell does, which is also visible in the opposite sign of ψ in Figure 3-13. The outer-bank cell is also well visible in Figure 3-14, where ψ * 100 / (HU) is plotted for the 060 cross-section.

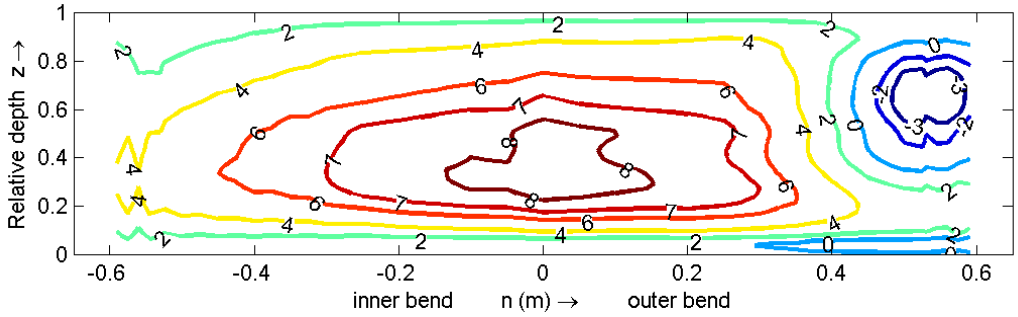

Figure 3-14 Normalized (by 100/(U_{bulk}*H)) pseudo stream function ψ, according to measurement, cross-section 060

Figure 3-15 to Figure 3-17 give insight in the distributions of the depth averaged cross-stream circulation strength and the differences in this quantity between the LES and simulation Q89_1_D3D. Starting with the results of the LES (see Figure 3-15) most phenomena observed in the results of the measurements can be recognized here as well. Four phenomena can be observed whereas two of them show a strong similarity with phenomena observed in the downstream velocity (see section 3.2).

a.) Firstly, the effects of the secondary cells at the straight inflow are visible as small fluctuations over the width of the depth averaged cross-stream function. Here also four little peaks are visible.

b.) Secondly there is the outward shift of the core of cross-stream circulation. Here the core is wider. A narrow strip in the inner bend shows here also high values. This strip is not visible in the measured data, presumably because of lack of data in the inner bend.

c.) In the straight outflow, the core is not attached to the outer wall but stays approximately in the centre region and disappears faster than the core of the downstream velocity does.

d.) At the start of the outer bend, a strip with a low cross-stream velocity is visible. The strip disappears towards the end of the bend. This strip looks alike the strip which was visible in the outer bank in Figure 3-8 and can be related to the outer-bank cell too.

For the cross-stream circulation the same holds as what was said about the depth averaged downstream velocity. The LES gives a good prediction of the depth averaged cross-stream circulation. Therefore the results of the LES will be used to compare with the results of simulation Q89_1_D3D.

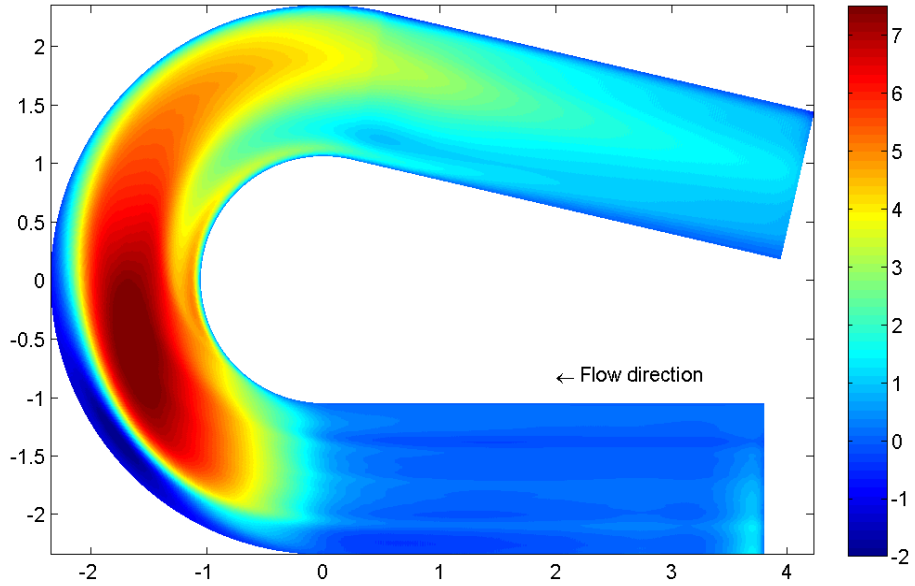

Figure 3-15 Distribution of the depth averaged cross-stream circulation strength ψ, according to LES, normalized by: 100/(U_{bulk}*H)

Comparing Figure 3-15 with the results of simulation Q89_1_D3D simulation (Figure 3-16) we see that:

a.) The same holds here as for the downstream velocity. There are no secondary cells visible in the straight inflow part of the flume.

b.) In the first part of the bend, the core of the cross-stream circulation extends over the full width of the flume while for the LES, the outer bend shows negative values. In the second part, the width of the core decreases. The decrease is especially visible in the inner bend. At the end of the inner bend there is a narrow strip visible with a slightly increased cross-stream with respect to its immediate surroundings, which can be recognized as the same narrow strip which is visible in the LES results but with a lower strength.

c.) When looking at the straight outflow, the width of the core of the cross-stream circulation decreases further, in the same way as the LES does.

d.) For simulation Q89_1_D3D, there is a small strip of decreased cross-stream circulation along the outer bend, but this strip starts half in the bend and extends towards the end instead of starting at the entrance of the bend and disappearing around ninety degrees in the bend. There is no relation with an outer-bank cell as we will see later.

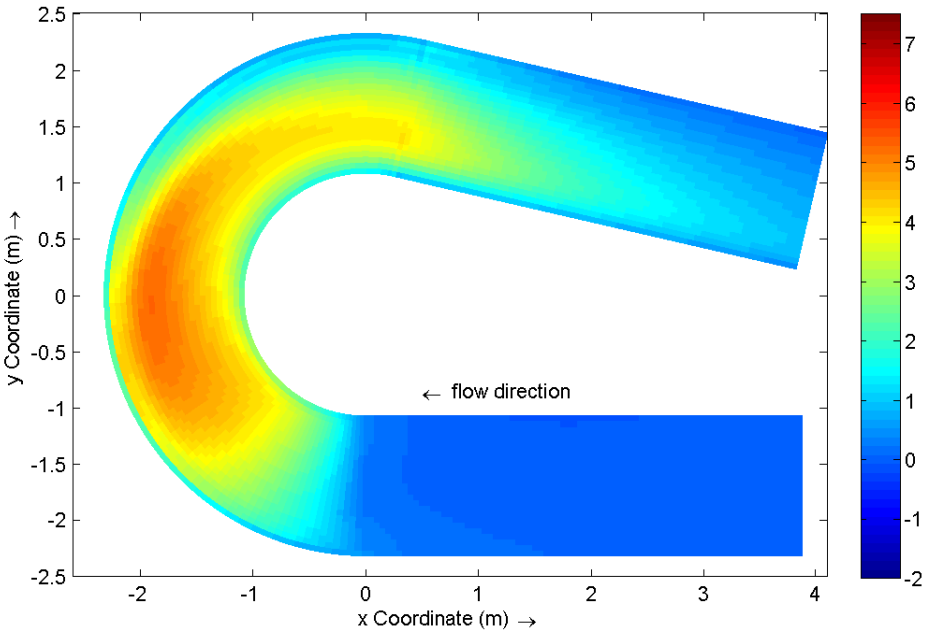

Figure 3-16 Distribution of the depth averaged cross-stream circulation strength ψ according to Delft3D-FLOW simulation Q89_1_D3D, normalized by 100/(U_{bulk} *H).

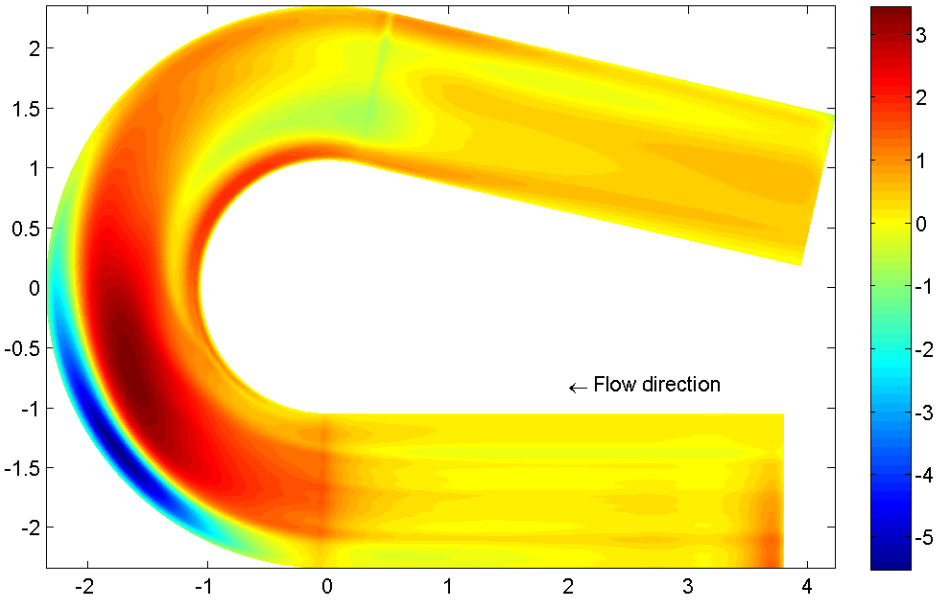

Figure 3-17 Distribution of (ψ_{Q89_LES} - $\psi_{Q89\_1\_D3D}$), normalized by 100/(U_{bulk} *H).

Besides that, the maximum of the depth averaged cross-stream circulation of the LES and simulation Q89_1_D3D are located at different locations. The maximum of the LES is located around the centre line, extended towards the outer bend, just before the ninety degree cross-section, while the maximum of simulation Q89_1_D3D is located from the centre line towards the inner bend around (before and after) the ninety degree cross-section.

Figure 3-17 shows the difference between the LES and simulation Q89_1_D3D. The maximum difference in the depth averaged cross-stream circulations is about 70% of the maximum value according to the LES. This maximum difference is an overestimation by simulation Q89_1_D3D. Remarkable is the fact that the maximum overestimation by

simulation Q89_1_D3D is close to the maximum underestimation. This has to do with the outer-bank cell (the narrow strip in the outer bend).

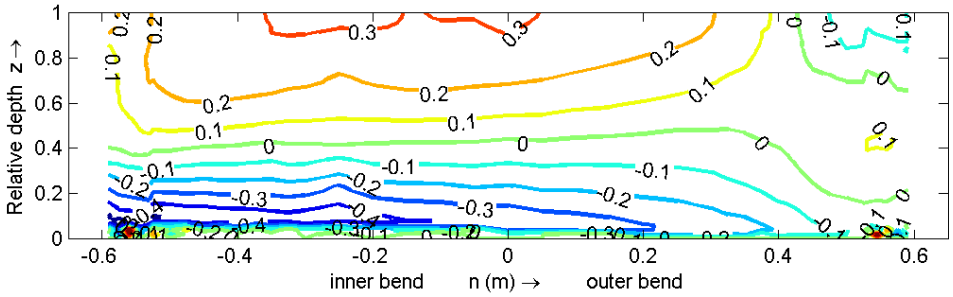

Figure 3-18 Normalized transverse velocity (v/U) according to the measurements, cross-section 060

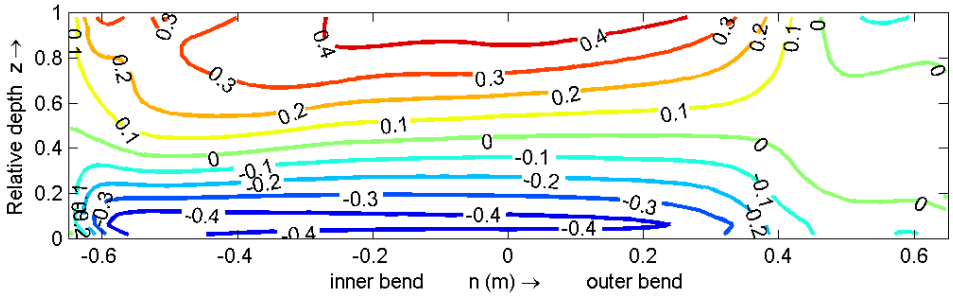

Figure 3-19 Normalized transverse velocity (v/U) according to the LES, cross-section 060

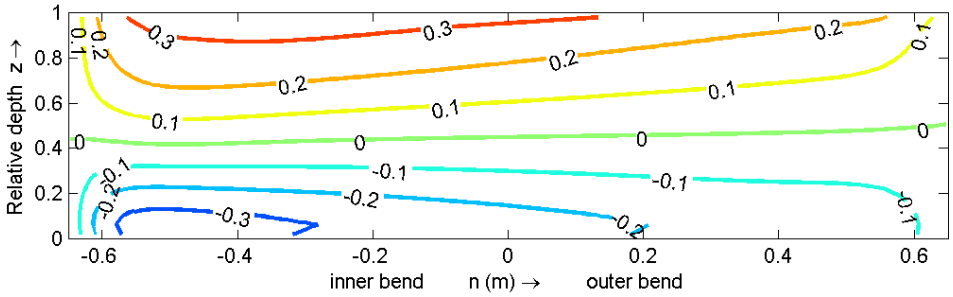

Figure 3-20 Normalized transverse velocity (v/U) according to RANS, cross-section 060

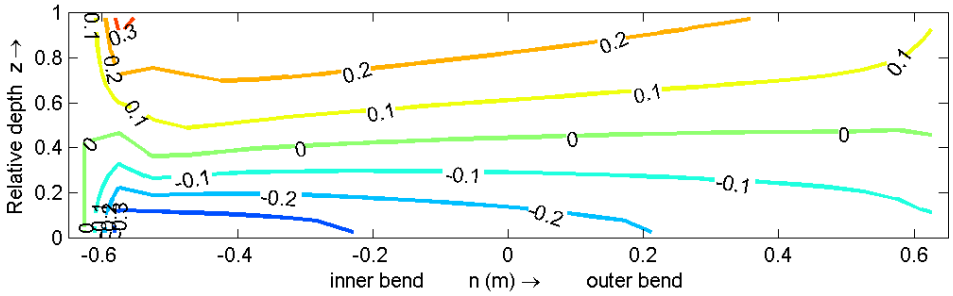

Figure 3-21 Normalized transverse velocity (v/U) according to simulation Q89_1_D3D, cross-section 060

Figure 3-18 to Figure 3-21 show contour plots of the transverse velocity for the measurements, the LES, the RANS simulation and simulation Q89_1_D3D for the 060 cross-section. The comparison with the RANS simulation is done to see to what extend the hydrostatic pressure assumption affects the transverse flow (see also section 2.3.4). Comparing the results for the RANS simulation with the results of simulation Q89_1_D3D we see no big difference. There is only a difference along the surface where simulation Q89_1_D3D shows lower velocities compared to the RANS simulation. This confirms the idea that the use of the hydrostatic pressure assumption in this case is applicable. Comparing the plots of simulation Q89_1_D3D with the plots of the LES and the measurements, the under prediction of the transverse

velocity by simulation Q89_1_D3D in the lower 30% of the flow becomes clear. This underestimation reaches a maximum of about 50% of the measured transverse velocity at the 060 cross-section. Also visible is the missing of the outer-bank cell in simulation Q89_1_D3D. The LES over predicts the transverse velocities at the water surface.

It can be said that the Delft3D-FLOW simulations are a good approximation for RANS simulations. The RANS simulation (and simulation Q89_1_D3D) under predict the transverse velocities and misses several phenomena (the flow separation and outer-bank cell). Van Balen *et al.* (2009b) and Blanckaert and de Vriend (2003) conclude that the choice of the turbulence model has a large effect on the transversal velocities. It is known that the outer-bank cell is caused by anisotropic turbulent stresses which can not be predicted by the standard k-ε model (van Balen *et al.* 2008). These conclusions can explain why the Delft3D-FLOW package is unable to reproduce the outer-bank cell but it remains unclear why it under predicts the transverse velocities in the lower part of the flume.

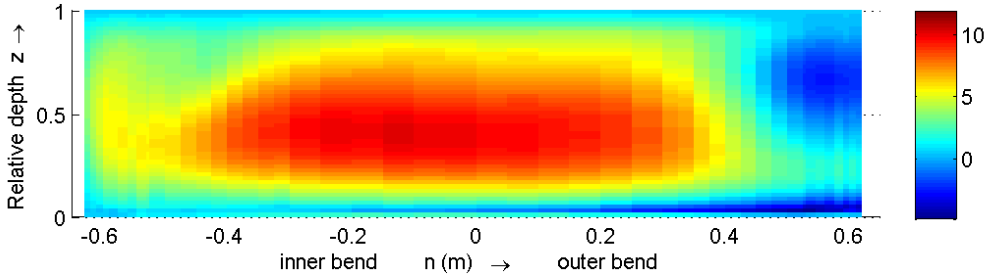

Figure 3-22 Normalized quantity ψ, in cross-section 090 according to the measurements, ψ is normalized by 100/(U_{bulk} *H)

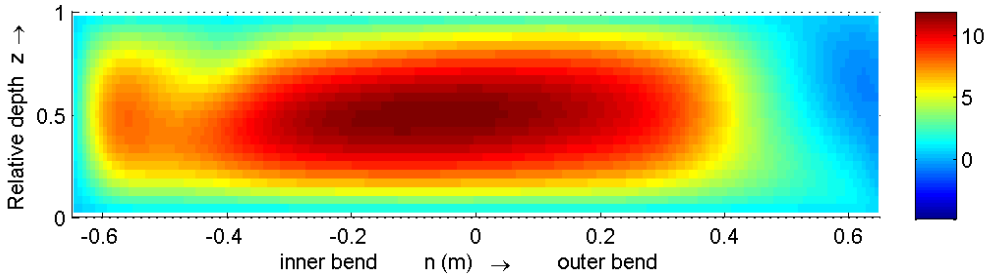

Figure 3-23 Normalized quantity ψ, in cross-section 090 according to the LES, ψ is normalized by 100/(U_{bulk} *H)

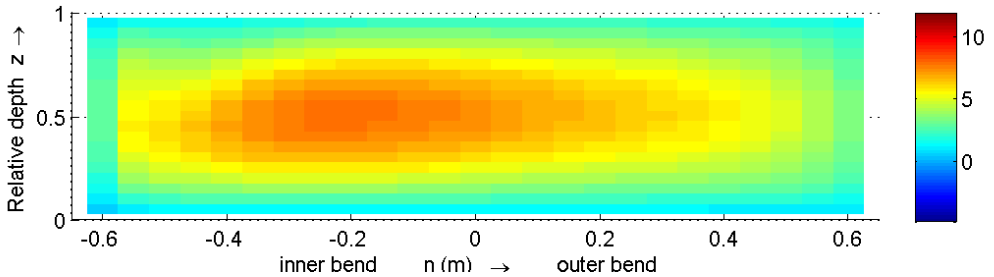

Figure 3-24 Normalized quantity ψ, in cross-section 090 according to simulation Q89_1_D3D, ψ is normalized by: 100/(U_{bulk} *H)

The figures in Appendix C.4 show the normalized pseudo stream function (ψ*100/(H*U)) for all the measured cross-sections of the Q89 experiment. The normalized pseudo stream function is also calculated for the LES and simulation Q89_1_D3D in those cross-sections. These figures give good insight in the development of the cross-stream circulations and the shortcomings of the simulations. Several phenomena can be recognized from the figures:

Centre region cell

The centre region cell starts to exist at the beginning of the bend and increases till cross-section 090 (see Figure 3-22 to Figure 3-24 where the normalized pseudo stream function (ψ*100/(H*U)) for the 090 cross-section for all three data sets is shown). The centre region cell still exists in the straight outflow but the strength of the cell decreases further and further along the straight outflow. All three data sets show the centre region cell. Simulation Q89_1_D3D under predicts the strength of the centre region cell quite a bit along the whole bend. The LES over predicts the centre region cell up to the 090 cross-section. After that, the LES slightly under predicts the strength of the centre region cell.

Outer-bank cell

The outer-bank cell is only represented by the measurements and the LES (see Figure 3-22 to Figure 3-24 the blue region in the upper corner). Simulation Q89_1_D3D do not show the outer-bank cell, this has to do with the lack of a good prediction of the turbulent quantities by the k-ε model, which is used in the Delft3D-FLOW package. Van Balen *et al*., (2008), tell us that the outer-bank cell comes into existence because of anisotropic turbulent stresses. The k-ε model is unable to predict anisotropic turbulent stresses and the outer bank will not appear in the Delft3D-FLOW simulation. The outer-bank cell observed in the LES and the measurements starts to exist from the beginning of the bend. For the LES it grows somewhat faster than it does according to the measurements. Further along the bend the outer-bank cell starts to decrease. For the LES it is already disappeared at the 120 cross-section (compare Figure 3-25 and Figure 3-26) while according to the measurements, it does not disappear completely in the bend and even after the bend there is something like an outer-bank cell visible. The cause of the disappearance of the outer-bank cell in the LES is not clear.

Internal shear layer

From cross-section 060 in the bend all data sets show a distortion (decrease of the height) of the centre region cell at about one time the water depth from the inner wall (-0.5). Especially the LES shows a clear reduction of the centre region cell at this point. The strength of this reduction increases strong in the 090 cross-section (the reduction of the centre region cell is visible in Figure 3-22 to Figure 3-24 and also Figure 3-25 to Figure 3-27). It seems that there is a relation between the reduction and the shift of the core of the downstream velocity.

For simulation Q89_1_D3D the internal shear layer is less clear visible in the quantity ψ. The existence of the internal shear layer starts somewhat later in the bend, in the 120 cross-section it becomes quite good visible (see also Figure 3-27 and the figures with the depth averaged downstream velocities, Figure 3-7, Figure 3-8 and Figure 3-9). At the end of the bend, the internal shear layer starts to decrease and so the centre region cell becomes more plain, the reduction in the inner bend disappears.

Negative valued bar at the bottom

The measured data shows an area where ψ gets negative values at the bottom along the whole flume. This is a very narrow bar. Both the LES and simulation Q89_1_D3D do not predict negative values of ψ at the bottom. It is unclear what the cause of this increase in this are is.

In the following of this research, the results for the m25, 060 and 150 cross-section will be compared. In the m25 cross-section the flow is not yet affected by the bend. In this cross-section the straight channel flow can be analyzed. The 060 cross-section can be seen as (nearly) fully developed flow, the 150 cross-section gives the flow around the exit of the bend. The flow develops in between the m25 and 060 cross-sections, from straight channel flow to (approximately) fully developed bend flow. From the 090 cross-section to the straight outflow,

the flow develops back to straight channel flow. There are still some effects visible in the straight outflow which are caused by the bend but they disappear as the flow continues over the straight reach.

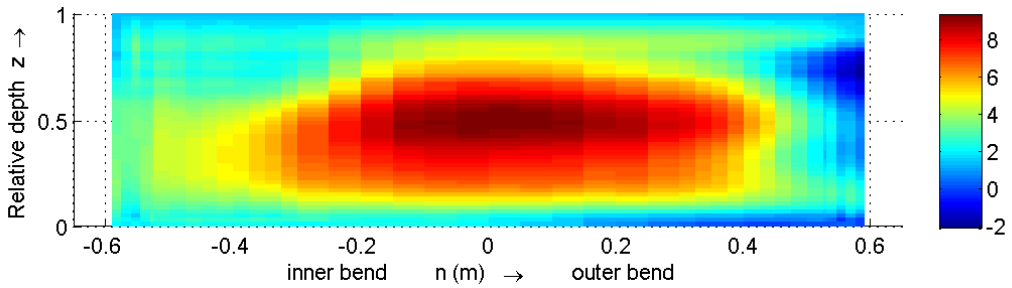

Figure 3-25 Normalized quantity ψ, in cross-section 120 according to the measurements, ψ is normalized by 100/(U_{bulk} *H)

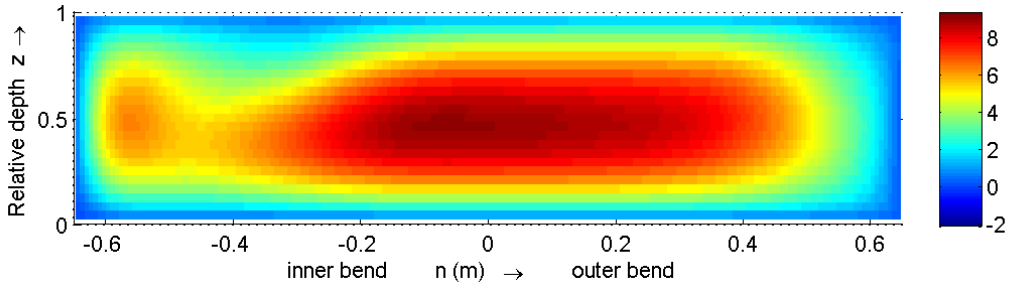

Figure 3-26 Normalized quantity ψ, in cross-section 120 according to the LES, ψ is normalized by 100/(U_{bulk} *H)

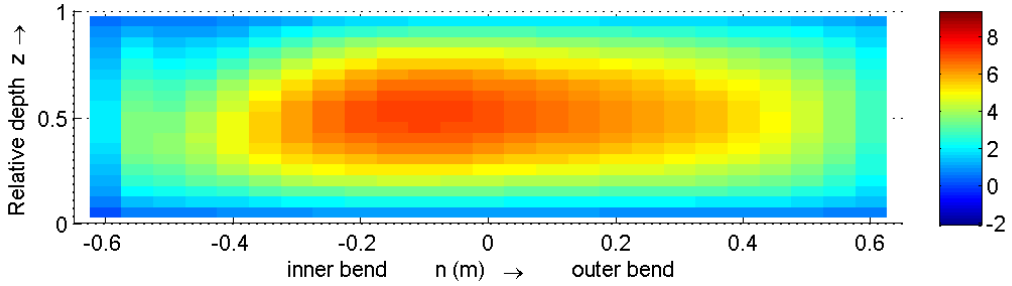

Figure 3-27 Normalized quantity ψ, in cross-section 120 according to simulation Q89_1_D3D, ψ is normalized by: 100/(U_{bulk} *H)

3.4 Vorticity and the vorticity balance

Now we have seen the differences in the transverse velocity and the pseudo stream function between the measurements, LES and simulation Q89_1_D3D, we will focus on the causes of these differences and there will be tried to explain these differences. This will be done on the basis of the downstream vorticity (ω_s) balance as described by van Balen *et al*. (2009b):

$$\frac{\partial \omega_s}{\partial t} = ADV + CFG + ISO + HOM + SKW + DNU + DIFF \qquad (3.5)$$

Where:

ADV = advection of ω_s
CFG = centrifugal effects which cause ω_s
ISO = anisotropy of the turbulent stresses
HOM = inhomogeneity of the turbulent stresses

SKW = the redistribution of ω_s by skeweness of the velocity field (excluding terms that can be associated with centrifugal effects
DNU = downstream non-uniformity of the turbulence
DIFF = diffusion of ω_s

All terms on the right hand side of equation (3.5) were evaluated, except the diffusion term (DIFF). The complete analysis is described in Appendix C.5 to C.11. In this section the downstream vorticity, the advection-(ADV), the centrifugal-(CFG) and the anisotropy-(ISO) term are discussed.

3.4.1 Vorticity

The downstream vorticity is defined as:

$$\omega_s = \frac{\partial w}{\partial r} - \frac{\partial v}{\partial z} \qquad (3.6)$$

The results for the downstream vorticity in the m25, 060 and 150 cross-sections (see Figure 2-3) are given in Appendix C.5. The quantity ω_s is normalized by H/U_{bulk}.

M25 cross-section

The vorticity in the m25 cross-section is nearly zero for simulation Q89_1_D3D. The LES and the measurements show alternating bars which correspond with the presence of the secondary flow cells in the straight inflow.

060 cross-section

In the 060 cross-section, the comparison of ω_s for the LES and the measurements is quite good. As was remarked before, the outer-bank cell is not visible in the results of simulation Q89_1_D3D. Both the LES and the measurements show the outer-bank cell and some kind of a cell in the upper part of the cross-section from -0.55 m to -0.3 m from the centre (the red circle in Figure 3-28). In both cells the vorticity has positive values while in the most of the cross-section the vorticity has negative values. The positive valued vorticity is mainly caused by the flow separation and the reduction of the transverse velocity due to this. Especially in the lower part, inner bend (the blue circle in Figure 3-28), the vorticity becomes strongly negative. The values of the vorticity according to simulation Q89_1_D3D are, in general, lower than the LES and the measurements.

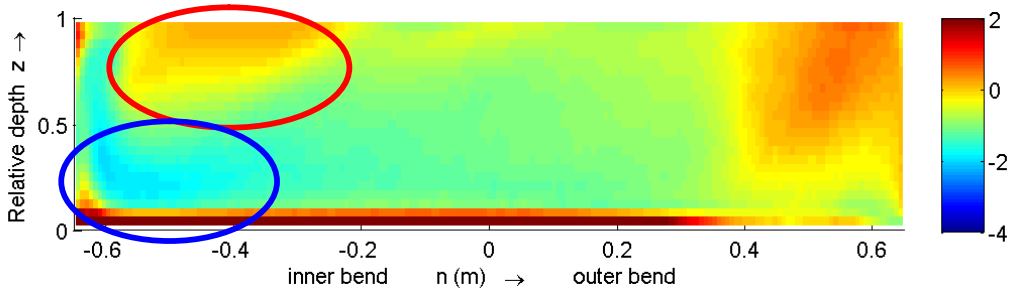

Figure 3-28 ω_s, normalized (with H/U_{bulk}), for cross-section 060, according to the LES. The range of the color bar is shortened with respect to the range of the data

Cross-section 150

In cross-section 150, the strength of the outer-bank cell is decreased for the LES (see Figure 3-29) and measurements. The strength of the vorticity decreases due to the internal shear layer (the two circles).

It can be concluded that the vertical velocities and the gradient of the vertical velocities in transverse direction, are only important at the side walls. This is the place where the 'up welling' and 'down welling' of the secondary flow takes place.

Vorticity is mainly generated along the walls, the borders of the outer-bank cell and the internal shear layer where the velocity gradients are high. Simulation Q89_1_D3D predicts too strong negative values most of the time and misses the outer-bank cell.

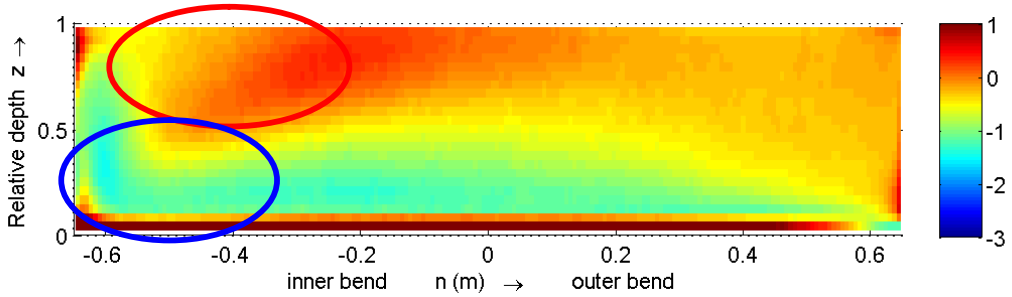

Figure 3-29 ω_s, normalized (with H/U_{bulk}), for cross-section 150, according to the LES. The range of the colour bar is shortened with respect to the range of the data

3.4.2 Advection

In this section the advection term (ADV) of the downstream vorticity balance equation is shortly discussed.

The advection term is defined as (see also van Balen *et al.*, 2009b):

$$ADV = -\left(\frac{u}{r}\frac{\partial \omega_\theta}{\partial \theta} + v\frac{\partial \omega_\theta}{\partial r} + w\frac{\partial \omega_\theta}{\partial z} \right) \qquad (3.7)$$

For all three data sets (measurement, LES and simulation Q89_1_D3D) the advection term can be calculated. Some remarks have to be made on the calculations of the *downstream* derivatives of the measurements. The downstream derivatives according to the measurements are calculated between two consecutive measured cross-sections which means that the distance '*1/r*dθ*' is a large distance.

The results and a more extensive discussion for the m25, 060 and 150 cross sections are given in Appendix C.6. Here only the most important results are described. The advection term is normalized by $H^2/U_{bulk}^2 * 1000$.

From the analysis of the advection it turned out that the advection is a significant term. The advection is related to the regions where the downstream vorticity is generated. This is especially visible in Figure 3-31. The advection attains high values along the walls, the internal shear layer and the borders of the outer-bank cell (the blue circle). The patterns for all three datasets are approximately the same (compare Figure 3-30 to Figure 3-32) besides that simulation Q89_1_D3D misses the outer-bank cell. The outer-bank cell is less clear for The strength of the advection term predicted by simulation Q89_1_D3D is also lower than was measured and predicted by the Q89_LES.

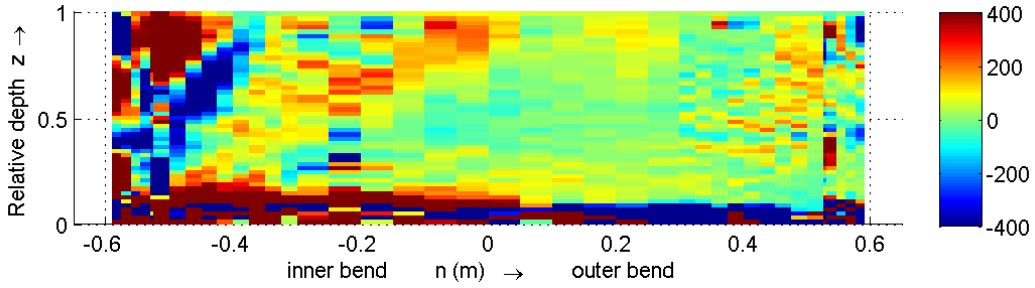

Figure 3-30 Normalized (1000*H^2/U_{bulk}^2) ADV for cross-section 060, according to the measurements. The range of the colour bar is shortened with respect to the range of the data

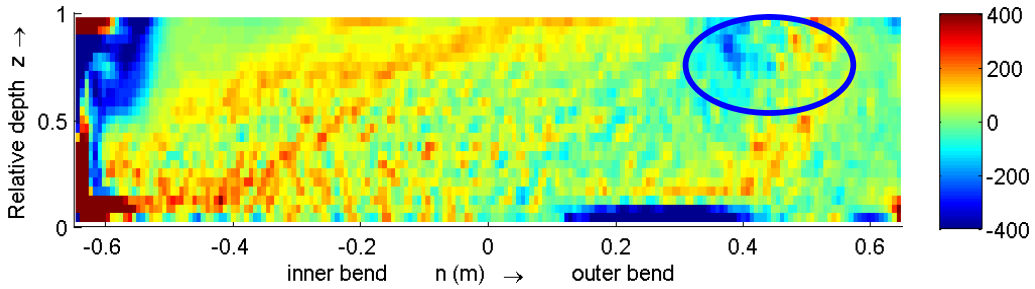

Figure 3-31 Normalized (1000*H^2/U_{bulk}^2) ADV for cross-section 060, according to the LES. The range of the colour bar is shortened with respect to the range of the data

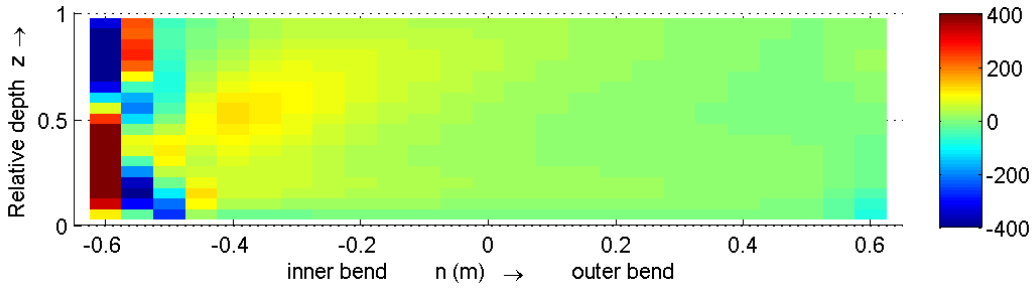

Figure 3-32 Normalized (1000*H^2/U_{bulk}^2) ADV for cross-section 060, according to simulation Q89_1_D3D. The range of the colour bar is shortened with respect to the range of the data

3.4.3 Centrifugal term

In Appendix C.7 the contour line plots of the centrifugal term (CFG) for the m25, 060 and 150 cross-section are given. There is chosen for a plot with contour lines to give a clear visualization of the pattern because of the data is very wide ranged. The centrifugal term is given as:

$$\frac{1}{r}\frac{\partial}{\partial z}\left(u^2+\overline{u'^2}\right) \qquad (3.8)$$

where u is the velocity in downstream direction, u' is the turbulent fluctuation of the downstream velocity, the over bar means averaging in time and r is the radius. The CFG-term is normalized by 1000*H^2/U_{bulk}^2.

For the LES and the measurements the development of the outer-bank cell is clearly visible in the CFG-term (Figure 3-36 and Figure 3-37). The outer-bank cell is already visible in the m25 cross-section in both the measured and LES data (Figure 3-33 and Figure 3-34). In the straight inflow, the Q89_LES shows in the inner bank an other cell which is much stronger than the outer-bank cell. Simulation Q89_1_D3D does not show the outer-bank cell and the inner bank

cell. Both cells can be caused due to the anisotropy of the turbulent stresses as was concluded by Van Balen *et al.* (2008) as we will see later on.

In the 060 cross-section, all three data sets show the internal shear layer but the shear layer is about 40% under predicted by simulation Q89_1_D3D. The strength of the outer-bank cell is a little over predicted by the LES. Simulation Q89_1_D3D generally under predicts the CFG-term. For the 150 cross-section, the outer-bank cell disappears for the LES (Figure 3-40) but is still visible in the measured data (Figure 3-39).

The CFG-term has high negative values at the bottom of the flow. This can be explained by the high gradient in the transverse velocity in the vertical direction caused by bottom friction.

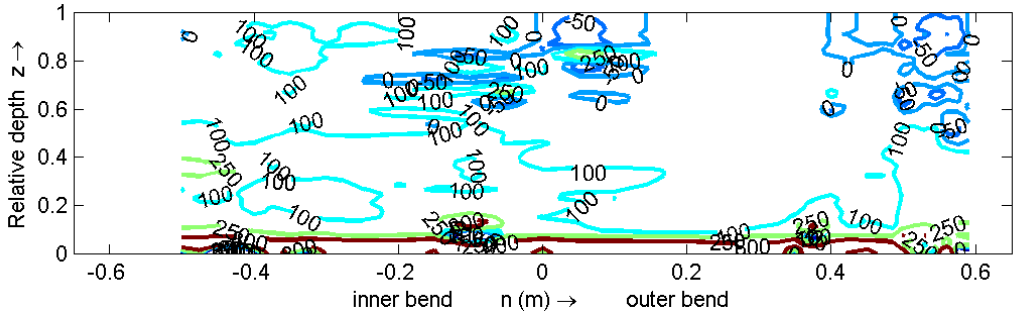

Figure 3-33 Contour plot of CFG-term, according to measurements, cross-section m25, normalized by $1000*H^2/U_{bulk}^2$.

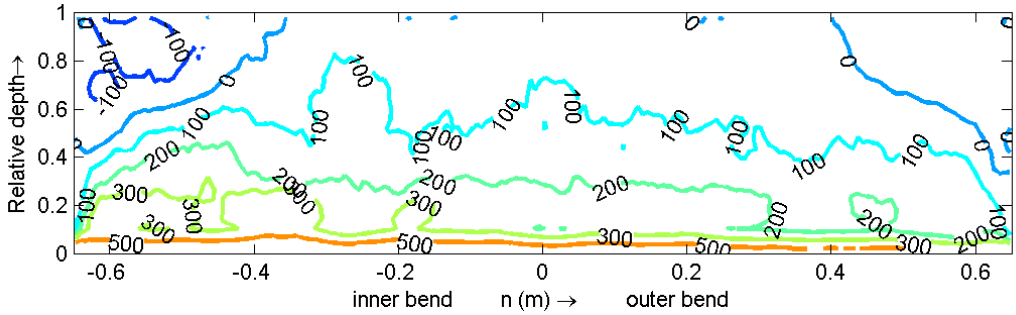

Figure 3-34 Contour plot of CFG-term, according to the Q89_LES, cross-section m25, normalized by $1000*H^2/U_{bulk}^2$.

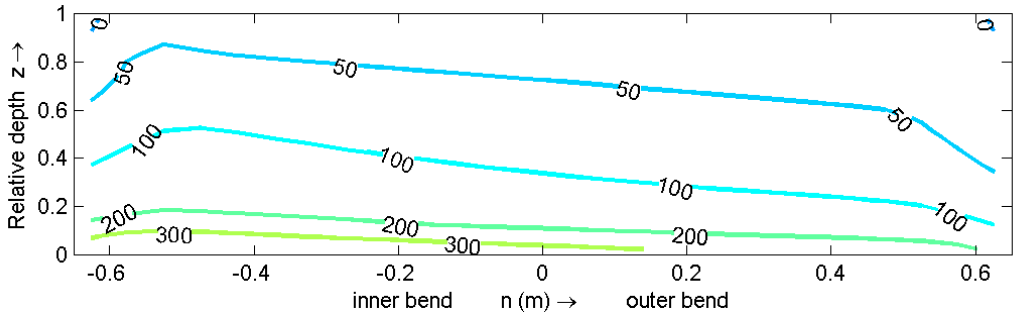

Figure 3-35 Contour plot of CFG-term, according to simulation Q89_1_D3D, cross-section m25, normalized by $1000*H^2/U_{bulk}^2$.

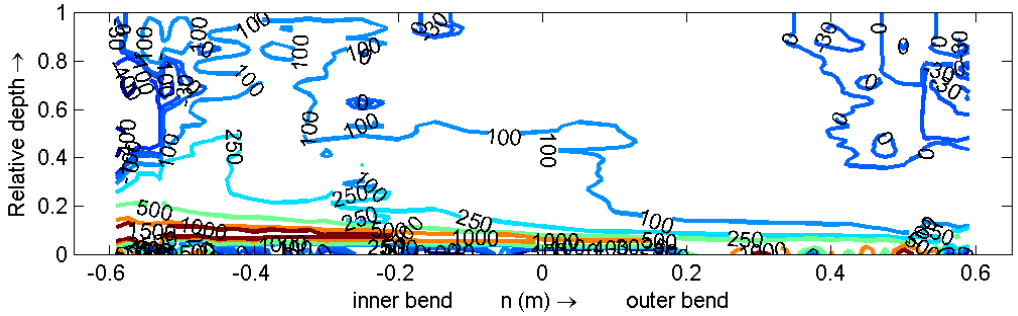

Figure 3-36 Contour plot of CFG-term, according to measurements, cross-section 060, normalized by $1000*H^2/U_{bulk}^2$.

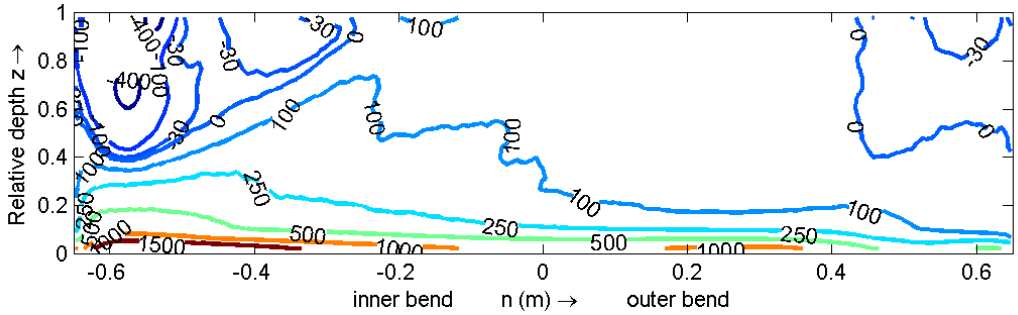

Figure 3-37 Contour plot of CFG-term, according to the Q89_LES, cross-section 060, normalized by $1000*H^2/U_{bulk}^2$.

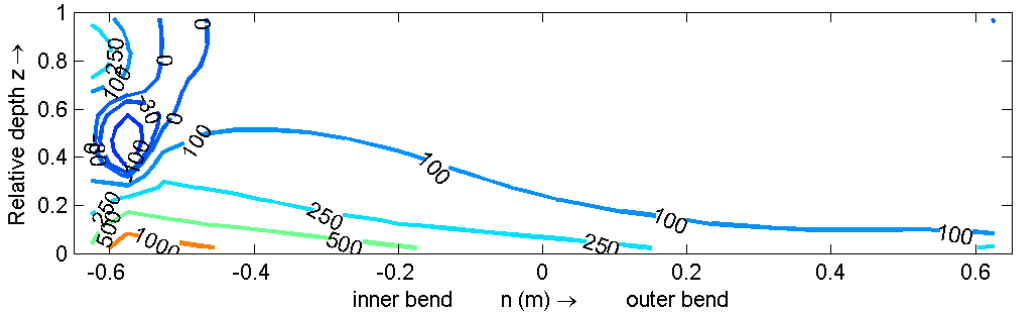

Figure 3-38 Contour plot of CFG-term, according to simulation Q89_1_D3D, cross-section 060, normalized by $1000*H^2/U_{bulk}^2$.

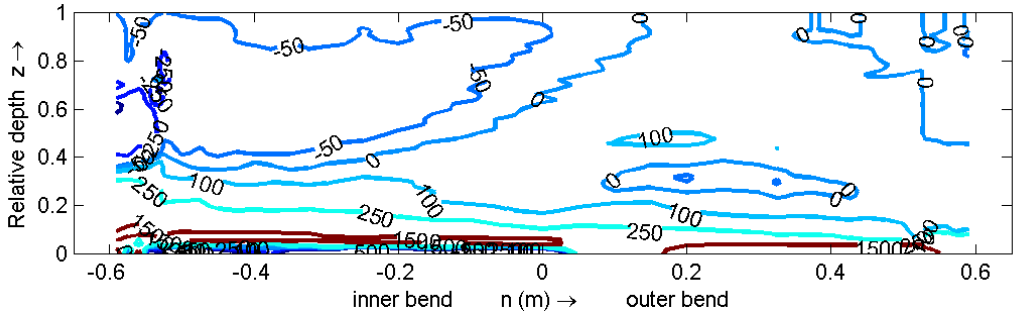

Figure 3-39 Contour plot of CFG-term, according to measurements, cross-section 150, normalized by $1000*H^2/U_{bulk}^2$.

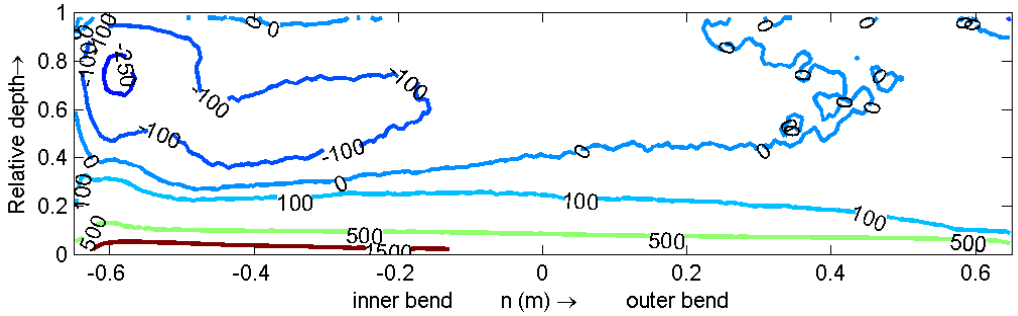

Figure 3-40 Contour plot of CFG-term, according to the Q89_LES, cross-section 150, normalized by $1000*H^2/U_{bulk}^2$.

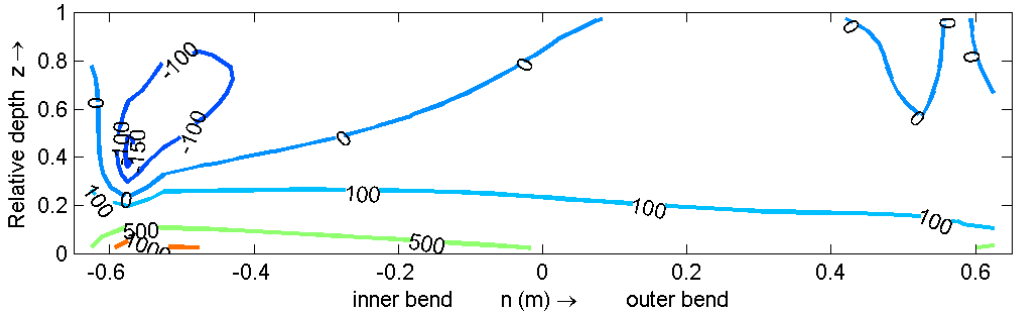

Figure 3-41 Contour plot of CFG-term, according to the Q89_1_D3D, cross-section 150, normalized by $1000*H^2/U_{bulk}^2$.

3.4.4 Anisotropy

In Appendix C.8 are the figures given of the ISO-term for the m25, 060 and 150 cross-sections. A more extensive discussion of the ISO-term is given in Appendix C.8.

The ISO-term represents the anisotropy of the turbulent stresses and is defined as (see also van Balen *et al.*, 2009b):

$$\mathrm{ISO} = \frac{\partial^2}{\partial r \partial z}\left(\overline{v'^2} - \overline{w'^2}\right) + \frac{1}{r}\frac{\partial \overline{v'^2}}{\partial z} \qquad (3.9)$$

Where v' and w' are the turbulent fluctuation of the transverse respectively the vertical velocity. The term is normalized by $1000 * H^2/U^2$.

The main differences in the anisotropy term between on the one side simulation Q89_1_D3D and on the other side the Q89_LES and the measurements are the under prediction by simulation Q89_1_D3D and the absence of the outer-bank cells (compare Figure 3-44 (D3D) with Figure 3-42 and Figure 3-43). The blue circles indicate the regions with the increased anisotropy of the turbulent stresses. This finding is in agreement with the findings of van Balen (2010) who stated that the outer-bank cell is initiated by the anisotropy in the turbulent stresses. A linear k-ε model (as used in simulation Q89_1_D3D) is not able to predict this anisotropy.

Along the inner wall there is also an increase of the anisotropy visible for all three datasets. Presumably this increase is caused by the internal shear layer.

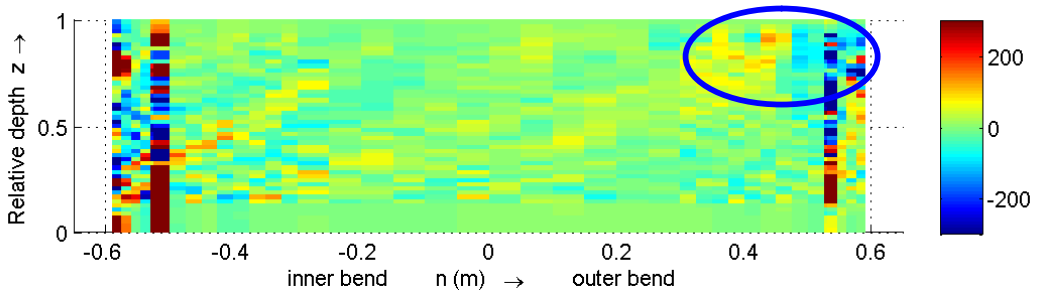

Figure 3-42 ISO-term, according to measurement, cross-section 060, normalized by 1000*H^2/U_{bulk}^2, shortened colour bar

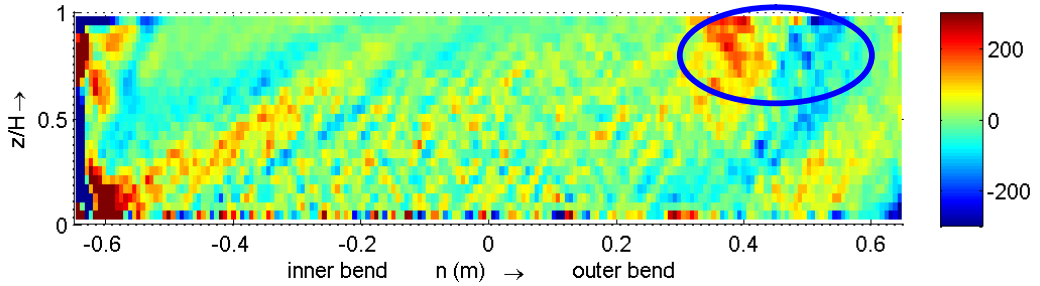

Figure 3-43 ISO-term, according to the Q89_LES, cross-section 060, normalized by 1000*H^2/U_{bulk}^2, shortened colour bar

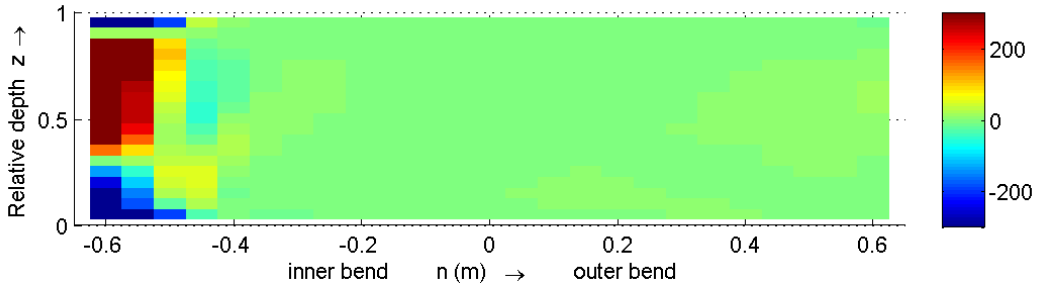

Figure 3-44 ISO-term, according to simulation Q89_1_D3D, cross-section 060, normalized by 1000*H^2/U_{bulk}^2, shortened colour bar

3.5 Turbulent stresses

In Appendix C.12 the figures are given of the turbulent stresses ($\overline{u'v'}$, $\overline{u'w'}$ and $\overline{v'w'}$) in cross section 060. The figures are normalized by U_{bulk}^2. The turbulent stresses $\overline{u'v'}$ are also given in the cross-sections m25 and 150. The $\overline{u'v'}$ stresses are closely related to the wall and bottom shear stresses.

The $\overline{u'v'}$ stresses were quite well predicted by the Q89_LES for all three cross-sections. One significant difference can be seen in cross-section 060 at the transition of the outer-bank cell and the primary secondary cell. The Q89_LES shows here a very strong increase of the turbulent stresses while this is nearly complete absent by the measurements (compare Figure 3-45 and Figure 3-46). The turbulent stresses according to simulation Q89_1_D3D are strongly underestimated (Figure 3-47). Only along the walls are the results comparable. In cross-section 150 the comparison is as poor as it is in cross-section 060.

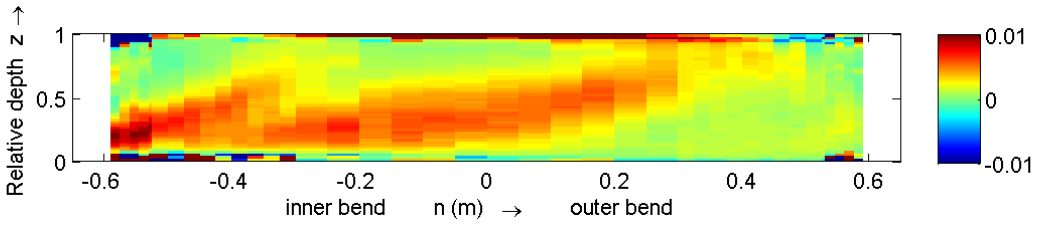

Figure 3-45 $\overline{u'v'}$, normalized by U_{bulk}^2, according to the measurements, cross-section 060

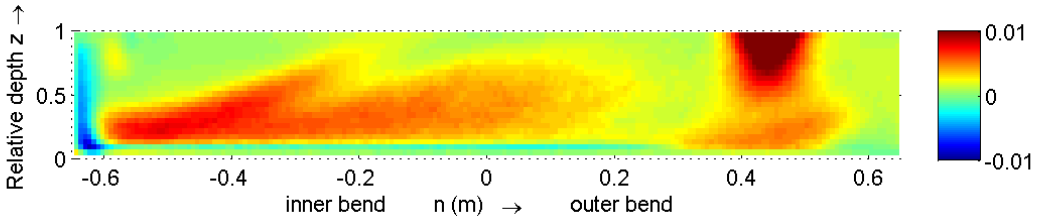

Figure 3-46 $\overline{u'v'}$, normalized by U_{bulk}^2, according to the Q89_LES, cross-section 060

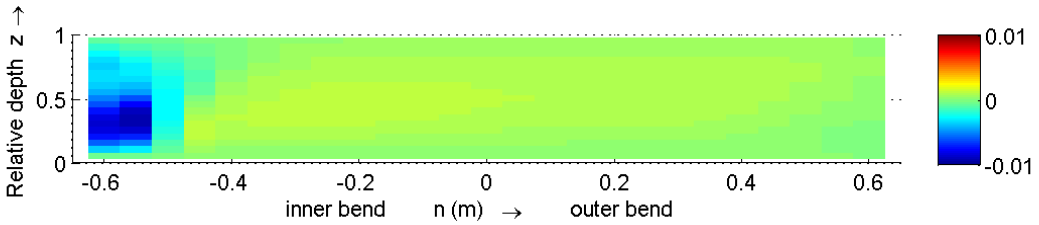

Figure 3-47 $\overline{u'v'}$, normalized by U_{bulk}^2, according to simulation Q89_1_D3D, cross-section 060

For the $\overline{u'w'}$ stresses in cross-section 060, the predictions of the Q89_LES are somewhat less accurate but the pattern in the upper part of the flow is comparable. The effects of the outer-bank cell are visible in the turbulent stresses. In the lower part of the flume the $\overline{u'w'}$ stresses are under predicted by the Q89_LES. The predictions by simulation Q89_1_D3D is better than for the $\overline{u'v'}$ stresses but the pattern does not match completely (see Figure 3-48 to Figure 3-50).

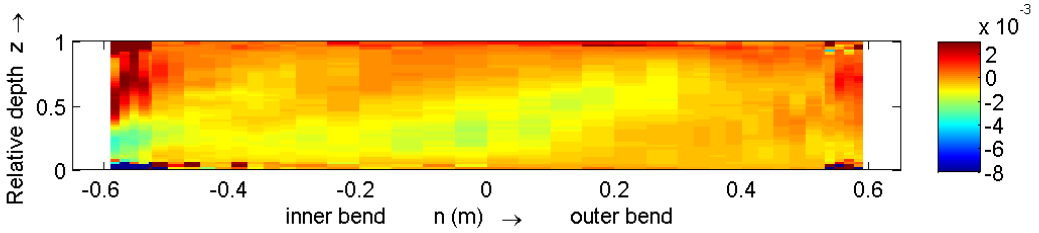

Figure 3-48 $\overline{u'w'}$, normalized by U_{bulk}^2, according to the measurements, cross-section 060

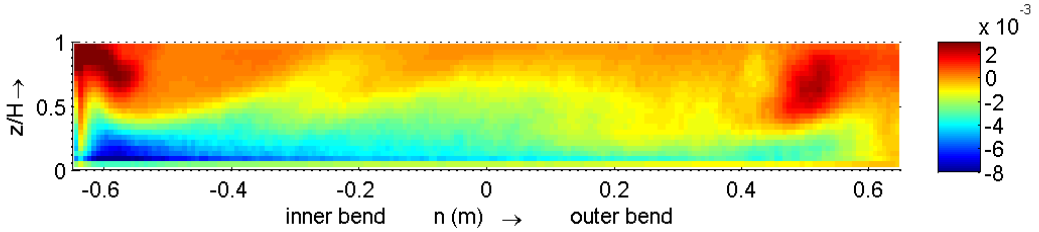

Figure 3-49 $\overline{u'w'}$, normalized by U_{bulk}^2, according to the Q89_LES, cross-section 060

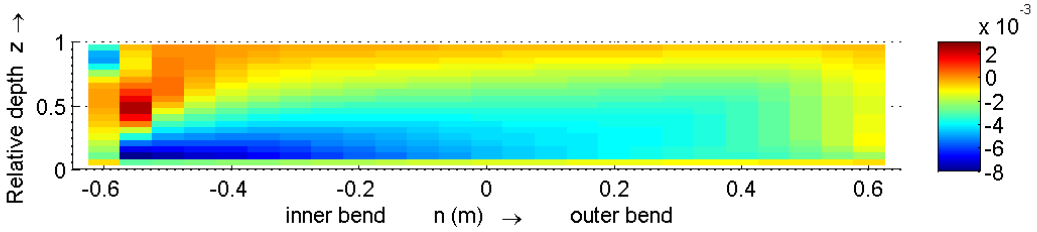

Figure 3-50 $\overline{u'w'}$, normalized by U_{bulk}^2, according to simulation Q89_1_D3D, cross-section 060

Finally looking at the $\overline{v'w'}$ stresses (Figure 3-51 to Figure 3-53.), it can be said that all three data sets predict most features in the right place. Of course, the outer-bank cell does not appear in the results of simulation Q89_1_D3D but for all three data sets, the $\overline{v'w'}$ stresses are positive along the walls and negative in the centre region. The negative values according to the Q89_LES are much higher, in absolute sense, than according to the measurements and simulation Q89_1_D3D.

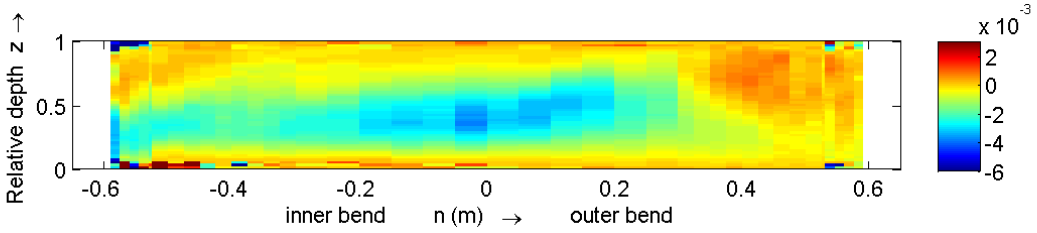

Figure 3-51 $\overline{v'w'}$, normalized by U_{bulk}^2, according to the measurements, cross-section 060

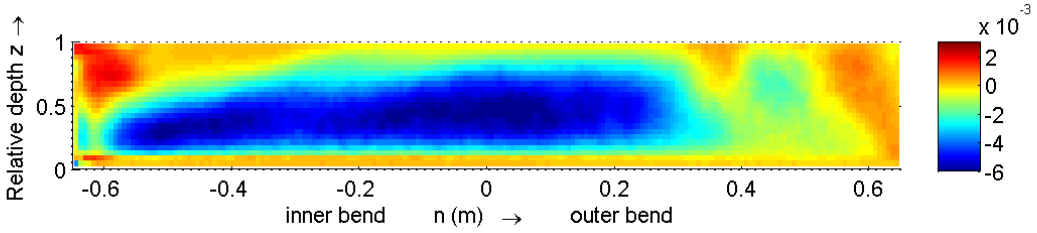

Figure 3-52 $\overline{v'w'}$, normalized by U_{bulk}^2, according to the Q89_LES, cross-section 060

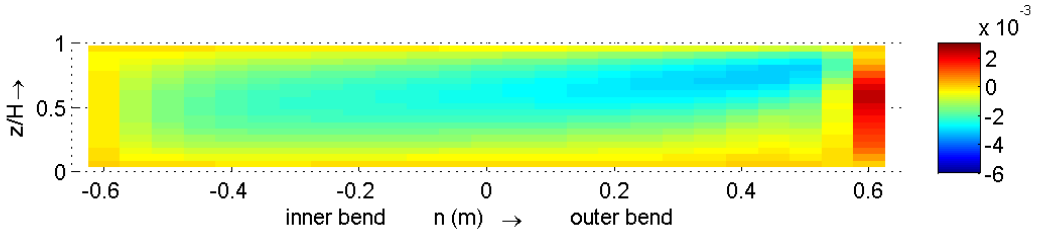

Figure 3-53 $\overline{v'w'}$, normalized by U_{bulk}^2, according to simulation Q89_1_D3D, cross-section 060

It can be concluded that most turbulent stresses are well predicted by the Q89_LES. In some cases the Q89_LES over predicts the turbulent stresses. Delft3D-FLOW underestimates most turbulent stresses. Especially the $\overline{u'v'}$ turbulent stresses are badly predicted by Delft3D-FLOW. This is not surprising because these stresses are partly determined by the horizontal eddy viscosity which strongly depends on the vertical eddy viscosity. The eddy viscosity is assumed to be isotropic which is questionable in this case. This wrong prediction of the turbulent $\overline{u'v'}$ stresses can have a significant effect on the results of the distribution of the

transverse and downstream velocities because these stresses represent the momentum exchange of transverse and downstream momentum in these directions.

3.6 Turbulent Kinetic energy

The turbulent kinetic energy (TKE) tells us at which places turbulent energy is available.

Figure 3-54 to Figure 3-56 show the depth averaged TKE according to the measurements, the LES and Delft3D-FLOW simulation. The TKE is given as: $\left(u'^2 + v'^2 + w'^2\right)/2$. The depth averaged TKE is normalized by 0.5 * u_*^2, whereas u_* is given $\sqrt{(g)}\, U_{bulk}/C$. From these figures it is clear that both the Q89_LES and simulation Q89_1_D3D overestimate the TKE in the bend. The TKE increases in the bend. The patterns of the depth averaged TKE differ too. For the Q89_LES, the increase of the TKE starts more upstream than according to the measurements and simulation Q89_1_D3D. The Q89_LES shows also some small strips of increased TKE along the inner and outer wall. The maximum of the TKE is found in the inner bend of the flume around cross-section 120.

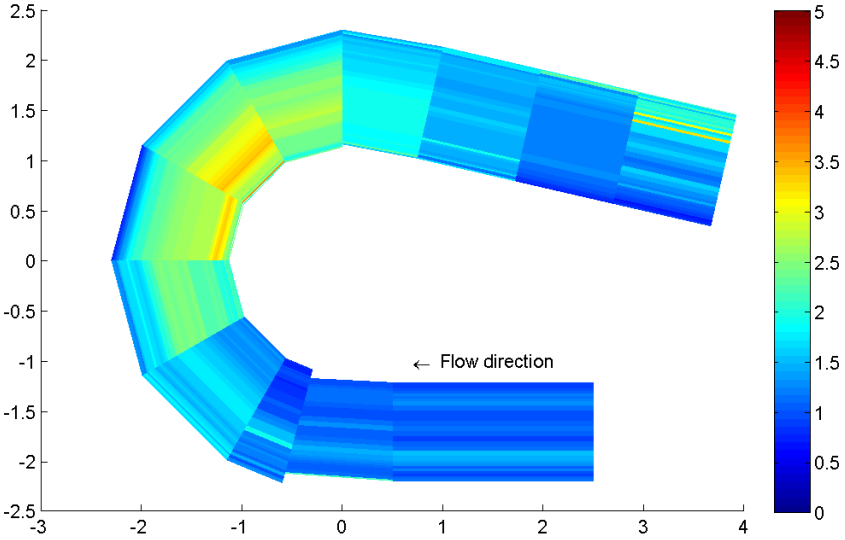

Figure 3-54 Depth averaged turbulent kinetic energy according to the measurements, normalized by 0.5 *u_*^2

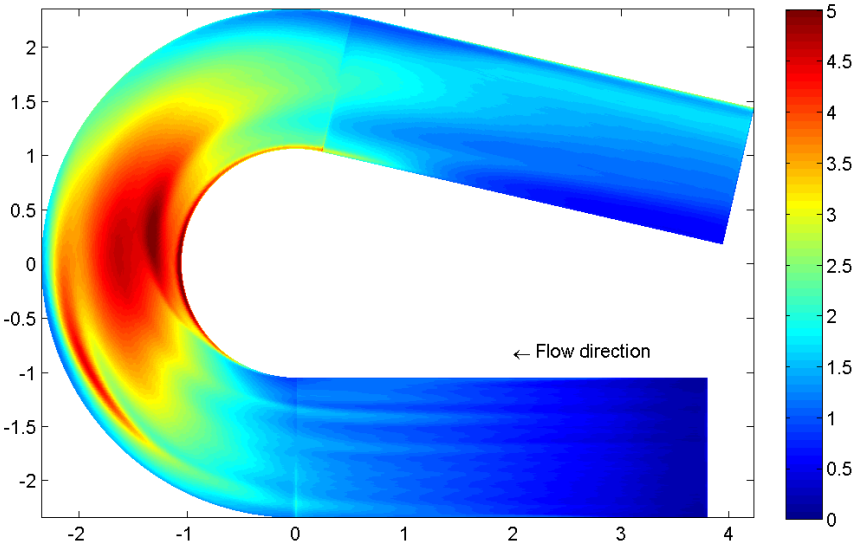

Figure 3-55 Depth averaged turbulent kinetic energy according to Q89_LES, normalized by 0.5 *u_*^2

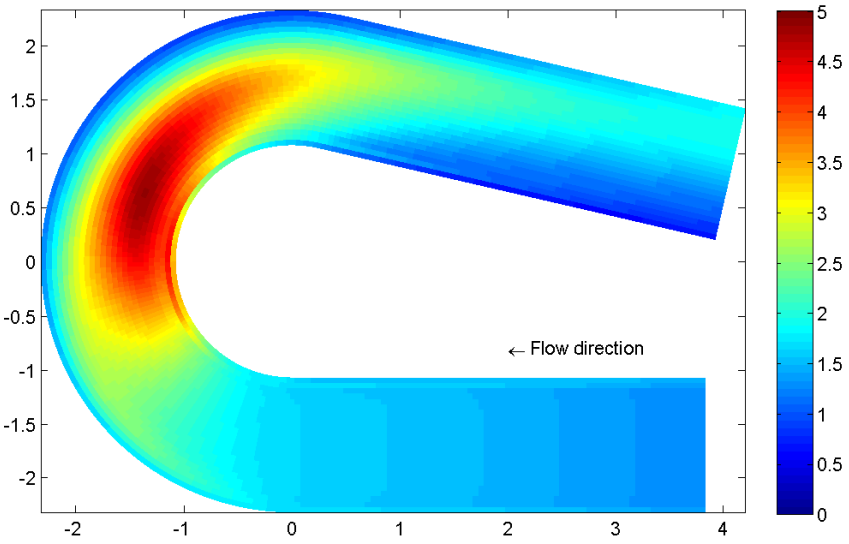

Figure 3-56 Depth averaged turbulent kinetic energy according to SIM Q89_1_D3D, normalized by 0. 5 *u_*^2

In Appendix C.13 some figures are shown representing the cross-sectional distributions of the TKE for several cross-sections. In Figure 3-57 to Figure 3-59 the distribution of the turbulent kinetic energy (TKE) for the straight inflow is shown. The TKE increases towards the bottom for all three data sets which is caused by the resistance of the bottom. The measurements and Q89_LES give more irregular patterns which show the effect of the circulatory cells in the straight inflow. These cells are absent in simulation Q89_1_D3D. The Q89_LES shows substantially lower values for the TKE.

Along the bend, the pattern of the distribution of the TKE is for all three data sets approximately the same (compare Figure 3-60 to Figure 3-62). The major difference for simulation Q89_1_D3D is the missing of the outer-bank cell. For the Q89_LES and the measurements the outer-bank cell is visible in an increase of the TKE. An other difference is the overestimation of the TKE by both the Q89_LES and simulation Q89_1_D3D. The overestimation of the TKE disappears in the straight outflow. The distribution of the TKE shows us that most TKE is distributed along the bottom. This shows the relation between the dissipation of the energy and the turbulence. Along the bottom the bottom resistance causes turbulence and dissipation of energy.

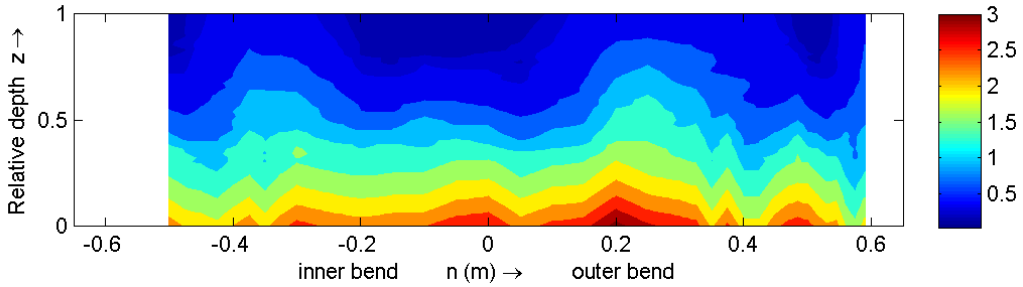

Figure 3-57 Turbulent kinetic energy (measured, m25), normalized by (0.5 *u_*^2)

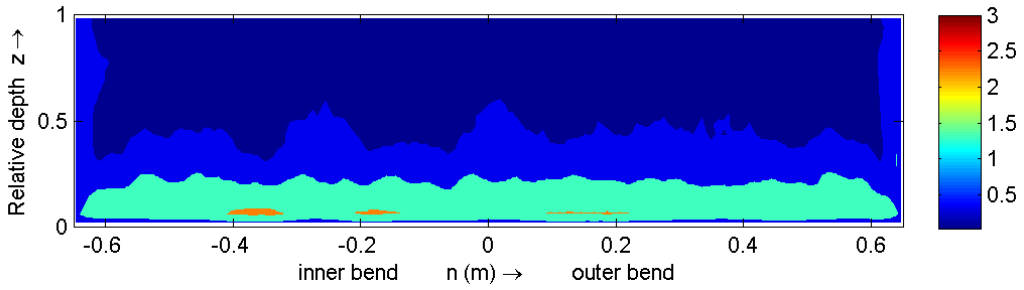

Figure 3-58 Turbulent kinetic energy (Q89_LES, m25), normalized by (0.5 *u_*^2)

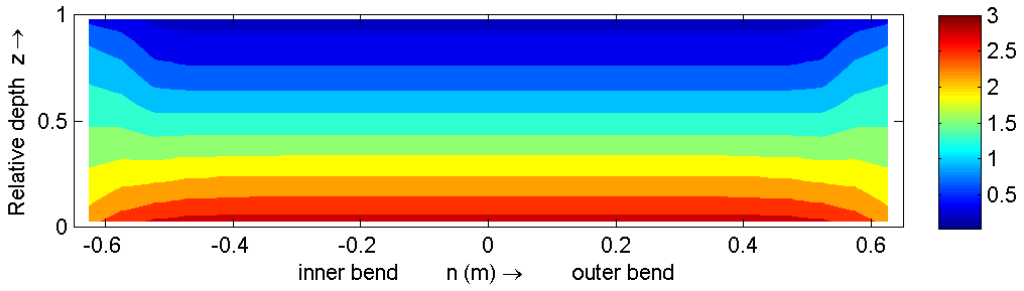

Figure 3-59 Turbulent kinetic energy (simulation Q89_1_D3D, m25), normalized by (0.5 *u_*^2)

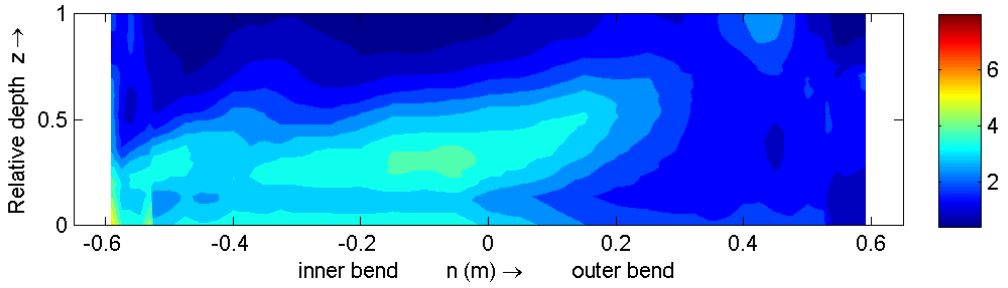

Figure 3-60 Turbulent kinetic energy (measured, 060), normalized by (0.5 *u_*^2)

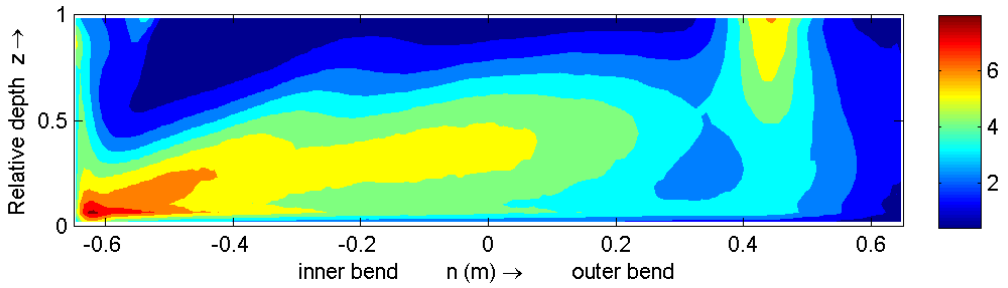

Figure 3-61 Turbulent kinetic energy (Q89_LES, 060), normalized by (0.5 *u_*^2)

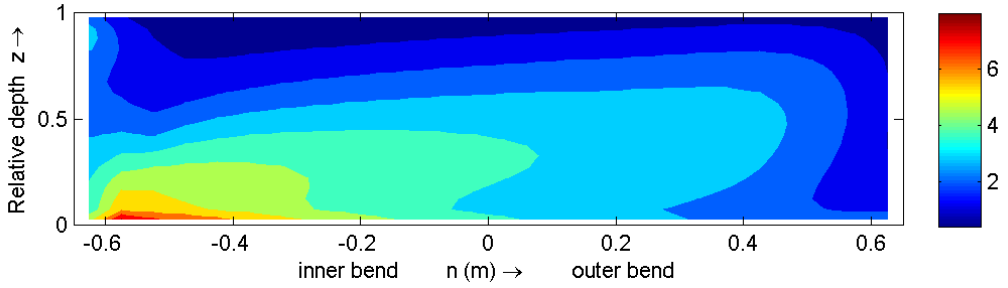

Figure 3-62 Turbulent kinetic energy (simulation Q89_1_D3D, 060), normalized by (0.5 *u_*^2)

It can be concluded that the TKE is overestimated by both the Q89_LES and the Delft3D-FLOW simulation. Simulation Q89_1_D3D misses the effect of the outer-bank cell. The TKE is related to the bottom resistance because of the generation of turbulence along the bottom which causes dissipation of energy.

3.7 The effect of an increased viscosity

In the first part of this chapter we analyzed the flow over the flat-bed and the capability of Delft3D-FLOW to predict this flow. In this section the effect of the viscosity on the flow is investigated. The results of simulation Q89_2_D3D is compared with the results of simulation Q89_1_D3D. In simulation Q89_2_D3D the horizontal background viscosity is increased to $\nu_{hor,back} = 10^{-2}$ m^2/s compared to simulation Q89_1_D3D (see Table 2-4). Together with the results of the first part of this chapter we can conclude whether the increase of the viscosity will benefit the quality of the prediction and how they affect the results. All quantities involved in this comparison are calculated and normalized as was done for simulation Q89_1_D3D.

3.7.1 The water level

Figure 3-63 shows the predicted water level according to simulation Q89_1_D3D (A) and according to simulation Q89_2_D3D (B). From this figure it follows that an increase of the viscosity results in a decrease of the water level. The lower water level is mainly visible in the straight inflow and at the end of the bend the water levels for both simulations are nearly equal. This is also clear from Figure 3-64 where the water level along the centre line is plotted for simulation where the water level along the centre line is plotted for simulation Q89_1_D3D, Q89_2_D3D, the Q89_LES and the measurements. Simulation Q89_2_D3D underestimates the water level in the straight entrance but the water level (see Figure 3-64 where the water level along the centre line is plotted) in the bend is better estimated than according to simulation Q89_1_D3D. The transverse water level gradients are nearly equal (Figure 3-65), the gradients according simulation Q89_2_D3D are a little smaller. As we will see later on, the flow with the increased viscosity contains less turbulent kinetic energy and also less dissipation. This results in less steep gradients because the flow is an equilibrium flow between dissipation and the gravitational forces.

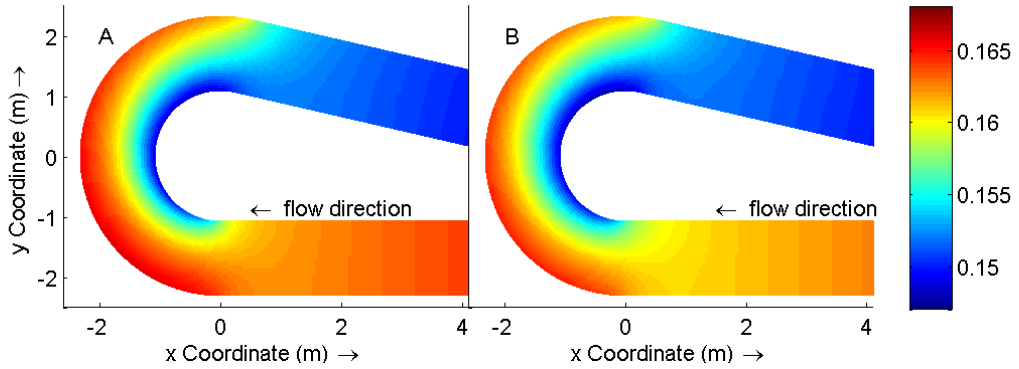

Figure 3-63 Comparison of the water level, A is according to simulation Q89_1_D3D, B is according to simulation Q89_2_D3D

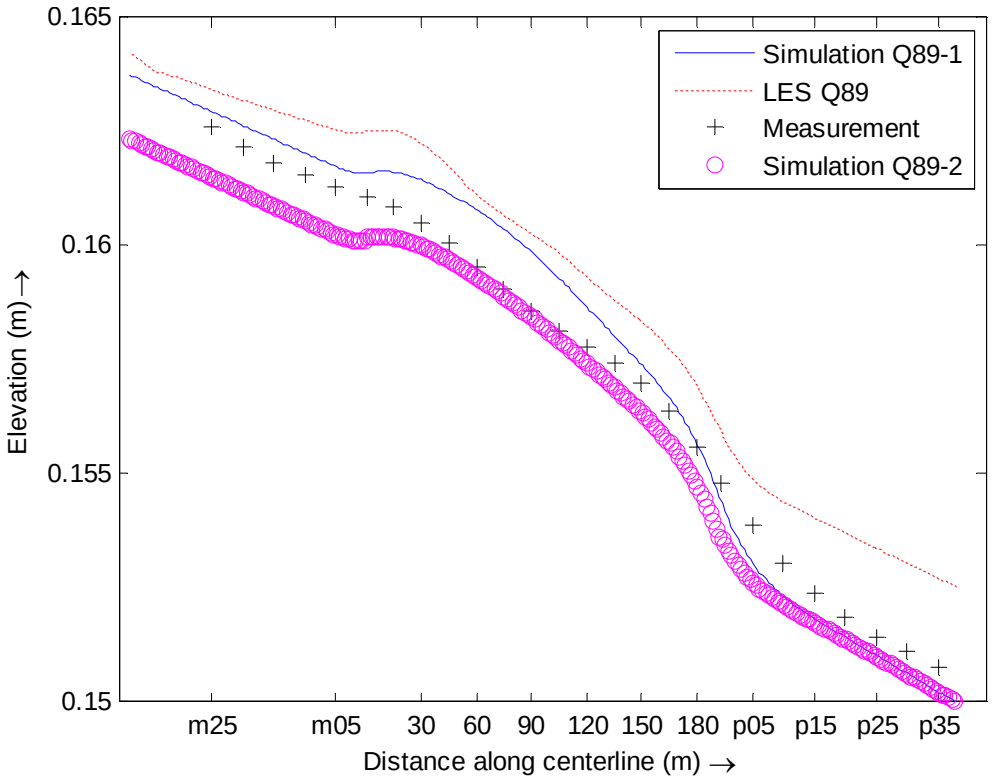

Figure 3-64 Water level along the centre line according to several data sets

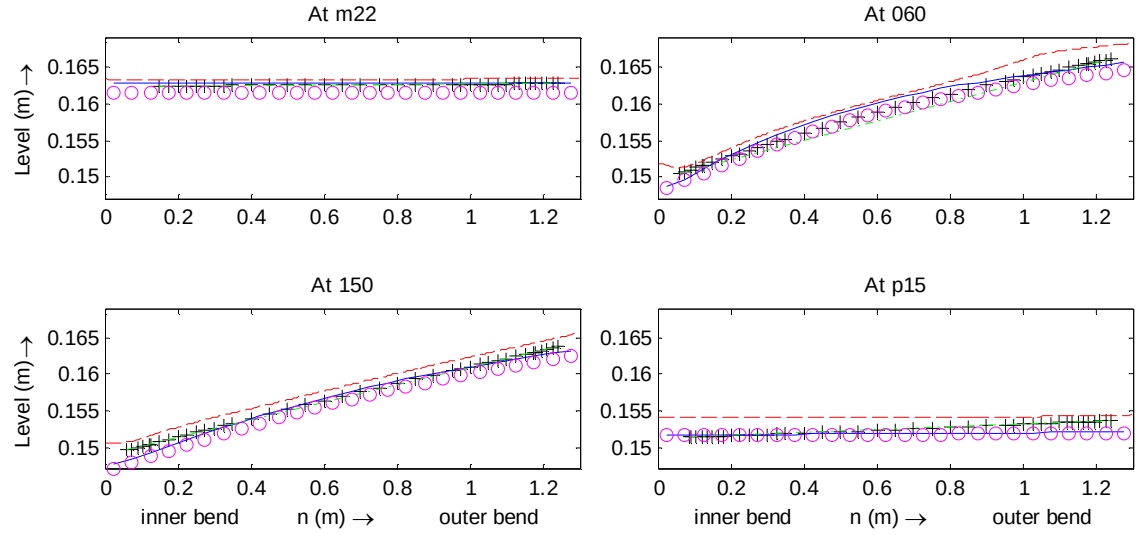

Figure 3-65 Transverse water levels for the same data sets as in Figure 3-64 (legend of Figure 3-64 is used)

3.7.2 Downstream velocity

The downstream depth averaged velocities are given in Figure 3-66. The velocities estimated by simulation Q89_2_D3D are more smoothed. The peak values and the lowest values are flattened compared to the values of simulation Q89_1_D3D. Especially in the last part of the flume it is clearly visible that the downstream velocity is more smoothed over the width when the viscosity is increased. Comparing the cross-sectional plots of the downstream velocity (see Figure 3-67 to Figure 3-69 or Figure D-1 to Figure D-6), the smoothing is clearly visible, indicating the exchange of streamwise momentum. Simulation Q89_1_D3D shows higher and more concentrate peak values and regions than simulation Q89_2_D3D. This is especially visible in the cross-sections 060 and 150 (see Figure 3-67 to Figure 3-69).

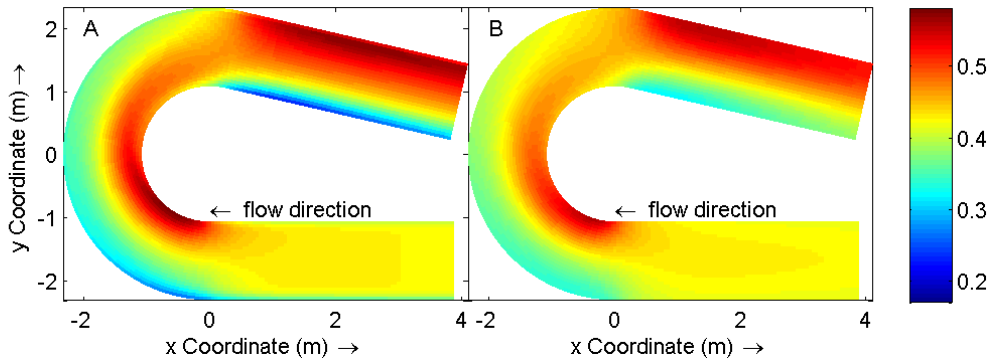

Figure 3-66 Comparison of the depth averaged downstream velocity, A is according to simulation Q89_1_D3D, B is according to simulation Q89_2_D3D (not normalized)

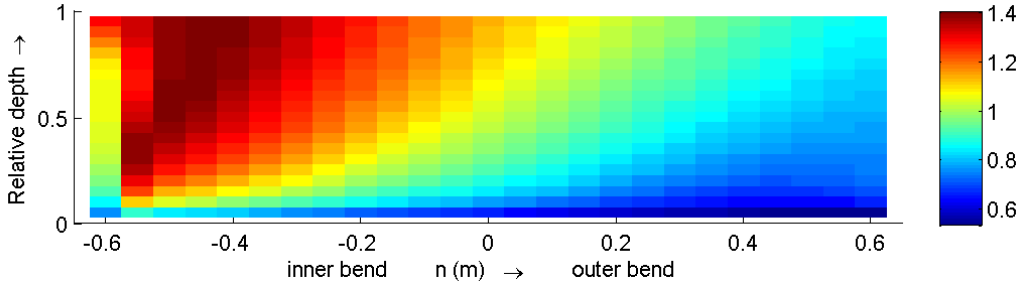

Figure 3-67 Downstream velocity in cross-section 060 according to simulation Q89_1_D3D, normalized by U_{bulk}

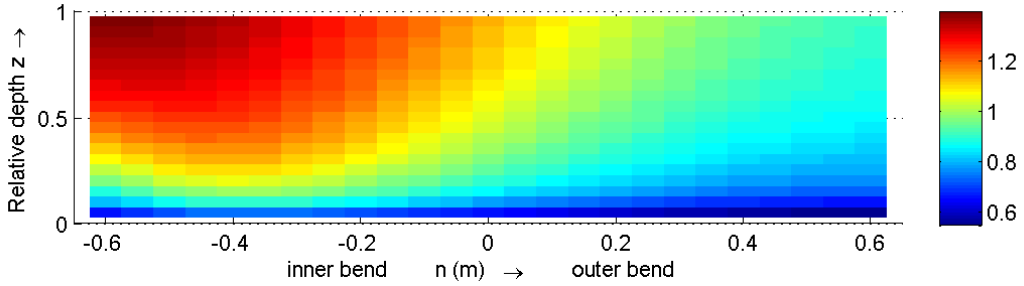

Figure 3-68 Downstream velocity in cross-section 060 according to simulation Q89_2_D3D, normalized by U_{bulk}

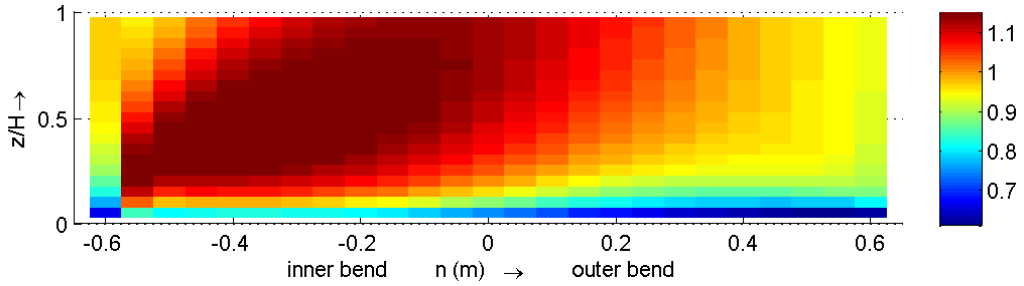

Figure 3-69 Downstream velocity in cross-section 150 according to simulation Q89_1_D3D, normalized by U_{bulk}

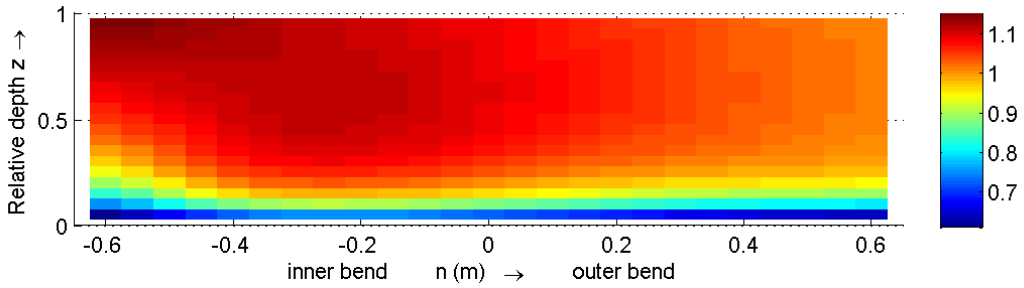

Figure 3-70 Downstream velocity in cross-section 150 according to simulation Q89_2_D3D, normalized by U_{bulk}

3.7.3 Transversal velocity

Figure 3-71 shows the depth averaged pseudo stream function (ψ) for both simulation Q89_1_D3D and simulation Q89_2_D3D. This pseudo stream function is a measure for the transversal velocities and is calculated as was explained in section 3.3. In the figure the same effects are visible as we saw in the Figure 3-66 of the downstream velocity. Peaks are lower and the velocities are more spread and smoothed. The shift of the core of the transversal velocities to the inner bend is nearly absent for simulation Q89_2_D3D. In the straight outflow, the transversal velocities vanish more rapidly. Along the bend the effect of the wall on the flow is larger. This is due to the larger momentum exchange in the horizontal direction. Taking a look at the cross-sectional plots of the transversal velocities by comparing Figure 3-72 and Figure 3-73, the differences observed in the depth averaged plots are also present. The increased viscosity causes more smoothing and lower peak values. Simulation Q89_1_D3D already underestimated the transversal velocities, simulation Q89_2_D3D does it even more because the momentum is more diffused.

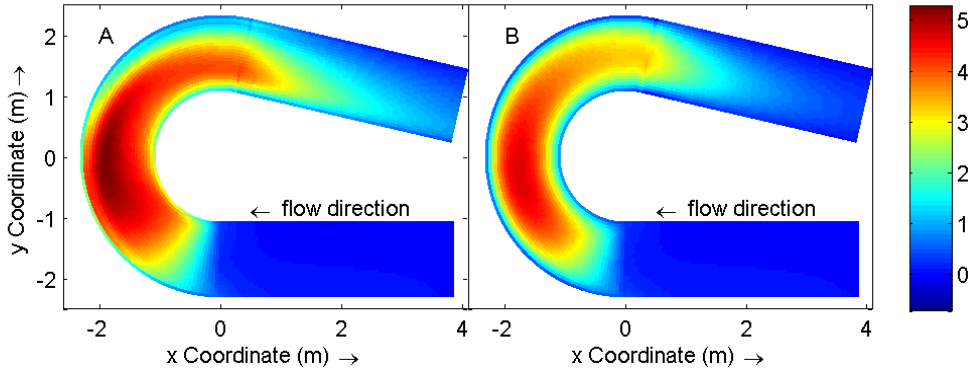

Figure 3-71 Comparison of the depth averaged pseudo stream function (100*ψ/(U_{bulk} H)), A is according to simulation Q89_1_D3D, B is according to simulation Q89_2_D3D

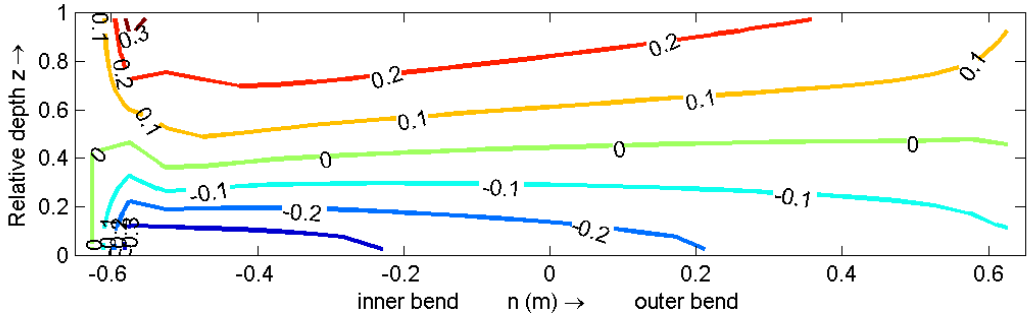

Figure 3-72 Normalized transverse velocity (v/U) according to simulation Q89_1_D3D, cross-section 060

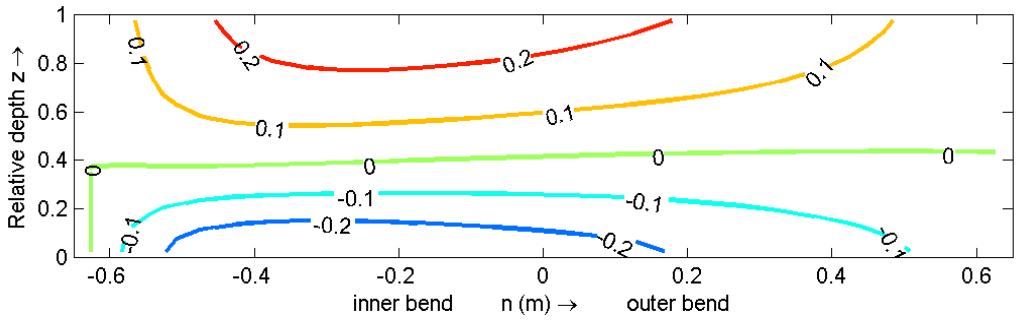

Figure 3-73 Normalized transverse velocity (v/U) according to simulation Q89_2_D3D, cross-section 060

3.7.4 Turbulent velocities

Because the turbulent stresses are determined with the use of the Boussinseq hypothesis which relates the eddy viscosity to the turbulent stresses, it is expected that an increase of the (horizontal) eddy viscosity results in an increase of the turbulent shear stresses. In Appendix D.3 the cross-sectional plots of the normalized turbulent shear stresses (velocities) are given for simulation Q89_2_D3D. The main differences between the Q89_1_D3D simulation and simulation Q89_2_D3D occur in the $\overline{u'w'}$ and $\overline{v'w'}$ shear stresses. The only difference in the $\overline{u'v'}$ stresses is an increase of the peak values in the bend and some smoothing in the straight inflow. In cross-section 060 (see Figure 3-75) the increase is significant (a three times higher peak value).

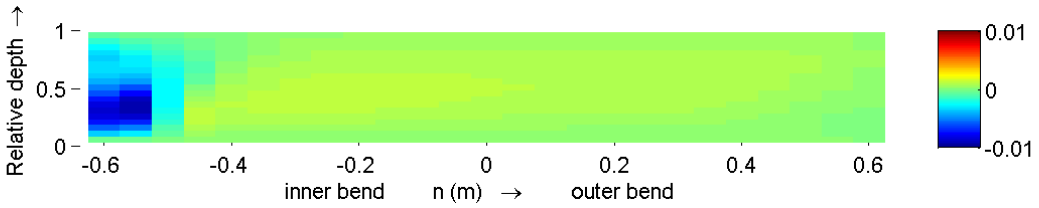

Figure 3-74 Normalized $\overline{u'v'}$ according to simulation Q89_1_D3D, cross-section 060, normalized by U_{bulk}^2

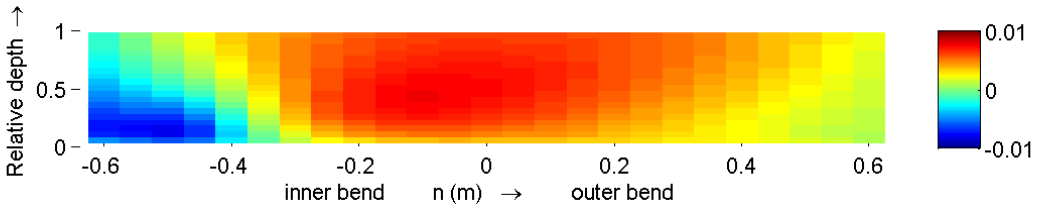

Figure 3-75 Normalized $\overline{u'v'}$ according to simulation Q89_2_D3D, cross-section 060, normalized by U_{bulk}^2

The magnitude of the shear stresses $\overline{u'w'}$ and $\overline{v'w'}$ is an order larger in simulation Q89_2_D3D than in simulation Q89_1_D3D (compare Figure 3-76 with Figure 3-77 and Figure 3-78 with Figure 3-79). The patterns are also changed. These changes can be clarified taking into account the Boussinesq hypotheses (equation (2.9)). The increase of the shear stresses $\overline{u'w'}$ and $\overline{v'w'}$ can be attributed to the change of the horizontal eddy viscosity which is an order larger in simulation Q89_2_D3D than in simulation Q89_1_D3D. The reason that the $\overline{u'v'}$ does not change so much can be clarified by the fact of the smoothing of the downstream velocity over the width. Because the gradients are smaller, the relative increase of the shear stresses $\overline{u'v'}$ is less than the relative increase of the eddy viscosity.

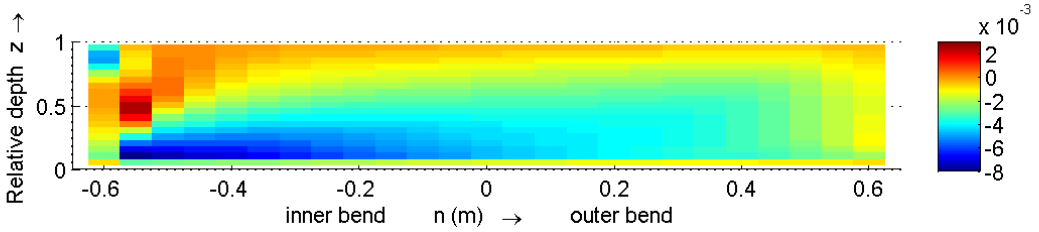

Figure 3-76 Normalized $\overline{u'w'}$ according to simulation Q89_1_D3D, cross-section 060, normalized by U_{bulk}^2

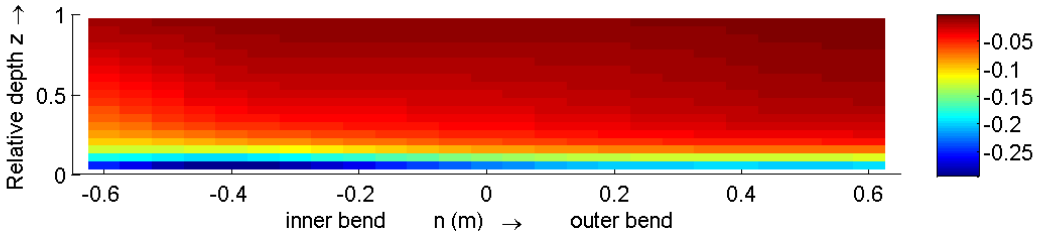

Figure 3-77 Normalized $\overline{u'w'}$ according to simulation Q89_2_D3D, cross-section 060, normalized by U_{bulk}^2

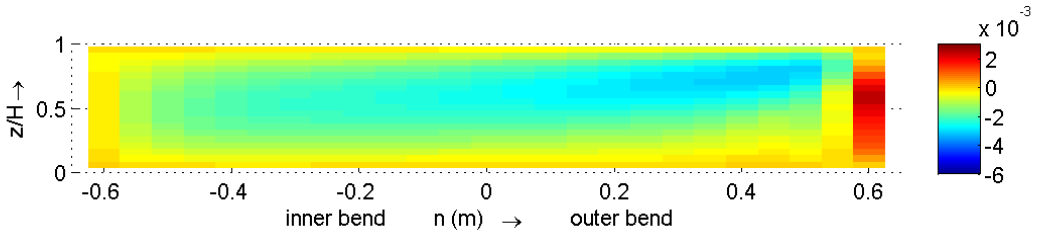

Figure 3-78 Normalized $\overline{v'w'}$ according to simulation Q89_1_D3D, cross-section 060 normalized by U_{bulk}^2

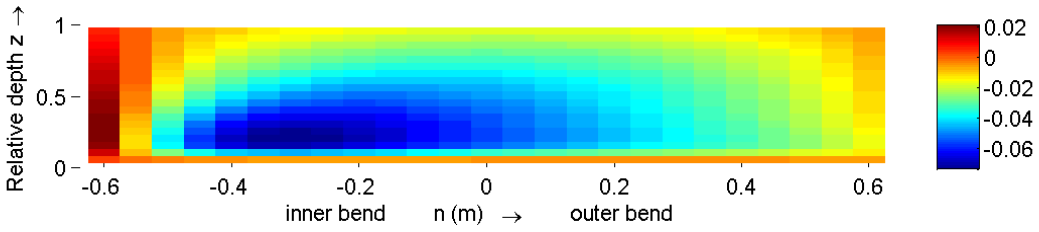

Figure 3-79 Normalized $\overline{v'w'}$ according to simulation Q89_2_D3D, cross-section 060, normalized by U_{bulk}^2

3.7.5 Turbulent kinetic energy

A plot of the depth averaged turbulent kinetic energy (TKE) is given in Figure 3-80. From this figure it is visible that an increase of the horizontal eddy viscosity results in a decrease of the depth averaged TKE. Along the bend and the outflow the TKE decreases. In Appendix D.4 the cross-sectional plots of simulation Q89_2_D3D are given for the cross-sections m25, 060 and 150.When comparing the 060 cross-sectional plots of the TKE of simulation Q89_1_D3D (Figure 3-81) and simulation Q89_2_D3D (Figure 3-82) it is visible that the peaks are lower in the case with increased viscosity and details are smoothed out and not any longer visible in the picture.

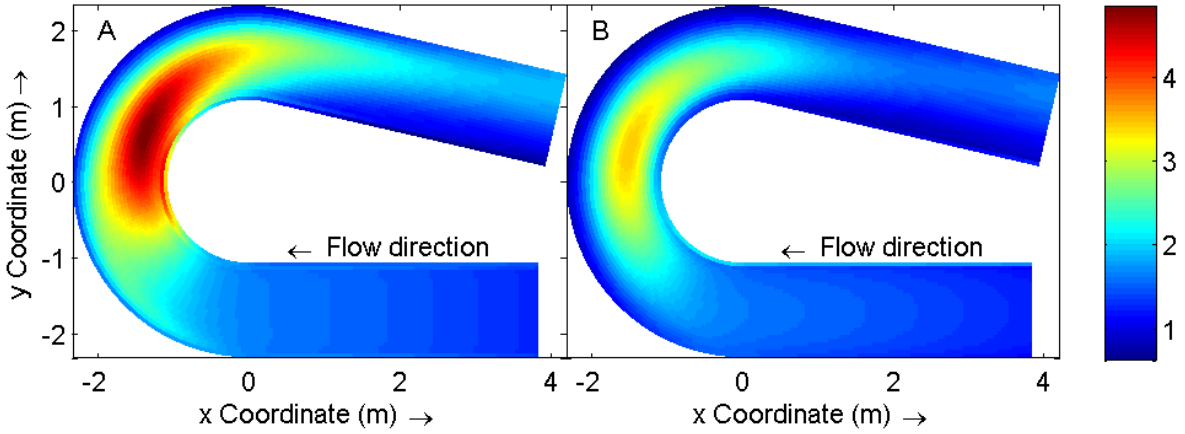

Figure 3-80 Normalized (by 0.5 * u_*^2) depth averaged turbulent kinetic energy , A is according to simulation Q89_1_D3D, B is according to simulation Q89_2_D3D

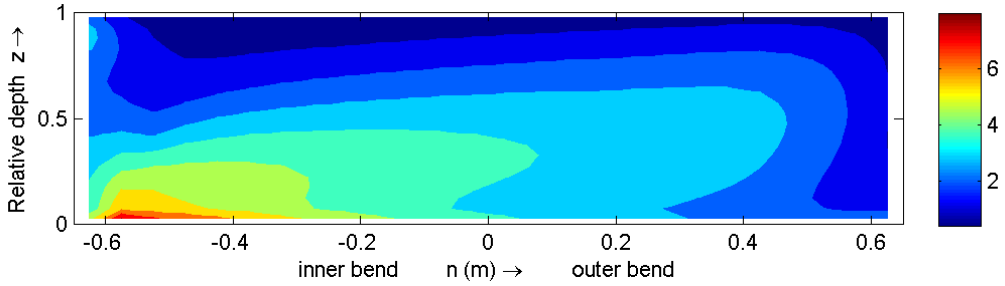

Figure 3-81 Turbulent kinetic energy (simulation Q89_1_D3D, 060), normalized by (0.5 * u_*^2)

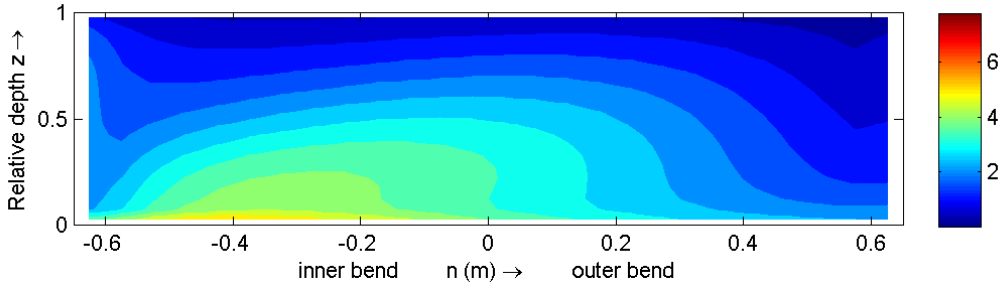

Figure 3-82 Turbulent kinetic energy (simulation Q89_2_D3D, 060), normalized by (0.5 * u_*^2)

3.8 Conclusion

It can be concluded from the analysis above that most flow quantities are well modelled by the Q89_LES (which is in accordance with the results of the research done by van Balen (2010)). Phenomena that occur in the flow are also visible in the results of the Q89_LES. Simulation Q89_1_D3DThe Delft3D-FLOW simulation, however gives less accurate results for certain details of the flow. It misses the secondary cells in the inflow and the outer-bank cell in the bend (which is a specific case of a secondary cell). The outward shift of the core of the flow is more or less absent too. It starts only at the end of the bend. The phenomena are visible in the downstream and transverse depth-averaged velocities of the Q89_LES and the measurements but not in the results of the Delft3D-FLOW simulation. Moreover, Delft3D-FLOW underestimates the transverse velocities in the lower part of the flume.

We analysed the downstream vorticity balance to see which terms cause the differences in the phenomena.

With respect to the different terms of the downstream vorticity balance, the following things can be said:

Vorticity is mainly generated along the walls, the internal shear layer and the borders of the outer-bank cell. The advection of the vorticity contributes to the distribution of this generated vorticity and therefore it is a relatively important term.

The centrifugal effects are very important and are strongly related to the transverse velocities. The centrifugal effects are important in the whole cross-section. It is a driving force in the outer-bank cell and the centre region cell. Besides that it is also important in the inner bank where the internal shear layer exists.

The anisotropy of the vertical and transverse turbulent velocities is in most of the cross-section unimportant, only along the boundaries it gains importance, which can be explained by the fact of the presence of the boundaries which cuts the possibility of the turbulent stresses to expand into the direction normal to the wall (because of the impermeable wall). In the outer-bank cell it initiates the distortion of the velocity profile which in its turn provides the centrifugal forces to drive the outer-bank cell.

The other terms of the downstream vorticity balance are less important for the estimation of the right transverse velocities.

Table 6-5 gives an overview of all terms, and shows which terms are under/over predicted by Delft3D-FLOW, and which terms are important in a specific area of a cross section. Table 6-5 holds only for the bend, not for the straight inflow or outflow.

	Under/Over predicted by Delft3D-Flow			**Relative importance**		
Term	**Inner Bend**	**Centre**	**Outer Bend**	**Inner Bend**	**Centre**	**Outer Bend**
ADV	-	Under	Under	Important	Important	Important
CFG	Slightly Under	Under	Under	Important	Important	Important
ISO	-	Under	-	Important	Important	UnImport.
HOM	Under	Under	Under	UnImport.	UnImport.	UnImport.
SKW	Under	Under	Under	Important	Important	UnImport.
DNU	-	Under	Under	UnImport.	UnImport.	UnImport.

Table 6-5 Overview of different terms

The turbulent stresses are better estimated by the Q89_LES than by Delft3D-FLOW, this holds particularly for the $\overline{u'v'}$ turbulent stresses which are important for momentum exchange between the downstream and transverse velocities. The poor estimation of the turbulent stresses by Delft3D-FLOW is caused by the way the eddy viscosity is determined. Use is made of a k-epsilon model which is unable to predict anisotropic turbulent stresses. These anisotropic turbulent stresses initiate the outer-bank cell.

The turbulent kinetic energy is overestimated by both the Q89_LES and simulation Q89_1_D3D.

The horizontal eddy viscosity is taken equal to the vertical eddy viscosity in simulation Q89_1_D3D. During simulation Q89_2_D3D, the horizontal eddy viscosity is approximately constant and is taken an order of magnitude larger than the vertical eddy viscosity. From simulation Q89_2_D3D it follows that an increase of the viscosity results in more smoothing and lowering of the peaks of the velocities due to the increased exchange of momentum. The transverse velocities are underestimated by simulation Q89_1_D3D and simulation

Q89_2_D3D. The underestimation increases when increasing the (horizontal) eddy viscosity. The eddy viscosity is a measure for a part of the momentum exchange in a turbulent flow. In this way it can be clarified that the increase of the horizontal eddy viscosity results in more smoothed distribution of the velocities. The value of the eddy viscosity is flow depended but it is also a variable that influences this flow. The vertical eddy viscosity in the Delft3D-FLOW simulations is determined by the k-ε model and in this way flow dependent (depends on transport of k and ε).

The viscosity is used to predict the turbulent stresses. As we saw in section 3.7, a change of the viscosity results in a relatively large change of the turbulent stresses (especially the $\overline{u'w'}$ and $\overline{v'w'}$ stresses). The turbulent stresses did not match with the measured turbulent stresses too. We also saw that the details of the flow are smoothed out.

4 Results of the equilibrium-bed case

In chapter 3 we have analyzed the flat-bed case by comparing the experiment (conducted at the EPFL) with the LES (conducted at the TU Delft) and the Delft3D-FLOW simulation. In this chapter the equilibrium-bed experiment (M89) will be compared with the results obtained from the simulations (both the M89_LES and the M89_1_D3D). This is done to see how the simulations perform in more practical problems. Most settings for the simulations have the same value as for the flat-bed simulation. The settings for the simulations are described in section 2.3 and Table 2-4. The structure of this chapter is approximately the same as in chapter 3. The first section contains the discussion of the water level, the second section is dedicated to the comparison of the downstream velocity. After that the transverse velocities are compared. Section 4.4 contains the comparison of the turbulent stresses and in the last section some conclusions are drawn.

4.1 Water level

Figure 4-1 shows us both the measured water level according to the Q89 and M89 experiment. The streamwise water level gradient according to the M89 measurements changes a lot compared to the water level gradient of the Q89 experiment. The water level difference over the total length of the flume for the Q89 is 0.1628m – 0.1508 m = 0.0120 m (measured from cross-section m25 to p35). If we compare this with the water level difference of the M89 (0.1422 m – 0.1194 m = 0.0228 m), it appears that the downstream water level gradient of the M89 experiment is much larger than the downstream water level gradient according to the Q89 experiment. This can be explained by the fact that in the M89 experiment the bottom is formed by morphological mechanisms which increased the bed roughness due to the formation of ripples and dunes. Due to the increased resistance, a larger downstream gradient is needed to convey the same flow. The tilting of the water level is also visible in the results of the M89 experiment.

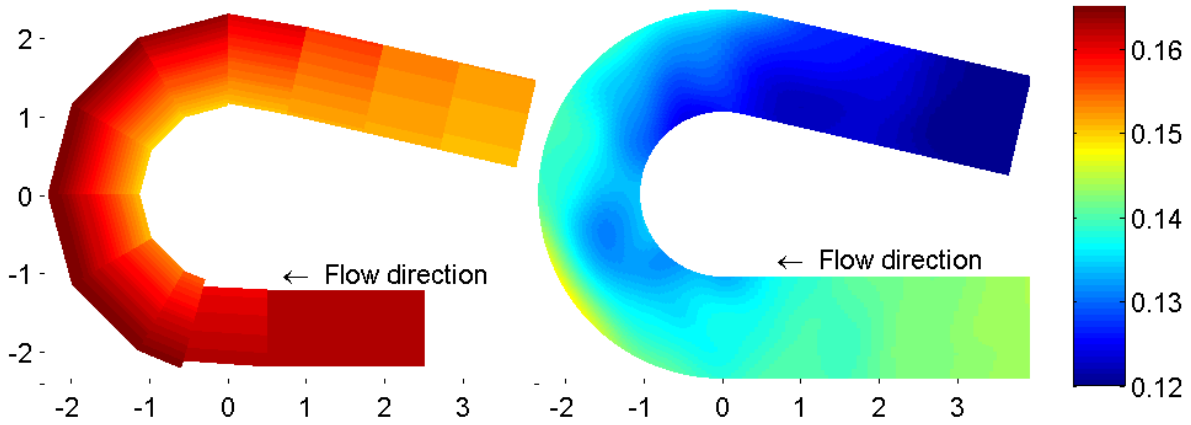

Figure 4-1 Water level according to measurements (left: Q89, measured with ADVP at cross-sections, right: M89, measured with limni meter at a 1 cm * 5 cm grid)

It is assumed that the vertical accelerations are relatively unimportant compared to the pressure in the vertical momentum balance. If this is true, the water level according to the M89_LES can be determined from the pressures with the help of the hydrostatic pressure assumption. The water level according to the M89_LES is calculated according to the following relations (the same as were used in section 3.1, equations (3.1)):

$$\frac{\partial h}{\partial r} = \frac{1}{\rho g}\left(\frac{\partial p}{\partial r}\right)_s \qquad \text{and} \qquad \frac{\partial h}{\partial r} = \frac{1}{\rho g}\left(\frac{\partial p}{\partial \theta}\right)_s$$

The averaged pressure is related to the average water level of 0.141 m (taken from the measurements). The result is shown in Figure 4-3.

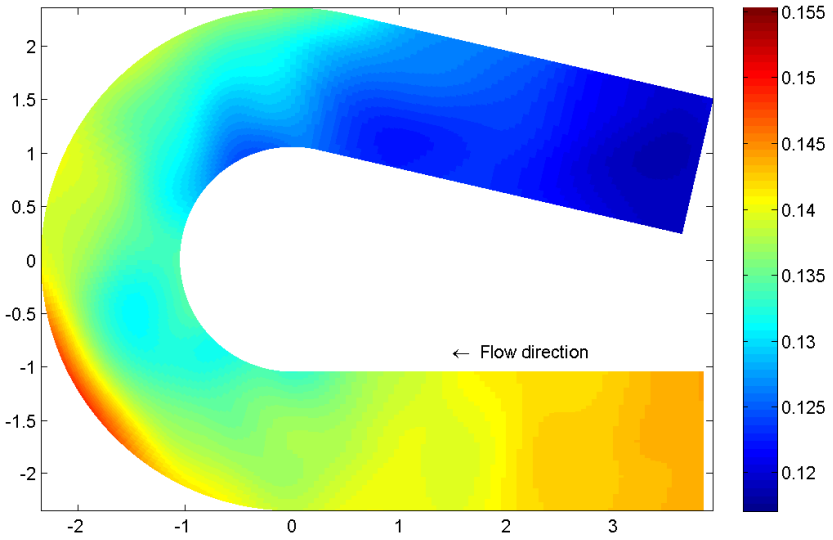

Figure 4-2 Water level according to measurements (M89, measured with limni meter)

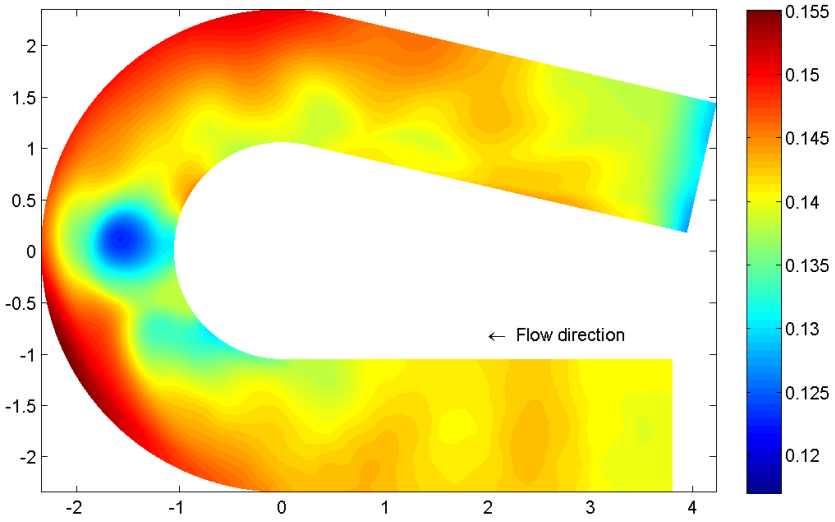

Figure 4-3 Water level according to the M89_LES

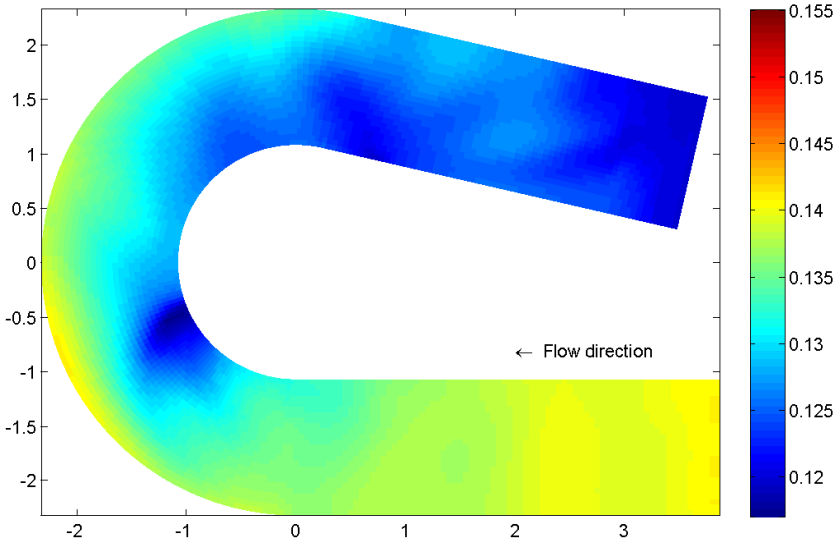

Figure 4-4 Water level according to simulation M89_1_D3D (M89)

Comparing the water level according to the measurements (see Figure 4-2) with the results of the M89_LES and simulation M89_1_D3D (see Figure 4-3 and Figure 4-4) the predictions are less accurate than they were for the flat-bed case. The water level according to the M89_LES is in most places higher than according to the measurements. Around the 090 cross-section the water level shows a dip which is barely visible in the measurements. Another difference is the high water level in the outflow and the high gradient at the very end of the flume. The measurements and simulation M89_1_D3D seems to be more comparable. Simulation M89_1_D3D underestimates the water level a little, especially along the outer bend. A strong decrease of the water level is visible in the inner bend like the dip we saw in the results of the M89_LES. This decrease is larger for simulation M89_1_D3D than according to the measurements.

Looking at the transverse water levels (Figure 4-5) we see that the water levels and the slopes in the straight inflow are nearly equal for all three data sets. At cross-section 060 the measurements show a dip along the whole width. The M89_LES shows a dip only at the inner bend (this is the beginning of the dip we came across in Figure 4-3) and simulation M89_1_D3D does not show a dip but only a water level with a nearly constant slope. The over prediction by the M89_LES is visible in the cross-sections 060, 150 and p13. In cross-section 150 the slopes of the M89_LES and the measurements are almost equal, the water level slope according to simulation M89_1_D3D is less steep as was measured which can be due to the relatively large eddy viscosity which smoothes out the downstream velocity and in that way, one of the driving mechanisms of the secondary flow, the centrifugal force. In the straight outflow (cross-section p13) the slope for all three data sets is almost equal. As a final remark it can be said that the dip in the water level is the most notable feature observed in the water level.

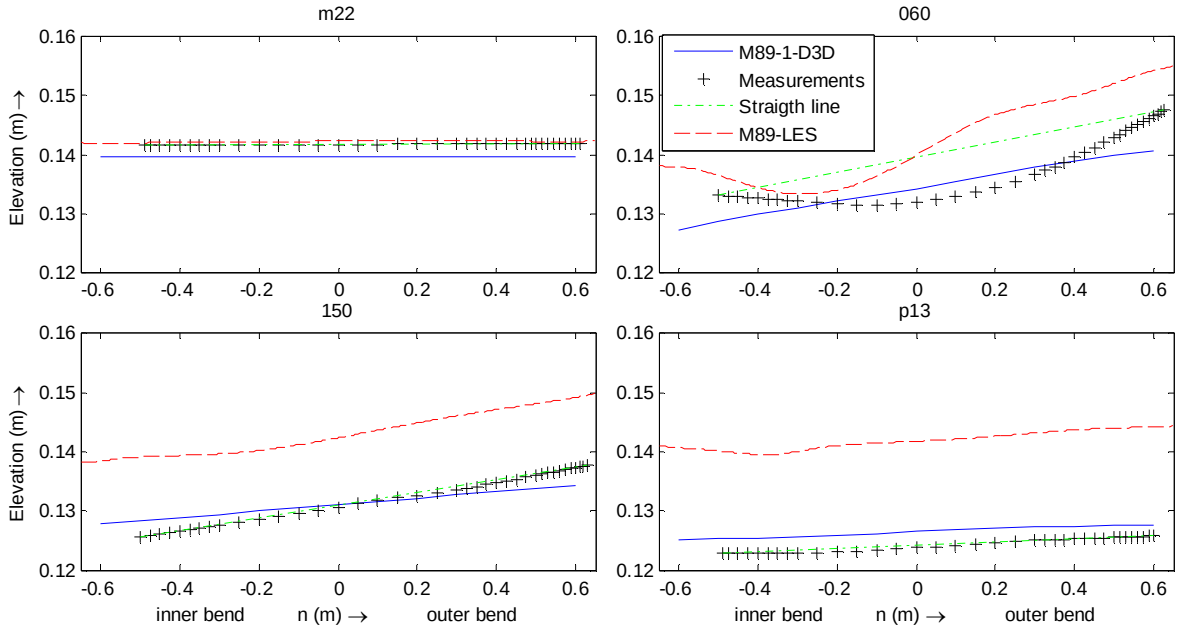

Figure 4-5 Transverse water levels of measurements at different cross-sections. The green dashed line is a linear line between the measured water level at the inner and outer bend

4.2 Downstream velocities

This section contains the comparison of the downstream velocity of all three datasets. Firstly we will see how the change of the bed topography from a flat-bed to the equilibrium-bed affects the downstream velocity.

Generally spoken, the depth averaged downstream velocity of the M89 experiment is larger than according to the Q89 experiment. Especially at the entrance of the flume and the bend, the velocities are larger. While the Q89 experiment shows an outward shift of the core of the downstream velocity, the M89 shows a shift of the core towards the inner bend. Between cross-section 060 and 120 the depth averaged downstream velocities along the inner bend are much smaller for the M89-experiment compared to the Q89-experiment. Blanckaert (2009) observed in this region a recirculation cell, which explains the very low velocities. The water level gradient in this region is very small and even in upstream direction (also visible in Figure 4-1 B). Together with the existence of the recirculation zone, this can explain the very small downstream velocities.

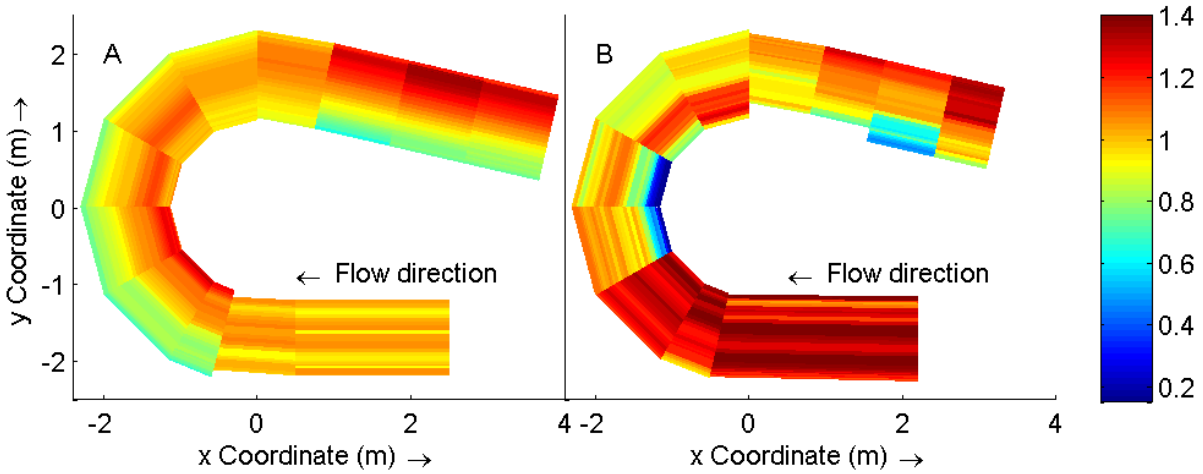

Figure 4-6 Depth averaged downstream velocity normalized by U_{bulk} according to measurements (A: Q89, B: M89)

Figure 4-7 to Figure 4-9 represent the depth averaged downstream velocities according to the M89-experiment, the M89_LES and the M89_1_D3D simulation. For all three data sets the depth averaged downstream velocity is quite uniformly distributed over the width in the straight inflow. It seemed that the total flow through the cross-section is underestimated by simulation M89_1_D3D. This is checked by integrating the velocity over the 060 cross-section to calculate the total flow through the cross-section. The flow is determined at 0.090 m^3/s which is about the upstream boundary condition of 0.089 m^3/s.

The flow according to the measurements is determined by integration and is about 0.092 m^3/s for cross-section 060. The integration is done with the trapezoidal rule in both the vertical and horizontal direction. The calculated flow is approximately the same as the upstream boundary condition of 0.089 m^3/s.

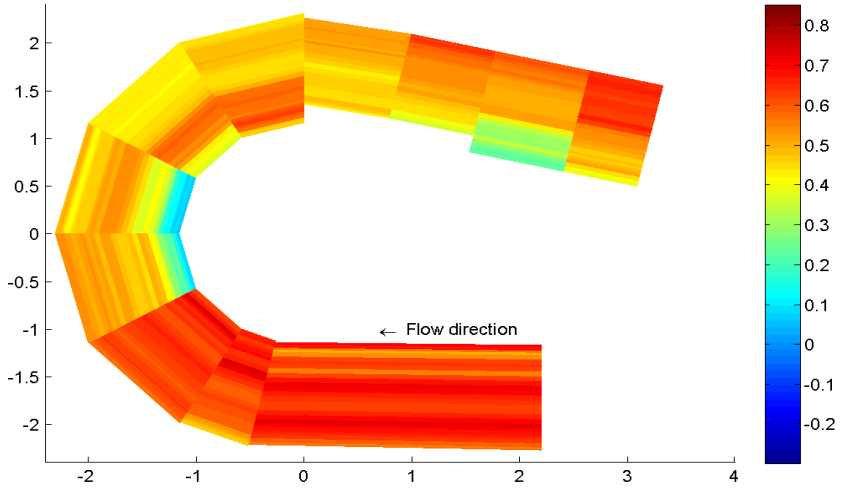

Figure 4-7 $U_{depth\ averaged}$, according to the measurements

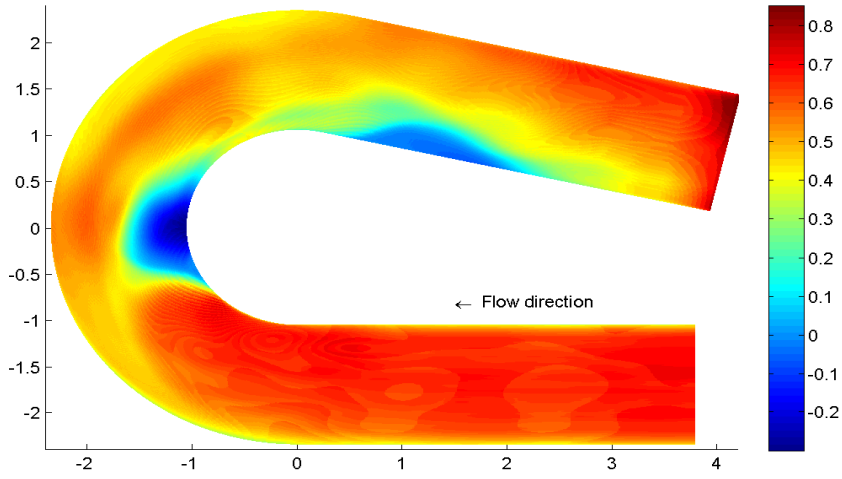

Figure 4-8 $U_{depth\ averaged}$, according to the M89_LES

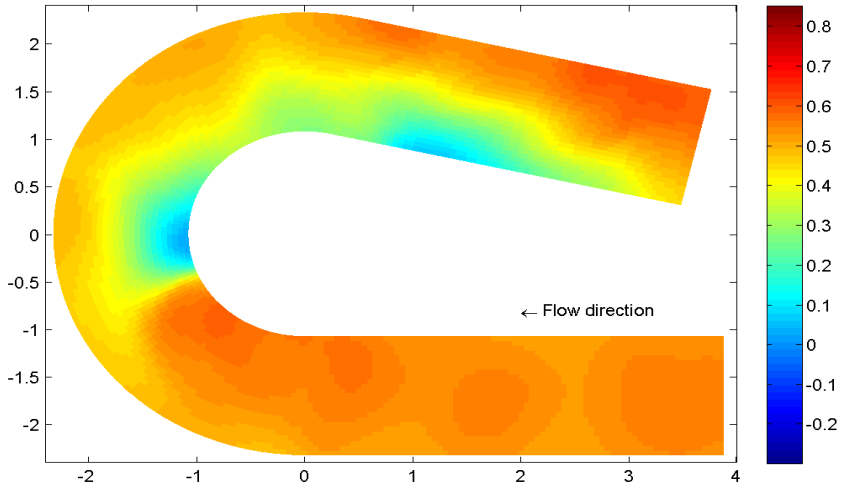

Figure 4-9 $U_{depth\ averaged}$, according to simulation M89_1_D3D

A further investigation of the figures shows two regions with a decrease of the downstream velocity. One strong decrease in the inner bend around the 090 cross-section and an other in the straight outflow along the inner wall. For the M89_LES the decrease of the velocity leads to negative flow velocities.

The negative streamwise velocities were also observed by Blanckaert (2009) but it is not clear from Figure 4-7 because the dip falls in between two cross-sections. It seems that the strong gradient of the streamwise velocities in the M89_LES results is partly caused by the bottom topography, in literature also called '*topographic steering*' (van Balen, 2010).

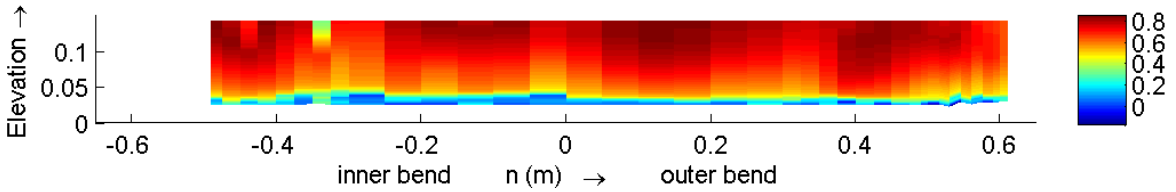

Figure 4-10 Downstream velocity according to the measurements, cross-section m22

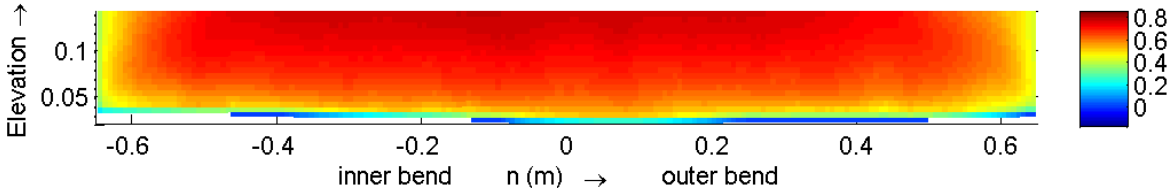

Figure 4-11 Downstream velocity according to the M89_LES, cross-section m22

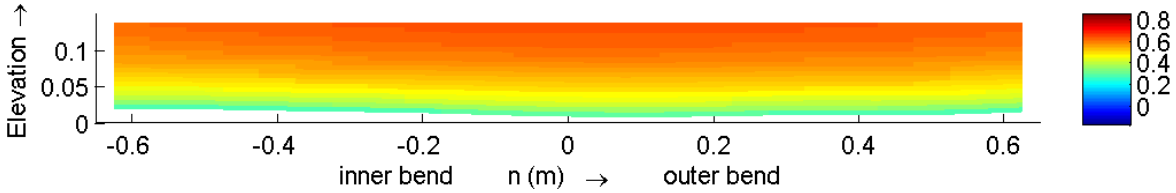

Figure 4-12 Downstream velocity according to simulation M89_1_D3D, cross-section m22

In the cross-sectional plot of the straight inflow (Figure 4-10 to Figure 4-12) the under prediction of the downstream velocity by simulation M89_1_D3D is clear. This underestimation is about 30 %. The M89_LES underestimates the downstream velocities as well but this underestimation is only a few percentages. The same is found in cross-section 060 (Figure 4-13 to Figure 4-15). The core of the streamwise velocity is situated in the centre of the flume. More toward the inner bend, the streamwise velocities decrease for both the measurements and the LES but not for the Delft3D-FLOW simulation.

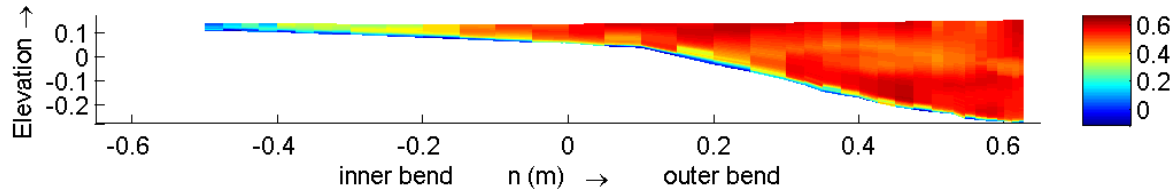

Figure 4-13 Downstream velocity according to the measurements, cross-section 060

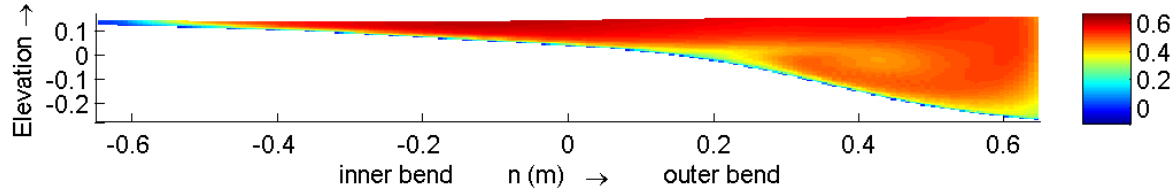

Figure 4-14 Downstream velocity according to the M89_LES, cross-section 060

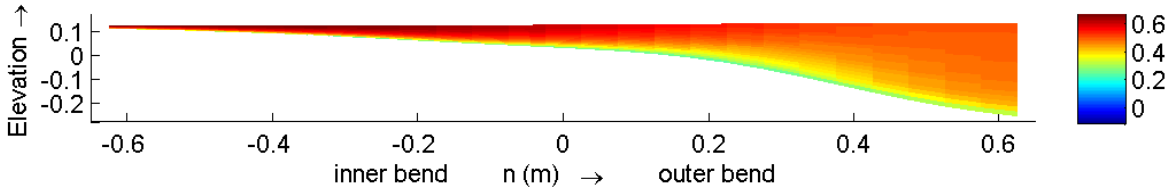

Figure 4-15 Downstream velocity according to simulation M89_1_D3D, cross-section 060

In cross-section 150 (Figure 4-16 to Figure 4-18) simulation M89_1_D3D still underestimates the downstream velocities. The core of the downstream velocity according to the measurements and the M89_LES is in the centre of the flume while it is in the deep part of the flume according to simulation M89_1_D3D. The M89_LES and measurements show a somewhat decreased downstream velocity compared to the strength in cross-section 060. This is in accordance with what was found in the depth averaged downstream velocity figures (Figure 4-7 and Figure 4-8).

For the equilibrium-bed experiment we can conclude that the LES estimates the downstream velocities better than Delft3D-FLOW. The downstream velocities are underestimated by Delft3D-FLOW and along the bottom the gradient is less steep because of the relative high viscosity. In the first half of the bend, the pattern is about the same as what was measured but changes in the last part of the bend. The core of the downstream velocity is situated in the deeper part of the flume according to Delft3D-FLOW while it is situated in the centre of the flume according to the measurements and the LES.

We can conclude that all three datasets show a kind of recirculation zone in the inner bend. Simulation M89_1_D3D underestimates the downstream velocities.

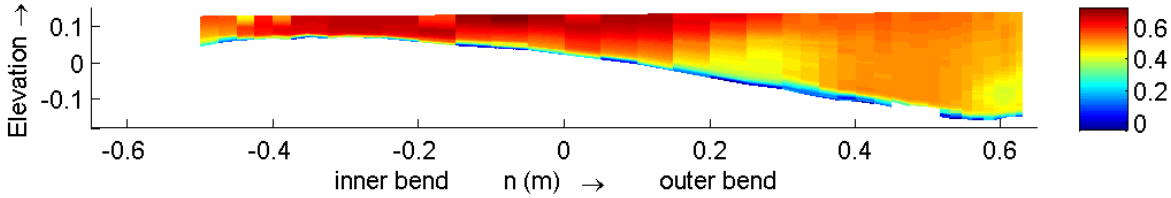

Figure 4-16 Downstream velocity according to the measurements, cross-section 150

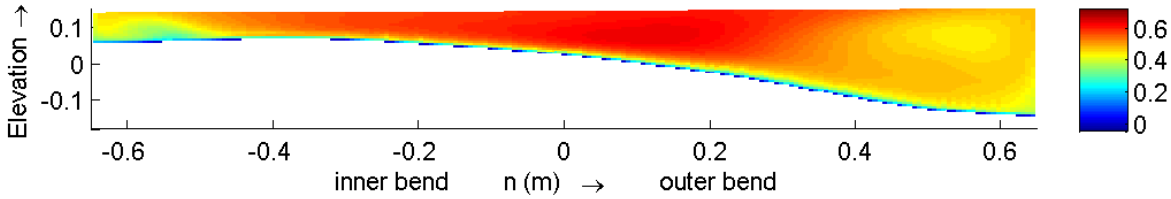

Figure 4-17 Downstream velocity according to the M89_LES, cross-section 150

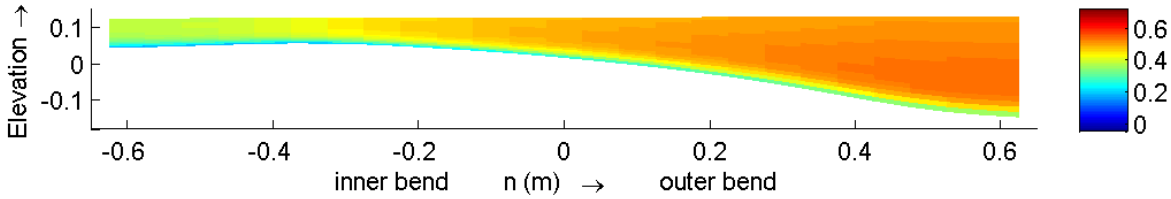

Figure 4-18 Downstream velocity according to simulation M89_1_D3D, cross-section 150

4.3 Transverse velocities

To gain insight in the distribution of the transverse velocity over the flume, use is made of the depth averaged pseudo stream function ψ as described in section 3.3. For the downstream velocity we saw larger velocities in the equilibrium-bed case than in the flat-bed case. For the depth average pseudo stream function ψ this is also true (see Figure 4-19). The difference start around cross-section 060 where ψ increases a lot in the outer bend for the equilibrium-bed case. From cross-section 090 the inner bend till the end of the flume, ψ shows large negative values. This suggest that the flow circulates in the other direction. A possible reason can be found in steering by the bottom topography. The start of the negative strip is at the point just after the deep dip in the water level.

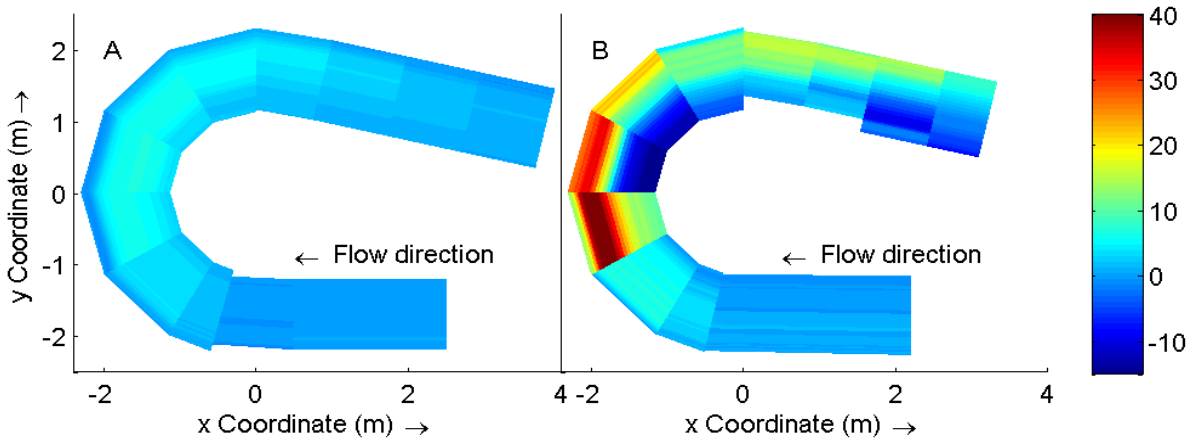

Figure 4-19 Normalized pseudo stream function (100*ψ/(U_{bulk}*H)); A: Q89, B: M89

The result for the depth averaged pseudo stream function is shown in Figure 4-20 to Figure 4-22 for the measurements, the LES and the Delft3D-FLOW simulation, respectively. The comparison between the LES and the measurements is quite good. Only some differences are visible at the locations where the flow approaches the critical velocity. Both data sets show a clear increase of ψ in the outer bend. The results of simulation M89_1_D3D are less accurate. The pseudo stream function ψ is largely underestimated in comparison to the measurements. A small increase of ψ is visible in the first half of the bend, starting at the centre line and ending at the inner bend.

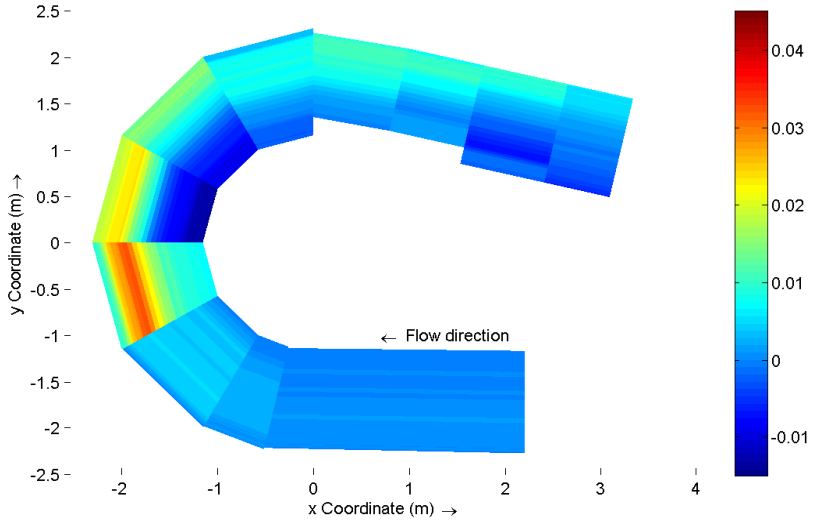

Figure 4-20 Distribution of the depth averaged pseudo stream function ψ, according to the measurements (not normalized)

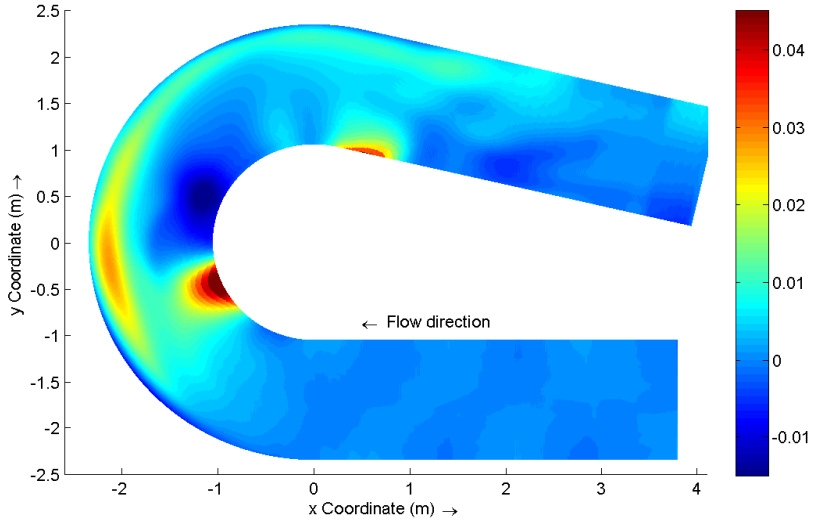

Figure 4-21 Distribution of the depth averaged pseudo stream function ψ, according to the M89_LES (not normalized)

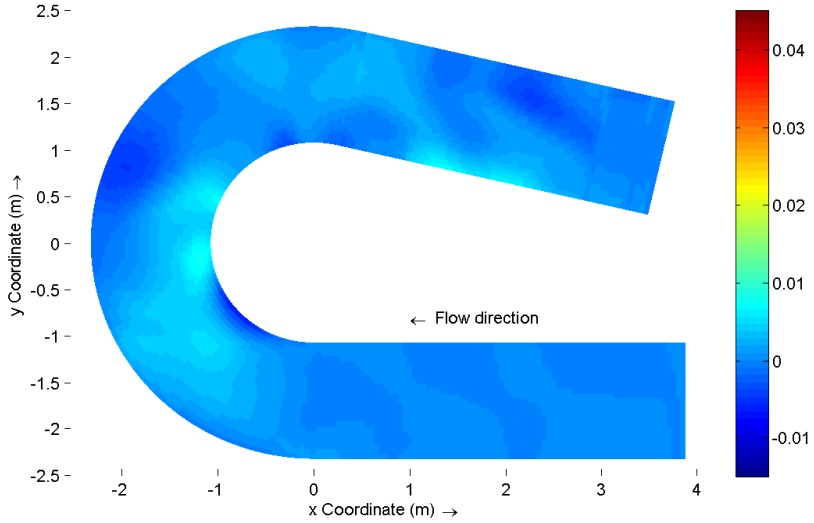

Figure 4-22 Distribution of the depth averaged pseudo stream function ψ, according to simulation M89_1_D3D (not normalized)

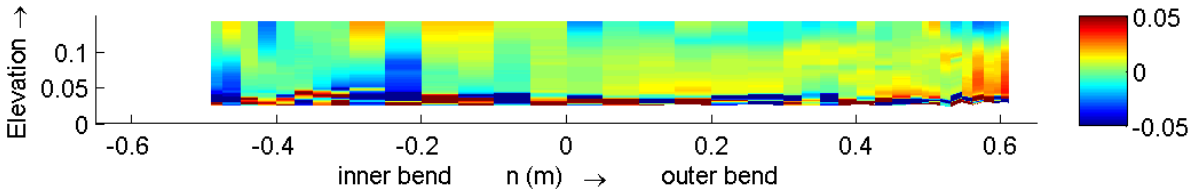

Figure 4-23 Transverse velocity according to the measurements, cross-section m22

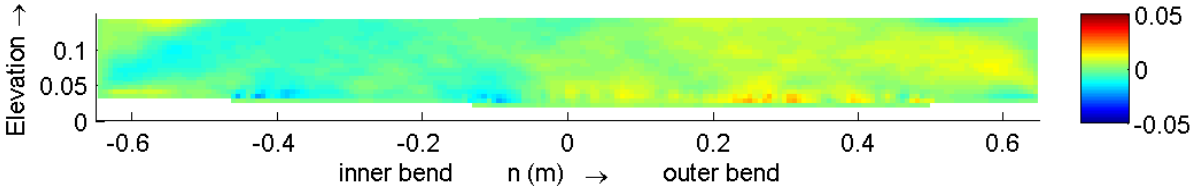

Figure 4-24 Transverse velocity according to the M89_LES, cross-section m22

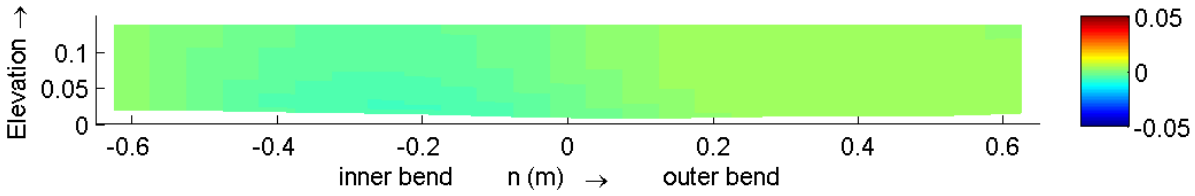

Figure 4-25 Transverse velocity according to simulation M89_1_D3D, cross-section m22

When looking at the cross-sectional plots (see Figure 4-23 to Figure 4-25), we see in the inflow some fluctuations, which are larger for the measurements than for the M89_LES and which are absent in the results of simulation M89_1_D3D. The fluctuations do not show the clear pattern of the secondary cells which was visible in results of the flat-bed experiment.

Cross-section 060 shows the primary secondary circulation cell (see Figure 4-26 to Figure 4-28). This cell is concentrated in the deep part of the flume. The outer-bank cell is not well visible in the results of the measurements. In the equilibrium-bed case, the LES is also not able to predict the transverse velocities exactly, it underestimates the transverse velocities. In the shallow part (the inner bend) the transverse velocity in the outward direction dominates. This results in a net outward flow which is present in at the start of the bend where the flow adapts to the bend. Both simulations underestimate the transverse velocities, the underestimation by simulation M89_1_D3D is 50% and is more than according to the M89_LES.

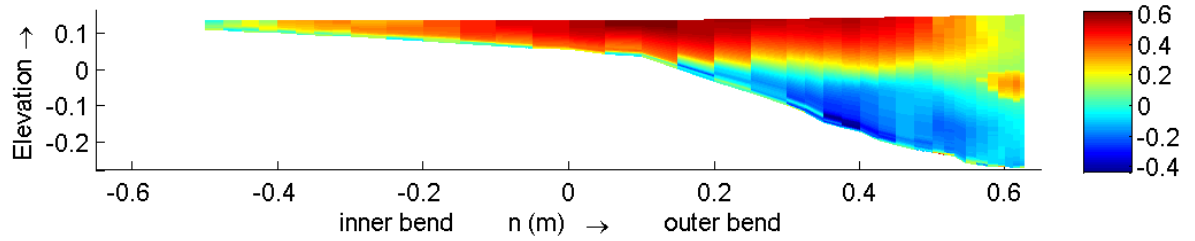

Figure 4-26 Transverse velocity according to the measurements, cross-section 060

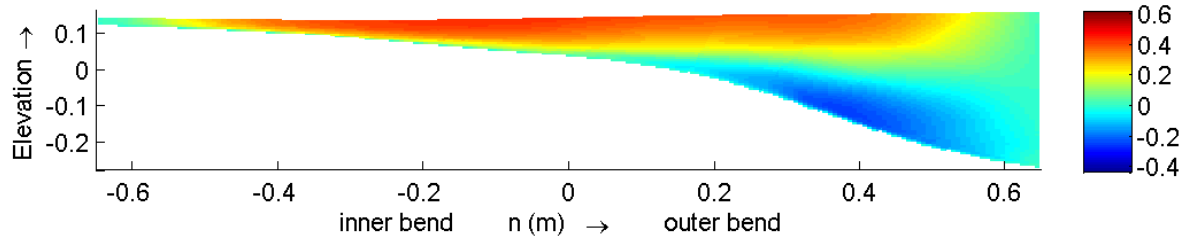

Figure 4-27 Transverse velocity according to the M89_LES, cross-section 060

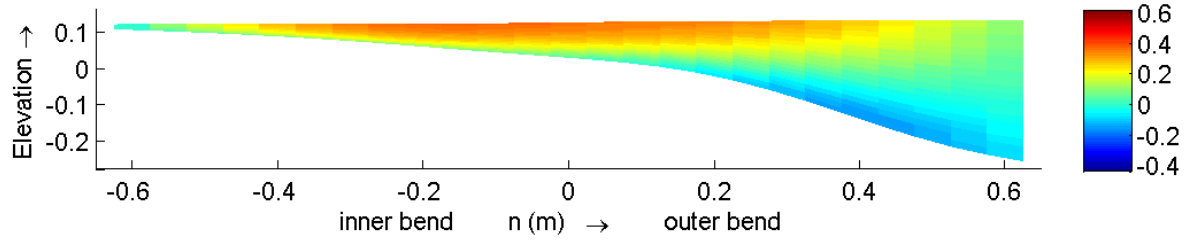

Figure 4-28 Transverse velocity according to simulation M89_1_D3D, cross-section 060

In cross-section 150 (Figure 4-29 to Figure 4-31) the primary secondary cell is completely situated in the deep part of the flume. The outer-bank cell has nearly vanished in the results of the measurements and the M89_LES and simulation M89_1_D3D does not show anything of the outer-bank cell. The transverse velocities in the inner part are strongly reduced. This is in accordance with the idea that the flow is adapted to the bend in this cross-section. The M89_LES gives approximately the same results as the measurements. The estimated

transversal velocities according to simulation M89_1_D3D are an order of magnitude smaller and so is the strength of the secondary cell. An explanation can be found in the decrease of the transversal water level gradient and the distribution and strength of the downstream velocity which both differs from what was measured. In general, it can be said that both the M89_LES and the M89_1_D3D simulation underestimate the transverse velocities. The underestimation increases in the second half of the bend and is larger for the M89_1_D3D than for the M89_LES.

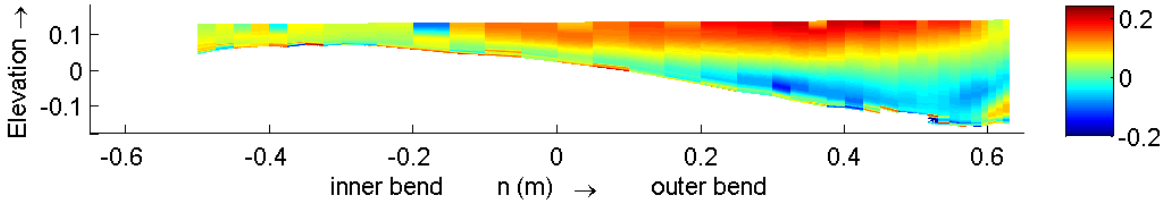

Figure 4-29 Transverse velocity according to the measurements, cross-section 150

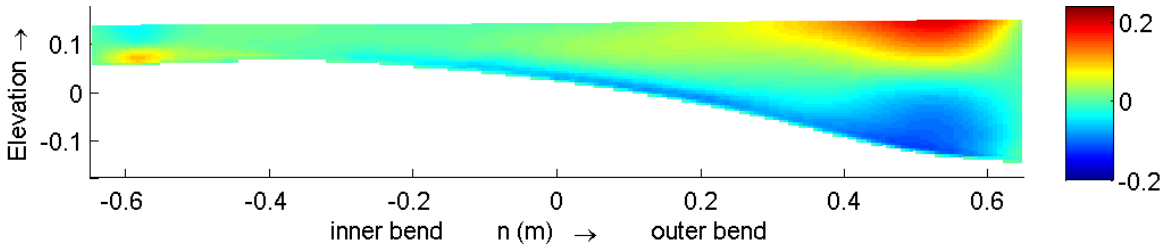

Figure 4-30 Transverse velocity according to the M89_LES, cross-section 150

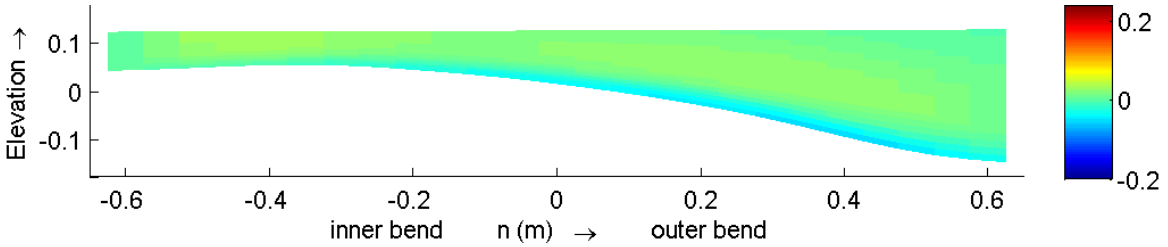

Figure 4-31 Transverse velocity according to simulation M89_1_D3D, cross-section 150

4.4 Turbulent stresses

Appendix E.3 shows some cross-sectional plots of the turbulent stresses. In this section we will particular focus on the turbulent velocities $\overline{u'v'}$. In Figure 4-32 to Figure 4-34 the turbulent $\overline{u'v'}$ velocities are given for cross-section 060. It is difficult to recognize clear patterns which are visible in more than one data set. For most of the flume, both the M89_LES and simulation M89_1_D3D gives a different prediction of the turbulent stresses. Even the strength of the stresses is an order of magnitude smaller than was measured. Simulation M89_1_D3D gives a more course and smoothed picture which is partly due to the relatively high horizontal eddy viscosity (10^{-2} m^2/s) and partly because of the course grid used. Van Balen (2010, chapter 8) concluded that a change of the bottom roughness mainly results in a change in the magnitude of the bottom shear stresses and not in a change in the distribution of the bottom shear stresses. Because the bottom shear stresses causes turbulence and turbulent stresses, it can be of importance to have a better prediction of the flow along the bottom. In both simulations the bottom and walls were modelled by the standard law-of-the-wall which defines the distance from the wall where the velocity is assumed to be zero. In reality there is more to do in the boundary layer, especially in the case of a morphologically

developed bed with dunes and ripples. Turbulence is created along the dunes and ripples and this will probably affect the distribution of the turbulent stresses.

Most turbulent stresses are underestimated by both the M89_LES and M89_1_D3D simulation. The patterns of the distribution are not comparable either. For the LES this is probably caused by shortcomings of the bottom boundary and for the Delft3D-FLOW simulation the turbulence model plays also a role.

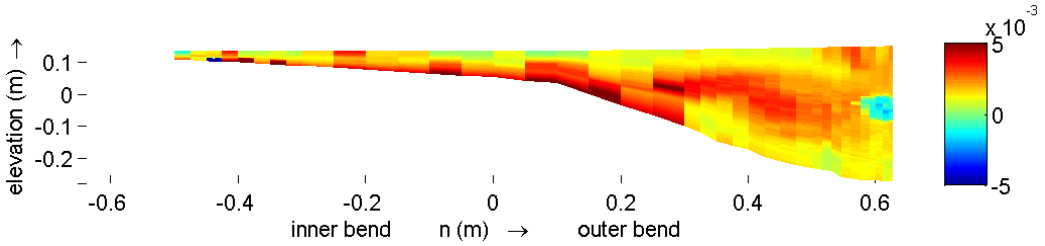

Figure 4-32 Turbulent velocity $\overline{u'v'}$ according to the measurements, cross-section 060

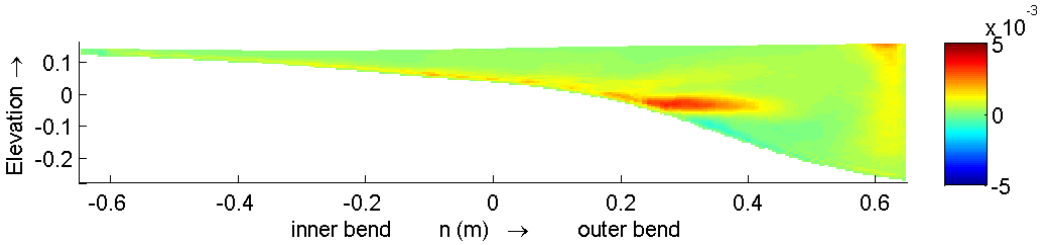

Figure 4-33 Turbulent velocity $\overline{u'v'}$ according to the M89_LES, cross-section 060

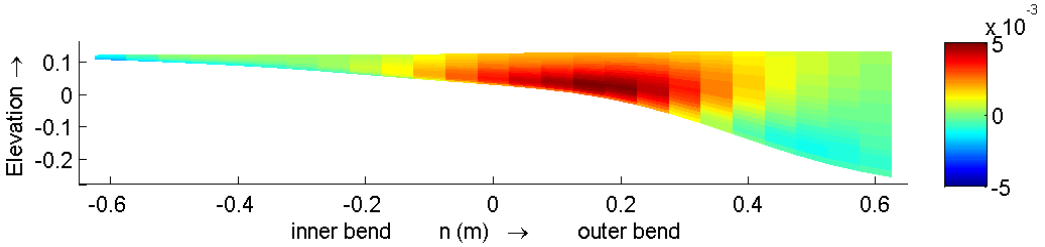

Figure 4-34 Turbulent velocity $\overline{u'v'}$ according to simulation M89_1_D3D, cross-section 060

4.5 Conclusion

In chapter 4 the results of the simulations (LES and Delft3D-FLOW) and the measurements for the equilibrium-bed were analyzed. The water level, the downstream and transverse velocities and the turbulent stresses were compared. In the comparison, the water level according to the LES differs most from what was measured. The water level is overestimated and shows a deep dip in the inner bend. The comparison with the Delft3D-FLOW simulation is better. The deep dip in the inner bend is also visible in the results of the Delft3D-FLOW simulation. The measurements show a dip too but this dip is less deep. The transverse gradients of the water level according to the Delft3D-FLOW simulation are flatter than what was measured.

From the comparison of the downstream velocities it can be concluded that these velocities are underestimated by Delft3D-FLOW but the distribution is comparable. The comparison with the LES is at most places relatively good. There are two places with a strong reduction of the downstream velocity visible in the depth averaged downstream velocity plots of the LES. One strong decrease in the inner bend around the 090 cross-section and an other in the straight outflow along the inner wall. These reductions are larger for the LES than for the

measurements. The water flows even in opposite direction in the inner bend (a recirculation zone). This reduction of the flow was also visible in the results of the measurements and in the results of simulation M89_1_D3D. This is partly caused by topographic steering because the bottom level is relatively high in that area.

The outer-bank cell is not any longer clearly visible in the transverse velocities of the measurements or the LES for the equilibrium-bed case. The predictions of the transverse velocities by simulation M89_1_D3D are even more underestimated than they were for the flat-bed case. Especially in the second half of the bend the secondary circulation disappears nearly completely in the Delft3D-FLOW simulation. This can partly be explained by the decrease of the transverse water level gradient and the distribution and strength of the downstream velocity which are the main driving mechanisms for the secondary circulation and both differ from what was measured. The LES gives better predictions but the transverse velocities are underestimated in the second half of the bend too.

The last quantities which were analyzed were the turbulent stresses. The comparison between the measurements on the one hand and both the M89_LES and simulation M89_1_D3D on the other hand, is poor. The strength is one order of magnitude underestimated and the patterns does not compare well either for both simulations. The cause of this mis-match can be the way the bottom boundary is schematized. The wall is modelled with the standard-law-of-the-wall which determines the distance from the wall where the velocity is zero. In reallity it is expected that there is more to do, especially in the case of the equilibrium-bed where dunes and ripples were present. It is possible that these morphologic features will create turbulence and affect the flow in an other way than is predicted by the law-of-the-wall. It must be said that the small-scale dunes and ripples were not visible in the measured equilibrium-bed in spite of the relatively fine measuring grid.

5 Discussion

5.1 Uncertainties in measured quantities

In this section some remarks are given on the possible errors in the measured data. For an extended review of the error sources you are referred to Blanckaert (2009, section 2.3 – 2.5).

Uncertainty in the experimental data set may be caused by a variety of factors, which may vary in space and in time. For ADVP measurements, for example, potential causes include the inaccuracy in the positioning of the instrument, the geometric and electronic configurations and the acoustic scattering level of the fluid.

Another possible error sources is the asymmetrical deployment of the receivers near the wall. In the centre of the flow the ADVP has a symmetrical configuration which is not possible near the walls because of the physical restrictions near the walls the ADVP is deployed there in an asymmetrical configuration which influences the measurements.

The ADVP is deployed in a housing which has to be moved on the water surface to perform the measurements. This housing will therefore disturb the water flow in a region of about 2 cm (in depth). An attempt to overcome this problem was tried by defining (manually) the region which is disturbed and extrapolating the data to the surface. The used extrapolation differs per measured quantity and are described by Blanckaert (2009, section 2.4). Afterwards the data is smoothed by the use of splines. This fitting of the data is a quite subjective procedure that aims at optimizing a compromise between smoothness of the analytical surface and proximity to the measured data without introducing systematic errors. This results in the experimental data that was used during this research.

Blanckaert (2009) gives an error for the water surface and the bottom topography (in case of the morphological experiment) of about 1 mm and 4 mm respectively. Besides that, it has to be mentioned that ripples and dunes with a magnitude of about the measuring grid size (1 cm by 5 cm) were not well measured. For the hydrodynamic quantities only a relative error is given, which is about 10 % for the time averaged velocities, about 15 % for the turbulent shear stresses and about 20 % for the turbulent normal stresses. Near the bottom (lowest 20%) the error in the measurements increases due to the high velocity gradient in the measuring volume and to parasitically echo's from the solid boundary.

The uncertainties in the represented depth averaged mean velocities and the pseudo-stream function ψ are estimated as less than 10%. The uncertainties of the derivatives of the time averaged velocities is about 20% and about 30% for the derivatives of the turbulent shear stresses. Here too it holds that the error increases towards the bottom which means that the reliability of the measured quantities used during this research decreases in the neighbourhood of the bottom.

5.2 Remarks about the simulations

Delft3D-FLOW

As a result of the use of staggered grid in Delft3D-FLOW different quantities are given at different locations in the grid. To compare them the quantities are linearly interpolated to a certain point to compare. This is for example the case for the velocities in transverse and downstream direction. This means that a slight error could be introduced due to interpolation of the simulation results.

It is questionable if the way the turbulent stresses are determined for the Delft3D-FLOW simulations during this research, is the right way. Use is made of the Boussinesq hypothesis

which relates the turbulent stresses to an eddy viscosity and a velocity gradient (see equation (2.9)). In the Delft3D-FLOW simulation there is chosen to relate all turbulent stresses to the average of the horizontal and vertical eddy viscosity calculated by Delft3D-FLOW. It is more likely that the horizontal turbulent stresses are related to the horizontal viscosity and the vertical turbulent stresses to the vertical eddy viscosity, because the horizontal eddies will cause the momentum exchange in horizontal direction and the vertical ones will cause the momentum exchange in the vertical direction. The question arises to which eddy viscosity the $\overline{u'w'}$ and $\overline{v'w'}$ (w' is the vertical component and u' and v' are the horizontal component of the shear stresses) should be related.

LES

The LES is performed with a rigid lid. The pressures that are available from the simulation are excluding the hydrostatic pressures because they are not relevant for the LES. The hydrostatic pressure is in every cross-section the same because of the rigid lid. The important quantity is the pressure gradient. To be able to compare the water levels of the different simulations properly it is necessary to transform the pressures from the LES to a water level excitation. In this report the vertical accelerations are neglected and the surface excitation is based on the pressures at the rigid lid. They are transformed to a water level excitation by means of the hydrostatic pressure assumption. The complete vertical momentum equation reads (in cylindrical coordinates):

$$\frac{\partial v}{\partial t}+u\frac{1}{r}\frac{\partial v}{\partial \theta}+v\frac{\partial v}{\partial r}+v\frac{\partial v}{\partial z}=g-\frac{1}{\rho}\frac{\partial p}{\partial z}+Diff \qquad (5.1)$$

The time derivative cancels out because of the steady state situation we are looking at. The gravitational force g is not included in the available pressures and is neglected too as well as the diffusion term. What remains is the balance between the vertical advective acceleration and the pressure gradient in the vertical.

$$\underbrace{u\frac{1}{r}\frac{\partial v}{\partial \theta}+v\frac{\partial v}{\partial r}+v\frac{\partial v}{\partial z}}_{adv.acceleration}=-\frac{1}{\rho}\frac{\partial p}{\partial z} \qquad (5.2)$$

The advective vertical acceleration is integrated from the bottom to the rigid lid and compared with the predicted pressure at the rigid lid and the bottom (see Figure 5-1). As we can see from this figure is that the pressure at the bottom fluctuates more but the magnitude is the same. The vertical accelerations are not important in the inner bend but they are in the outer bend. It is expected that the diffusion term has the same magnitude as the vertical acceleration because the pressures at the bottom and the surface are nearly equal so the diffusion term should balance the vertical acceleration to keep equilibrium in the momentum balance in the vertical direction. Having said that, it becomes clear that it is important to take the vertical accelerations into consideration when deriving the water level excitation for the outer bend. The relatively large importance of the vertical acceleration in this equilibrium-bed case means also that the hydrostatic pressure distribution may no longer be valid in this case. It could be worthwhile to investigate the M89-case using Delft3D-FLOW in the non-hydrostatic mode.

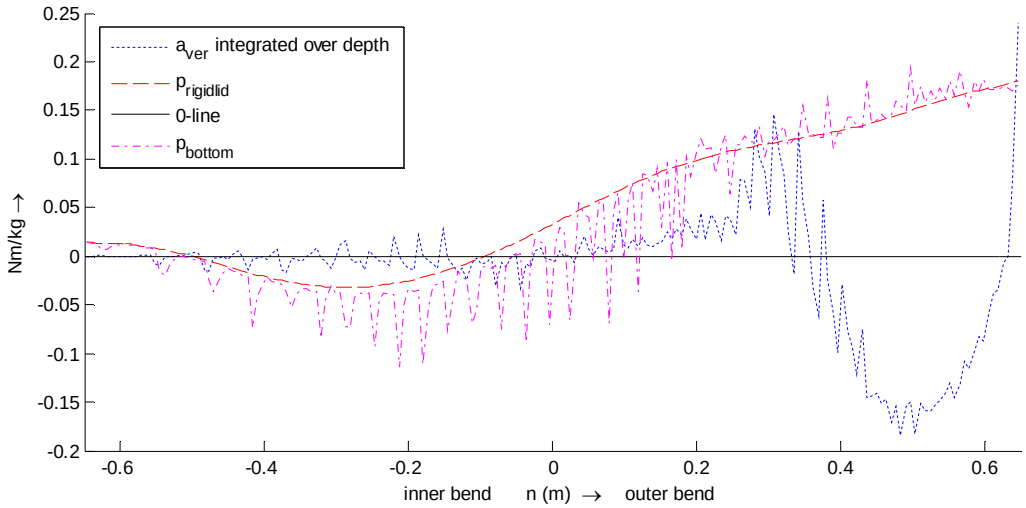

Figure 5-1 Cross-sectional plot (060) of the integrated vertical acceleration and the pressure at the surface according to the M89_LES

By scaling the water level, it is also needed to scale the velocities because with the use of a rigid lid, the flow is confined compared to the open channel flow. This operation is not applied to the following quantities of the LES:

- the transverse velocity profiles in the Q89 case
- the turbulent velocities in the Q89 case (including the TKE plots)
- the cross-sectional plots of the downstream velocities of the M89-case
- the cross-sectional plots of the transverse velocities of the M89-case
- the turbulent velocities in the M89-case

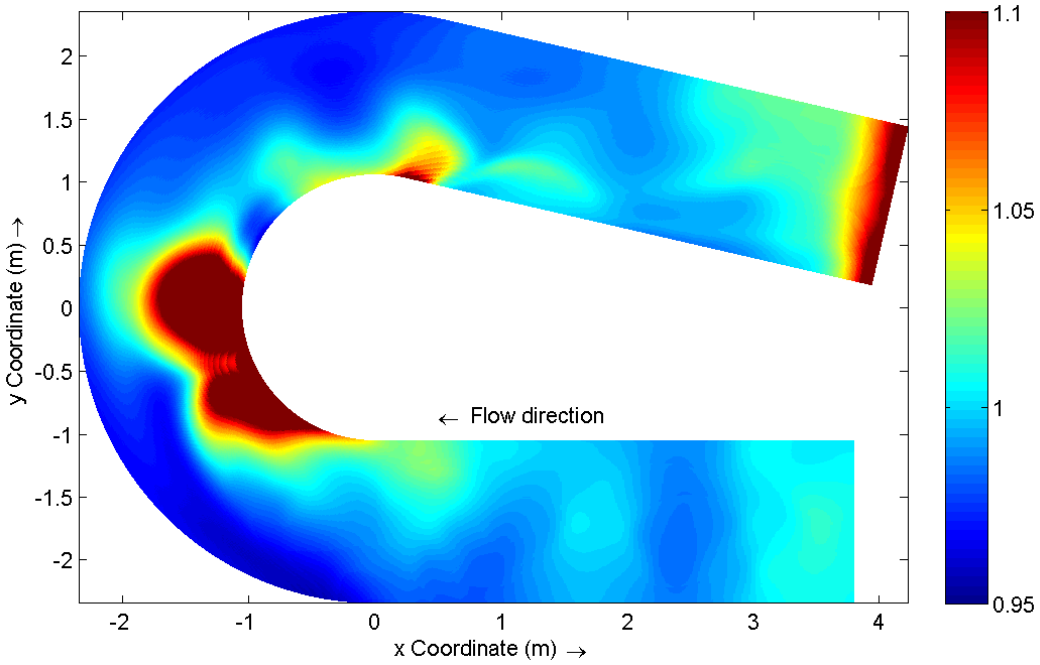

Figure 5-2 Factor to scale the velocities (d_{old} / d_{new}) for the M89_LES case

As a result of this, the velocities which are shown in the cross-sectional plots (M89_ and Q89_LES-results) are sometimes overestimated (at places where the water level is higher than

the rigid lid) and sometimes underestimated (the places where the water level is lower than the rigid lid).

In Figure 5-2 the scaling factor for the velocities in the equilibrium-bed case is plotted. As we can see, the scaling factor around the '*dip*' (inner bend) we came across in section 4.1 is relatively high. This means that the velocities should be higher than they were given according to the M89_LES case.

6 Conclusions and recommendations

This research was aimed at assessing the applicability of Delft3D-FLOW in sharp open-channel bends.

During this research there was attempted to find an answer to the following questions:

1.) To what extent is Delft3D-FLOW able to predict the hydrodynamic processes in sharp open channel bends?

2.) What are the differences between the Large Eddy Simulation (LES) and the Delft3D-FLOW simulation and how can these differences be explained?

3.) The effects of the turbulent viscosity on the flow are investigated.

To find the answers to these questions, three Delft3D-FLOW simulations are done and these are compared with detailed measurements and with the results of LES conducted at the TU Delft. The measurements were performed in a flume. Two different cases were evaluated, a flat-bed case and an equilibrium-bed case. For both cases LES results are available and for both cases Delft3D-FLOW simulations were done. To find an answer to the third question, a simulation was done for the flat-bed case with a horizontal background viscosity which was one order of magnitude larger than in the first flat-bed case simulation.

In this chapter we will summarize the findings we came across during this research and draw conclusions from it. In section 6.1 the conclusions are written and in section 6.2 some recommendations are given.

6.1 Conclusion

1.) To what extent is Delft3D-FLOW able to predict the hydrodynamic processes in sharp open channel bends?

From the analyzed quantities in the flat-bed case, it was found that especially the transverse velocities and the turbulent stresses are underestimated by Delft3D-FLOW. Phenomena were not predicted correctly (the internal shear layer) or missed completely (the outer-bank cell) in the Delft3D-FLOW simulation. After analyzing the downstream vorticity balance it turns out that the centrifugal effects are strongly related to the transverse velocities. The centrifugal-term of the downstream vorticity balance is also underestimated by Delft3D-FLOW and the anisotropy term does not show the effects of the outer-bank cell in the results of the Delft3D-FLOW simulation. It seems that the underestimation of the transverse velocity is caused by the underestimation of the centrifugal term. The centrifugal term is strongly related to the distribution of the downstream velocity which in its turn depends partly on the turbulent stresses.

In the equilibrium-bed case, the prediction of the flow becomes less accurate for the Delft3D-FLOW simulation. The underestimation of the transverse velocities by the Delft3D-FLOW simulation is larger (an underestimation of about 50%) in the equilibrium-bed case than for the flat-bed case. Also the prediction of the turbulent stresses by Delft3D-FLOW does not agree with what was measured. The turbulent stresses are underestimated and the patterns do not match which strengthens the idea of that the underestimation is partly caused by the not properly estimated turbulent stresses.

It can be concluded that the Delft3D-FLOW has problems to predict the transverse velocities properly. This was visible in both the flat-bed and the equilibrium-bed case. The same holds for the turbulent stresses. From this study it seems that there is a relation between the

underestimation of the transverse velocities and the not properly estimated turbulent stresses. The turbulence affects the distribution of the downstream velocity which in its turn affects centrifugal force, one of the driving mechanisms of the transverse velocities.

2.) What are the differences between the LES and the Delft3D-FLOW simulation and how can these differences be explained?

The prediction of the flow in the flat-bed case by the LES shows the outer-bank cell and shows the internal shear layer at the right place in the bend and the transverse velocities are well estimated. Where Delft3D-FLOW misses the outer-bank cell, predicted the internal shear layer only at the end of the bend and underestimated the transverse velocities severely, the LES was able to predict these features relatively well, which was also visible in the centrifugal term and the anisotropy term according to the LES. The reason why Delft3D-FLOW misses the outer-bank cell is the use of the linear k-ε model to predict the turbulent stresses. This model is not able to predict anisotropic turbulent stresses. This is in accordance with the findings of van Balen (2009) who stated that the anisotropic turbulent stresses initiate the distortion of the velocity profile which in its turn provides the centrifugal forces to drive the outer-bank cell. This idea is strengthened by the comparison of the turbulent stresses. The turbulent stresses are underestimated by the Delft3D-FLOW while the turbulent stresses according to the LES and the measurements compare well.

Comparing the M89_LES and the M89_1_D3D we see that for both simulations the predictions become less accurate compared to the measurements. Especially Delft3D-FLOW gives large underestimations of the transverse velocities. The prediction of the turbulent stresses by both the LES and the Delft3D-FLOW simulation do not agree with each other or with what was measured. The turbulent stresses are underestimated for both simulations and the patterns do not match. The underestimation of the turbulent stresses by Delft3D-FLOW can partly be caused by the shortcomings of the k-ε model as we saw in the flat-bed case. Besides that, the turbulent viscosity in the equilibrium-bed case is increased compared to the flat-bed case. The larger turbulent viscosity affects the turbulent stresses. The increase of the turbulent viscosity results in more exchange of momentum and a smoothing of the velocity profiles. This is further treated in the explanation about the effects of the turbulent viscosity on the flow. Another possible explanation for the mismatch of the turbulent stresses is sought in the effect of the bottom boundary on the generation of turbulence. It is expected that ripples and dunes will create turbulence in an other way as is predicted by the standard law-of-the-wall which was used in both Delft3D-FLOW and LES.

For both the equilibrium-bed and the flat-bed case it turned out that the predictions of the flow by the simulations became less accurate in the second half of the bend compared to the first half of the bend.

Delft3D-FLOW underestimates the transverse velocities and turbulent stresses and it misses the outer-bank cell in the flat bed case. The reasons for these under predictions and missing of the outer-bank cell can be found in the way the turbulent stresses are predicted which explains that the LES yields better results.

3.)What are the effects of the turbulent viscosity on the flow?

The way the turbulent viscosity affects the flow is investigated by changing the horizontal background viscosity in the Delft3D-FLOW simulation. It was visible that, due to the increase of the turbulent viscosity, the cross-sectional distributions of the downstream and transverse velocities were smoothed. Peaks were lower and momentum is more spread over the cross-section, details were smoothed out. This happens due to the increase of momentum exchange by the turbulence. Once again it must be said that the influence of the bottom roughness may

play an important role in the generation of turbulence. Especially in morphologic situations (the equilibrium-bed case) the dunes and ripples at the bottom will generate turbulence and deform the velocity distribution near the bottom.

Summarizing the results of this research in a nutshell, it can be said that in the comparison of the flat-bed case we concluded that an increase of the eddy viscosity reduces the transverse velocities because the momentum exchange increased and details and peaks are smoothed out. In the equilibrium-bed case the turbulent stresses are poorly reproduced by both the LES and Delft3D-FLOW simulation. The transverse velocities and details of the flow are not properly estimated. The LES does this better than Delft3D-FLOW model with the k-ε turbulence closure model, in the case of a flat-bed. This underpins the idea of the need of a good prediction of the turbulent stresses to be able to predict sharp bend flows in more detail.

6.2 Recommendations

Evaluating more options of Delft3D-FLOW

For the Delft3D-FLOW simulations, only the k-ε turbulence model was used which is applicable in the vertical. The horizontal eddy viscosity is only varied by increasing the horizontal background viscosity. From the comparison of those simulations and the results of the equilibrium-bed simulation the conclusion was drawn that the prediction of the turbulent stresses shows severe shortcomings. A meaningful addition to the simulations done in this research is the use of the HLES option of Delft3D-FLOW. This option can give a better estimation of the horizontal eddy viscosity and the turbulent velocities. It is expected that this will increase the quality of the predictions of the transverse velocities and other details of the flow.

As we saw in chapter 5, the vertical accelerations are quite important in the zone with upwelling (outer bank). For that reason a non-hydrostatic simulation is required.

An other improvement could be the use of a finer grid to get a better representation of the details of the flow. The cross-sectional plots of several quantities look quite rough due to lack of resolution. To give a quite good representation of effects with the size of the outer-bank cell (about 10 by 10 cm) a grid size of about 2 to 3 cm is required to give a reasonable representation of this feature. This will make it easier to see how details of the flow look. The drawback here is however the increase in computation time.

The relatively large horizontal background viscosity in simulation M89_1_D3D was chosen to damp large fluctuations that arose at the inflow boundary. It seemed that these fluctuations were caused by the combination of the boundary condition and the equilibrium-bottom topography. A mismatch between the inflow and the bottom-topography causes the flow to adapt strongly to the bottom topography at the entrance of the flume which results in strong fluctuations in the flow. Most quantities were smoothed out in simulation Q89_2_D3D due to the large horizontal background viscosity, as we saw in the comparison of simulation Q89_1_D3D (low horizontal background viscosity) with simulation Q89_2_D3D (high horizontal background viscosity). This was also visible in simulation M89_1_D3D. A better prediction of the flow over the equilibrium-bed can be achieved by the combination of better inflow conditions and a lower horizontal background viscosity. These conditions can be created by a longer straight inflow reach with a flat-bed. Another option is to keep the viscosity high in the near the inflow boundary and keep a more reasonable viscosity in the rest of the flume.

Extension of the analysis

The turbulent kinetic energy and the vorticity balance are not analyzed for the equilibrium-bed case. The analysis of these quantities will give a more complete comparison of the different data sets and more insight is gained in the flows and the shortcomings of the models.

As was said in the discussion about the calculation of the water level and several other flow quantities for the LES (section 5.2), the calculation of these quantities was not properly done. Because of the rigid lid approximation, some of the velocities should be scaled to compare them with the measurements and the Delft3D-FLOW simulations. This scaling is not performed for several velocities of the LES's. A better comparison of the LES with the results of the measurements and the Delft3D-FLOW simulation can be achieved by scaling the flow quantities of the LES (listed in section 5.2) with the right scaling factor d_{old} / d_{new}. With d_{old} the water depth in the case of the rigid lid and d_{new} the water depth calculated from the pressures predicted by the LES.

Improving Delft3D-FLOW

We concluded that there is a possible relation between the under estimation of the transverse velocities and the turbulence stresses. This idea was strengthen by the fact that the LES underestimated the transverse velocities and the turbulent stresses in the equilibrium-bed case too.

To improve the estimation of the turbulence stresses a non-linear k-ε model is suggested which is able to predict anisotropic turbulence (c.f. Kimura *et al.*, 2008) and also the outer-bank cell.

An other improvement, which will be beneficial for the LES too, can be the development of boundary conditions that include the generation of turbulence in the bottom layer. Especially in situations with developed bed forms this can lead to a better prediction of the turbulent stresses.

Upscaling

To use Delft3D-FLOW as a practical engineering tool in real life problems it is needed that the software package is validated with existing sharp-bend flows. Therefore it is needed to perform measurements of hydrodynamics in real river bends. Especially the transverse velocities and turbulence should be measured carefully.

7 References

Balaras, E., Benocci, C. and Piomelli, U., (1996), “Two-layer approximate boundary conditions for large-eddy simulations”, AIAA Journal, 34, 6, pp. 1111-1119

Blanckaert, K., and Graf, W. H., (2001). “Experiments on flow in an open-channel bend. Mean flow and turbulence” J. Hydraul. Eng.,127(10), 835–847.

Blanckaert, K., (2002), “Flow and turbulence in sharp open channel bends”, PhD-thesis Nr. 2545, Ecole Polytechnique Fédérale Lausanne, Switzerland.

Blanckaert, K., Glasson, L., Jagers, H.R.A., Sloff, C.J. (2003), “Quasi-3D simulation of flow in sharp open-channel bends with horizontal and developed bed topography”, Proc., Int. Symp. on Shallow Flows 1, 93-100

Blanckaert, K., de Vriend, H. J. de, (2003), “Nonlinear modelling of mean flow redistribution in curved open channels”, Water resources research, Vol. 39, No. 12

Blanckaert, K., and Lemmin, U. (2006). “Means of noise reduction in acoustic turbulence measurements.” J. Hydraul. Res., 44(1), 3–17.

Blanckaert, K., (2009, submitted for publications Water Resources Research, AGU), “Laboratory experiments on straight and sharply curved open-channel flows. Experimental techniques, data treatment and selected results”, Water resources research, Ecole Polytechnique Fédérale Lausanne, Switzerland.

“Delft3D-FLOW, Simulation of multi-dimensional hydrodynamic flows and transport phenomena, including sediments”, (2008), user manual, version 3.14, Rev. 5661, Deltares, Delft, The Netherlands

Demuren, A.O. and Rodi, W., (1984), “Calculation of turbulence-driven secondary motion in non-circular ducts”, Jounal of Fluid Mechanics, 140, pp.189-222

de Vriend, H.J. (1977), “A mathematical model of steady flow in curved shallow channels”, J. Hydr. Res., Delft, The Netherlands, 15(1), 37-54

de Vriend, H.J., (1981), "Steady flow in shallow channel bends" Rep. No. 81-3, Comm. on Hydraulics, Dept. Civ. Eng., Delft Univ. Techn., Delft

Hosoda, T., Sakurai, T., Kimura, I. and Muramoto, Y., “3-D computation of compound open channel flows with horizontal vortices and secondary currents by means of non-linear k-ε model”, J.of Hydroscience and Hydraulic Eng., 17 (1999), pp. 87-96

Hurther, D., and Lemmin, U. (1998). ‘‘A constant beamwidth transducer for three-dimensional Doppler profile measurements in open channel flow.’’ Measurement Science and Technology, 9(10), 1706–1714

Ikeda, S., M. Yamasaka, and J. F. Kennedy (1990), “Three-dimensional fully-developed shallow-water flow in mildly curved bends”, Fluid Dynamics Research 6, pp. 155-173, edited by the Japan Society of Fluid Mechanics, North-Holland, New York

Jansen, P.Ph. et al. (1979), “Principles of river engineering, The non-tidal alluvial river”, book, ISBN 0-273-01139-1, Pitman Publishing Limited, London

Johanneson, H. and Parker, G. (1989), “Velocity redistribution in meandering rivers”, J. Hydr.Engng, ASCE, 115(8), 1019-1039

Kalkwijk, J.P.T., and Booij, R. (1986), “Adaptation of secondary flow in nearly horizontal flow”, J.Hydraul. Res., 24(1), 19-37

Kimura, I., Uijttewaal, W.S.J., van Balen, W. and Hosoda, T. (2008), "Application of the non-linear k-ε model for simulating curved open channel flows", River Flow, Proceedings of the international conference on fluvial hydraulics, Izmir, Turkey, September 2008, Vol. 2, pp. 99-108

Lemmin, U., and Rolland, T. (1997). ''Acoustic velocity profiler for laboratory and field studies.'' J. Hydr. Engrg., ASCE, 123(12), 1089–1098

Nezu, I. & Nakagawa, H. (1993). "Turbulence in open channel flows", Int. Ass. Hydraul. Res. Monograph Series, AA Balkema, Rotterdam

Olesen, K.W. (1987), "Bed topography in shallow river bends", Report No. 87-1, Department Civil Engineering, Delft University of Technology, Netherlands

Pope, B. (2000), "Turbulent flows", Cambridge University Press, Cambridge, United Kingdom

Rozovskii, I.L. (1957). Flow of Water in Bends of Open Channels . Ac. Sc. Ukr. SSR, (English translation, Israel Program for Scientific Translations, Jerusalem, 1961)

Tennekes, H., and Lumley, J.L., "A first course in turbulence", MIT-Press

Uijttewaal, W.S.J., (2008), "Turbulence in hydraulics", reader, CT5312, Department Civil Engineering, Delft, University of Technology, Netherlands

van Balen, W., Uijttewaal, W.S.J., and Blanckaert, K., (2008), "LES and RANS computations of schematized river bends", River flow

van Balen, W., Uijttewaal, W.S.J., and Blanckaert, K. (2009a), "Large-eddy simulation of a mildly curved open-channel flow", under consideration for publication in Journal of Fluid Mechanics (2009)

van Balen, W., and Uijttewaal, W.S.J., and Blanckaert, K. (2009b), "Large-eddy simulations and experiments of single-bend open-channel flow at different water depths", under consideration for publication in Journal of Turbulence (2009)

van Balen, W., (2010), "Curved open-channel flows, a numerical study", PhD-thesis, Civil Engineering, TU Delft, The Netherlands

van Rijn, L.C., (1984), "Sediment transport, Part I: Bed load transport" Journal of Hydraulic Engineering, ASCE, 110(10), 1431-1456

Wu, W. (2007), "Computational River Dynamics", Taylor & Francis/Balkema, Leiden, Netherlands

Zeng, J., Constantinescu, G., Blanckaert, K., and Weber, L. (2008), "Flow and bathymetry in sharp open-channel bends: Experiments and predictions", Water Resources Research, vol.44, W09401

Nawoord

Via deze weg wil ik vele mensen danken voor hun hulp, inzet en tijd om mij te helpen gedurende mijn afstuderen. Ik heb veel kunnen leren van alles wat ik gedaan heb, ook de dingen die niet altijd mee zaten.

Mijn dank gaat uit naar Deltares waar ik, via Kees Sloff, de mogelijkheid kreeg om aan mijn afstudeerwerk te werken. Daarnaast wil ik ook de andere mensen binnen Deltares bedanken (Herman Kernkamp and Rob Uittenbogaard) voor hun hulp tijdens mijn afstudeerwerk. Willem, bedankt dat je zo goed als altijd bereikbaar was en tijd vrij hebt willen maken om me te helpen. Veel dingen ben ik door je uitleg beter gaan begrijpen. Ik wil Wim Uijttewaal bedanken voor zijn heldere uitleg en de duidelijke aanwijzingen. De andere commissieleden (Erik Mosselman, Kees Sloff en Huib de Vriend) dank ik voor hun tijd, altijd opbouwende opmerkingen en discussies gedurende de vergaderingen.

Ik wil mijn ouders en familie danken voor hun interesse en ondersteuning in materiële en immateriële zin en het geduld om te wachten tot ik eindelijk echt klaar was. Niet in het minst mijn vriendin Anneleen die me regelmatig aangemoedigd heeft om door te blijven knokken als het niet altijd meezat.

En ‘last but not least’: Dank aan God

Arco van Sabben

Delft, juni 2010